Charles University of Prague
Faculty of Mathematics and Physics

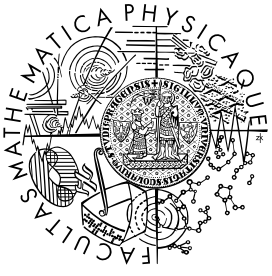

Anharmonic and solvation effects in vibrational spectroscopy

by
Mgr. Petr Daněček

Supervisor:
Doc. RNDr. Petr Bouř, CSc.

Consultant:
Doc. RNDr. Vladimír Baumruk, DrSc.

Prague 2007

Acknowledgements

It is a pleasure to thank the many people who made this thesis possible. I would like to give thanks namely to my supervisor, Doc. RNDr. Petr Bouř, CSc., for his guidance. Thanks are due also to many others, who helped me one way or another during my work: my consultant Doc. RNDr. Vladimír Baumruk, DrSc.; Melanie Glynn for proof-reading; and all colleagues. Last, but not least, much gratitude is due to my beautiful wife and two daughters for their patience. Their support has been invaluable.

Contents

Abstract

The aim of this work is to systematically investigate the role of anharmonic corrections and solvation effects in vibrational spectra and thus try to explore two important sources of errors in spectra simulations of molecules in polar liquids. Several anharmonic methods were implemented in one program package and applied to a number of small and medium-sized systems (up to 26 atoms), which enabled consistent comparison of performance of the methods.

All of the implemented anharmonic methods are based on the expansion of the nuclear potential in the fourth-order Taylor series. While all of the anharmonic methods significantly improved the region of hydrogen stretching vibrations, the agreement with experiment was not significantly improved in mid- and low- frequency region. According to the results, selection of a good electronic model is very important and errors in the *ab initio* potential easily surpass the anharmonic corrections. In agreement with previous results, it has been shown that a high-precision model must be used for evaluation of harmonic frequencies, but it may be sufficient to evaluate the anharmonic corrections at a lower level of electronic theory. Performance of a number of electronic methods and basis sets were compared for selected systems.

One of the issues investigated was numerical stability of the anharmonic methods. Most sensitive to potential variations were the perturbation methods, partly because many near-degenerate energy levels occur in larger systems. Therefore, a modified degeneracy-corrected formula was developed and successfully applied to a number of systems. The solvation effects were accounted for by including the polarizable continuum model into the electronic calculations. Inclusion of anharmonic and solvation corrections improved parts of spectra. However, a detailed peak-to-peak assignment was not possible due to the limited precision of the approximative electronic and vibrational methods used.

Finally, on model zwitterionic dipeptides, the Boltzmann averaging was used for lowest-frequency modes in order to investigate the effect of molecular flexibility on vibrational spectra.

CHAPTER 1

Introduction

Vibrational spectroscopy is one of the main spectroscopic methods employed by molecular biology and biophysics. It comes in many flavors and is an invaluable technique for studying the structure of molecules either in solid, liquid or gas phase. It is particularly useful for determining the structure and dynamics of biological molecules (or even whole living systems), for they can be studied by the Raman technique non-destructively in water, their natural environment. Time-resolved vibrational spectroscopy enables the visualization and tracking of fundamental events such as molecular reaction mechanisms or protein folding. Advanced systems utilizing high-power pulse lasers enable the study of the dynamics of fast processes occurring in the region of picoseconds. Vibrational spectroscopy has found its way from academic laboratories into practical applications across a range of diverse fields including: biomedical, pharmaceutical, agricultural, forensic and many more.

The most commonly used vibrational techniques are infrared absorption (IR) and Raman spectroscopy. While IR spectroscopy measures the decrease in the intensity of incident light due to excitation of vibrational energy levels in a molecule, Raman spectroscopy measures light inelastically scattered from a sample with a frequency different from that of incident light. Both methods have their chiroptical variants, collectively known as vibrational optical activity (VOA). The IR form is known as vibrational circular dichroism (VCD). In an analogy to electronic circular dichroism, VCD is a measurement of differential absorption of left- and right-polarized light. The Raman form, known as Raman optical activity (ROA), measures differential inelastic scattering with respect to left- and right-polarized light. The largest ROA signals are often associated with vibrations of the most rigid chiral parts of molecular structure and therefore ROA is particularly suitable for conformation studies of peptides. Although the first part of the work presented here concerns vibrational spectroscopy in general, the main focus lies in the interpretation and modeling of Raman and ROA spectra.

Raman scattering was first observed in 1928 [1]. Because it is such a weak effect (only one photon from a million scatters inelastically), it was not used widely until the development of laser and multichannel detectors. In the 1970s, the ability of chiral molecules to differentially scatter circularly polarized light was first predicted [2,3] and observed shortly afterward [4]. The number of photons scattered with different circular polarization is of three orders of magnitude weaker than the Raman signal. The ROA experiment therefore requires delicately sensitive instrumentation, which was not commercially available until 2003. Among the few laboratories which developed their own ROA spectrometers is the Institute of Physics of the Charles

University in Prague [5–7].

Vibrational spectra are generally very complex and consist of a large number of peaks. The peak intensity and position are sensitive to molecular structure and conformation, therefore the spectra are highly characteristic for each molecule. The analysis of measured spectra is not straightforward. In some applications it is sufficient to inspect spectra empirically by comparing marker bands with characteristic features of known structural motifs, but for detailed understanding and interpretation accompanying *ab initio* calculations are essential. Although a remarkably good agreement of calculation with experiment can be achieved on model systems [8], theoretical predictions for larger or medium-sized molecules give only qualitative results and differ significantly from experiment, especially in the high-frequency region of the spectra. One of the goals of this work is therefore to provide a theoretical support for interpretation of spectra measured by the high-quality ROA instrument at the Institute of Physics of the Charles University in Prague.

Due to the complexity of the calculations involved it is necessary to use many approximations to simplify the computational problem down to a feasible level. Thus several sources of errors are introduced. The most prominent one is the limited accuracy of electronic methods used for evaluation of the potential energy surface, on which the nuclei vibrate. The inaccurate potential energy surface (PES) is then further simplified to allow calculation of vibrational frequencies using, traditionally, the harmonic approximation. Moreover, unless studying molecules in the gas phase, the molecular vibrations may be strongly affected by interactions with other molecules of the same kind or by interactions with solvent molecules. Developments in these areas will be outlined in the following paragraphs and after that the structure of this document will be given.

Developments

The starting point for prediction of molecular properties is usually the harmonic approximation. Because it generally overestimates observed frequencies (especially the hydrogen stretching vibrations) some kind of correction is applied to account for anharmonic effects. Because the errors in calculations appeared largely systematic, scaling of force field constants by empirical factors had been suggested [9, 10]. The method can be remarkably successful [11], but it may fail when experimental reference data are not available. There has been also considerable effort to account for anharmonic effects directly by including the anharmonic part of the potential into the vibrational Schrödinger equation. However, calculation of the anharmonic potential is computationally demanding task. In the past many applications relied on empirical or semi-empirical force fields with parameters determined by fitting of an analytic function to experimental data, but the accuracy of such models is not very high [12, 13]. For small and medium sized molecules, accurate *ab initio* potential energy surface can be calculated at selected points around the equilibrium geometry and interpolated by use of standard approximation techniques [14]. This approach is particularly useful, when only interactions between a limited number of vibrational modes can be considered and thus only integrals of limited

dimension need to be evaluated [15, 16]. Another approach is to represent the potential by the lowest coefficients of Taylor series, determined from analytic second derivatives calculated at geometries displaced from the optimized geometry along nuclear coordinates [17]. Working in the basis of linear harmonic oscillator wave functions, only one-dimensional integrals need to be considered this way at the cost of truncating the higher coefficients of the Taylor expansion. In this work, PES was represented by a Taylor polynomial of the fourth order.

The beauty of the harmonic approximation is that it enables one to split the multidimensional Schrödinger equation into a set of independent one-dimensional problems with a simple analytic solution. For anharmonic potentials this is generally not possible and therefore approximative methods must be employed. The vibrational self-consistent field method (VSCF) developed by Bowman in 1978 [18] became very popular. The method includes anharmonic terms in the potential, yet retains separability of the harmonic approximation. Once the anharmonic potential is known, the method is efficient enough to be applied to large systems with thousands of degrees of freedom, such as was the case of the protein BPTI studied by Roitberg and Gerber [13]. The efficiency of VSCF comes at the price of lower accuracy, because the method neglects correlation of vibrational motions. Several extensions to VSCF have been therefore proposed, in a close parallel to methods applied in the electronic mean-field problem. The most general method is the vibrational configuration interaction (VCI), which looks for a solution expanded in some complete basis set, for instance linear harmonic oscillators (LHOs) or the VSCF solutions [19]. An alternative method is the vibrational perturbation theory (VPT), where the Rayleigh-Schrödinger perturbation method is used to correct either the harmonic [20, 21] or the VSCF approximation [22]. Recently, Christiansen formulated vibrational coupled cluster theory (VCC) [23]. In this work, multiple anharmonic methods were implemented: VCI in the basis of LHOs, VSCF, and VPT of the second order for both the VSCF and harmonic approximation.

For biochemical problems it is important that vibrational spectra can be collected in an aqueous environment. Because the conformational changes induced by solvation often have a large effect on the spectra, there is a need for computationally affordable model. Continuum models are very popular, where the solute molecule is placed in a cavity surrounded by a polarizable continuum, whose reaction field modifies the energy and the properties of the solute molecule [24]. Polarizable continuum models are flexible and efficient, but they partially neglect important effects, such as hydrogen bonding and dispersion interactions. More precise but computationally expensive is inclusion of explicit solvent molecules. In this work, the conductor solvent model CPCM was used [25].

Document structure

The document is organized as follows. In the introductory Chapter 1, a brief account on developments in the *ab initio* modeling of vibrational spectra of large molecules in liquid phase is given.

Chapter 2 is devoted to theory. First there is a reminder of basic concepts and notations

of quantum chemistry, then a review of electronic methods used in this study for evaluation of potential energy surface follows. Although PES constitutes mere input data in this work, the choice of proper electronic method for evaluation of PES is of utmost importance for modeling of vibrational spectra. The vibrational problem is then reviewed and the anharmonic methods VCI, VPT and VSCF are discussed. The theory required for understanding how the intensities of IR, VCD, Raman and ROA transitions can be determined, follows. The chapter finishes with a review of the conductor solvent model.

In the concluding Chapter 3, the results of anharmonic calculations performed on a number of systems are presented, starting from the benchmark two-dimensional Henon-Heiles potential up to real molecules containing 26 atoms. The chapter also briefly summarizes two papers published by the author of this work in the Journal of Computational Chemistry and the Journal of Chemical Physics. Some preliminary results for the next paper under preparation are included.

Theory

2.1 Basic concepts of quantum mechanics

In this section will be presented a cursory review of quantum mechanical principles and approximations ubiquitous in quantum chemical calculations.

In the quantum view of the world, a system at a time t is represented by a state vector $|\boldsymbol{\Psi}(t)\rangle$ in a Hilbert space. State vectors can be projected onto a particular basis, e.g. the coordinate basis $\{|\boldsymbol{r}\rangle\}$

$$\boldsymbol{\Psi}(\boldsymbol{r},t) = \langle \boldsymbol{r}|\boldsymbol{\Psi}(t)\rangle. \tag{2.1.1}$$

A system of N spinless particles in three-dimensional space can be described by a *wave function* $\boldsymbol{\Psi}(x_1, y_1, z_1, \ldots, z_N, t)$ of $3N+1$ variables. Physical observables are represented by self-adjoint operators, that is, ones whose matrix is *Hermitian*.[1] A distinct role is played by the *Hamiltonian* operator $\hat{\mathrm{H}}$, which gives the value of energy and also determines time evolution of a system through the *Schrödinger equation*

$$i\hbar\frac{\partial\boldsymbol{\Psi}(\boldsymbol{r},t)}{\partial t} = \hat{\mathrm{H}}\boldsymbol{\Psi}(\boldsymbol{r},t). \tag{2.1.2}$$

When the Hamiltonian does not depend on time, a stationary wave function can be separated into product functions

$$\boldsymbol{\Psi}(\boldsymbol{r},t) = \Psi(\boldsymbol{r})\,\varphi(t), \qquad \varphi(t) = \mathrm{e}^{-iEt/\hbar}, \tag{2.1.3}$$

and the Schrödinger equation can be simplified into

$$\hat{\mathrm{H}}\,\Psi(\boldsymbol{r}) = E\,\Psi(\boldsymbol{r}). \tag{2.1.4}$$

The stationary wave function changes as a function of time only by a complex phase, therefore the probability amplitude

$$\langle\Psi(\boldsymbol{r})\,\varphi(t)|\Psi(\boldsymbol{r})\,\varphi(t)\rangle \equiv \int \Psi^*(\boldsymbol{r})\,\varphi^*(t)\,\Psi(\boldsymbol{r})\,\varphi(t)\,d\boldsymbol{r}\,dt = \langle\Psi(\boldsymbol{r})|\Psi(\boldsymbol{r})\rangle \tag{2.1.5}$$

is constant.[2]

[1] A Hermitian matrix is identical to its transpose with complex conjugate elements. An operator is defined as an entity which, when acting on a vector, converts it into a vector. The operator $\hat{\mathrm{O}}$ is completely determined by its matrix representation O_{ij} in a complete basis $\{|i\rangle\}$ by the expansion $\hat{\mathrm{O}}|j\rangle = \sum_i O_{ij}|i\rangle$. Note that $O_{ij} = \langle i|\hat{\mathrm{O}}|j\rangle$.

[2] The asterisk symbol (*) denotes complex conjugate.

Our system of interest is a molecule which consists of N_n nuclei and N_e electrons. The stationary wave function of a molecule can be found by solving the time-independent Schrödinger equation

$$\left[-\sum_{\alpha_i \in \boldsymbol{R}} \frac{\hbar^2}{2M_i} \frac{\partial^2}{\partial R_{\alpha_i}^2} - \sum_{\alpha_i \in \boldsymbol{r}} \frac{\hbar^2}{2m_e} \frac{\partial^2}{\partial r_{\alpha_i}^2} + V(\boldsymbol{R}, \boldsymbol{r}) \right] \Psi(\boldsymbol{R}, \boldsymbol{r}) = E\, \Psi(\boldsymbol{R}, \boldsymbol{r}), \tag{2.1.6}$$

where $\boldsymbol{R} = \{x_1, y_1, \ldots, z_{N_n}\}$ are the nuclei positions, $\boldsymbol{r} = \{x_1, y_1, \ldots, z_{N_e}\}$ are the positions of electrons, m_e is mas of electron and M_i is mass of i-th nucleus.

In a vacuum without external fields and without relativistic effects, the only forces between the particles are Coulomb interactions. The potential then has the form

$$V(\boldsymbol{R}, \boldsymbol{r}) = \frac{e^2}{4\pi\varepsilon_0} \left[\sum_{i<j} \frac{1}{|\boldsymbol{r}_i - \boldsymbol{r}_j|} + \sum_{i<j} \frac{Z_i Z_j}{|\boldsymbol{R}_i - \boldsymbol{R}_j|} - \sum_{i,j} \frac{Z_i}{|\boldsymbol{R}_i - \boldsymbol{r}_j|} \right], \tag{2.1.7}$$

where the electron i at $\boldsymbol{r}_i$ has charge $-e$ and the nucleus at $\boldsymbol{R}_i$ has charge eZ_i.

An analytic solution to this mathematical problem exists only for the simplest case of atoms with a single electron, such as the hydrogen atom or the He^+ ion. For other systems it must be solved numerically by employing approximative methods. The dimension of the problem grows very quickly and many simplifications must be introduced. Because even the smallest nucleus is much heavier than an electron[3], the motions of electrons and nuclei can be separated and the wave function can be expressed as a product of the electronic and the nuclear part

$$\Psi(\boldsymbol{R}, \boldsymbol{r}) = \Psi_e(\boldsymbol{r}; \boldsymbol{R})\, \Psi_n(\boldsymbol{R}). \tag{2.1.8}$$

The equation is called *adiabatic approximation*, and it is justified by the fact that the electronic charge distribution adjusts almost instantaneously to slow changes in nuclear positions. When the Schrödinger equation is applied to the adiabatic wave function, it is common to neglect nuclear derivatives of the electronic wave function $\nabla_n \psi_e$ in the nuclei kinetic energy term

$$\begin{aligned} \frac{\partial^2}{\partial \boldsymbol{R}^2}\, \Psi_e(\boldsymbol{r}; \boldsymbol{R})\, \Psi_n(\boldsymbol{R}) &= \Psi_e\, \nabla_n^2 \Psi_n + \Psi_n\, \nabla_n^2 \Psi_e + 2\, (\nabla_n \Psi_n)\, (\nabla_n \Psi_e) \\ &\simeq \Psi_e\, \nabla_n^2 \Psi_n. \end{aligned} \tag{2.1.9}$$

In the *Born-Oppenheimer approximation* (BOA), Eq. 2.1.6 can be then written as

$$\left[-\sum_{\alpha_i \in \boldsymbol{r}} \frac{\hbar^2}{2m_e} \frac{\partial^2}{\partial r_{\alpha_i}^2} + V_{ee} + V_{en} \right] \Psi_e(\boldsymbol{r}; \boldsymbol{R}) = E_e(\boldsymbol{R})\, \Psi_e(\boldsymbol{r}; \boldsymbol{R}) \tag{2.1.10}$$

$$\left[-\sum_{\alpha_i \in \boldsymbol{R}} \frac{\hbar^2}{2M_i} \frac{\partial^2}{\partial R_{\alpha_i}^2} + V_{nn} \right] \Psi_n(\boldsymbol{R}) = E_n\, \Psi_n(\boldsymbol{R}). \tag{2.1.11}$$

[3]The proton-electron mass ratio is 1836.

The electronic part of the wave function now depends on the positions of nuclei only parametrically. If evaluated for different nuclear positions, the electronic energy is obtained as a function of $\boldsymbol{R}$. This function is known as the *potential energy surface*. Thus in the Born-Oppenheimer approximation, the nuclei move on a potential energy surface obtained by solving the electronic problem 2.1.10.

The mathematical separation of nuclear and electronic motions respects experimental observation, because transitions between electronic states are usually energetically well separated from vibrational and rotational transitions: electronic transitions correspond to energies of photons from the visible and ultraviolet region of spectra, but energy differences between vibrational states are measured in the infrared region. Similarly, energy differences between rotational states correspond to photons from the microwave region and are therefore well separated from the infrared region of vibrational transitions. Consequently, nuclear vibrations can be often treated separately from rotational motions. Before proceeding to this problem, approximate electronic methods of quantum chemistry will be outlined.

2.2 General techniques

2.2.1 The variational principle

An important approach for finding solutions to the eigenvalue equation

$$\hat{\mathrm{H}}\,|\Psi\rangle = E\,|\Psi\rangle \tag{2.2.1}$$

is the *variational principle*, which states that the expectation value of the Hamiltonian is larger or equal to the exact ground state energy

$$E_0 \leq \langle\Psi|\hat{\mathrm{H}}|\Psi\rangle, \tag{2.2.2}$$

where $|\Psi\rangle$ is normalized, that is, $\langle\Psi|\Psi\rangle = 1$. The inequality can be easily proved. The function $|\Psi\rangle$ can be expanded into the complete set $\{\Psi_n\}$ of orthonormal eigenfunctions of $\hat{\mathrm{H}}$, so that

$$\langle\Psi|\hat{\mathrm{H}}|\Psi\rangle = \sum_{i,j} c_i^*\, c_j\, \langle\Psi_i|\hat{\mathrm{H}}|\Psi_j\rangle = \sum_i |c_i|^2\, E_i \geq \sum_i |c_i|^2\, E_0 = E_0. \tag{2.2.3}$$

Thus the task of finding the ground state eigenfunction takes on the form of determining the optimum set of coefficients $\{c_i\}$. As will be shown, it can be solved by matrix diagonalization. Since the function $|\Psi\rangle$ is normalized, the coefficients are subject to the constraint

$$\langle\Psi|\Psi\rangle = \sum_i |c_i|^2 = 1. \tag{2.2.4}$$

The problem of minimizing the function $\langle\Psi|\hat{\mathrm{H}}|\Psi\rangle$ can be solved by the method of Lagrange multipliers. The Lagrange function is

$$\begin{aligned} \mathcal{L}(c_1, c_2, \ldots) &= \langle\Psi|\hat{\mathrm{H}}|\Psi\rangle - E\,(\langle\Psi|\Psi\rangle - 1) \\ &= \sum_{i,j} c_i^*\, c_j\, \langle\Psi_i|\hat{\mathrm{H}}|\Psi_j\rangle - E\left(\sum_i |c_i|^2 - 1\right). \end{aligned} \tag{2.2.5}$$

Note that the second term in the equation is zero and therefore the minimum of both $\langle\Psi|\hat{\mathrm{H}}|\Psi\rangle$ and $\mathcal{L}$ occurs at the same value of coefficients. The values c_i which minimize $\mathcal{L}$ are then sought by finding the extreme of $\mathcal{L}$

$$0 = \frac{\partial\mathcal{L}}{\partial c_k^*} = \sum_i c_i\, H_{ik} - c_k\, E, \qquad k = 1, \ldots \tag{2.2.6}$$

which yields the standard matrix eigenvalue problem

$$\sum_i H_{ij}\, c_i = E\, c_j. \tag{2.2.7}$$

In general, the basis $\{\Psi_n\}$ is infinitely large, but only a limited number of functions can be included in practice. Within a given finite subspace, the lowest eigenvalue is the best approximation to the ground state energy.

2.2.2 Perturbation method

Perturbation theory (PT) is a tool for finding an approximate solution to a problem which is too complicated to be solved exactly. It starts from an exact solution to a simpler problem and applies a small disturbance to the system. For instance, the harmonic potential describes the vibrational motion of molecules rather well and thus the anharmonic terms in the potential can be regarded as a perturbation. Another example is the interaction of electromagnetic radiation with molecules, inside of which much stronger electrostatic interactions take effect. The anharmonicity of the vibrational potential does not depend on time. In such case we talk about *time-independent perturbation theory*. On the other hand, electromagnetic radiation falls in the category of *time-dependent perturbation*, because the radiation electromagnetic field varies with time.

Time-independent perturbation theory

Assume that the system of interest can be described by a Hamiltonian $\hat{\mathrm{H}}$ which can be split into a part $\hat{\mathrm{H}}^{(0)}$ with known exact solutions and a small perturbation $\hat{\mathrm{W}}$. An arbitrary dimensionless parameter λ is introduced

$$\hat{\mathrm{H}} = \hat{\mathrm{H}}^{(0)} + \lambda\hat{\mathrm{W}}. \tag{2.2.8}$$

Because the Hamiltonian depends on λ, also the energy and wave functions depend on it. It is assumed that for a weak perturbation they can be written in terms of power series

$$\begin{aligned} E &= E^{(0)} + \lambda\, E^{(1)} + \lambda^2\, E^{(2)} + \cdots \\ |\Psi\rangle &= |\psi^{(0)}\rangle + \lambda\,|\psi^{(1)}\rangle + \lambda^2\,|\psi^{(2)}\rangle + \cdots\,, \end{aligned} \tag{2.2.9}$$

where $E^{(0)}$ is the energy of the unperturbed system and $\psi^{(0)}$ is the corresponding wave function. Inserting the power series into the Schrödinger equation 2.1.4 and comparing terms of each power of λ, one obtains an infinite series of simultaneous equations

$$\begin{aligned} \hat{\mathrm{H}}^{(0)}|\psi_i^{(0)}\rangle &= E_i^{(0)}|\psi_i^{(0)}\rangle \\ \hat{\mathrm{H}}^{(0)}|\psi_i^{(1)}\rangle + \hat{\mathrm{W}}|\psi_i^{(0)}\rangle &= E_i^{(0)}|\psi_i^{(1)}\rangle + E_i^{(1)}|\psi_i^{(0)}\rangle \\ \hat{\mathrm{H}}^{(0)}|\psi_i^{(2)}\rangle + \hat{\mathrm{W}}|\psi_i^{(1)}\rangle &= E_i^{(0)}|\psi_i^{(2)}\rangle + E_i^{(1)}|\psi_i^{(1)}\rangle + E_i^{(2)}|\psi_i^{(0)}\rangle \\ &\cdots \end{aligned} \tag{2.2.10}$$

The first-order correction to the i-th solution Ψ_i can be expanded in the basis set of unperturbed solutions $\psi_j^{(0)}$

$$\psi_i^{(1)} = \sum_j c_{ij}\,\psi_j^{(0)}. \tag{2.2.11}$$

When the second equation is multiplied by the bra vector $\langle\psi_i^{(0)}|$, the expression for the first-order energy correction is obtained

$$E_i^{(1)} = \langle\psi_i^{(0)}|\hat{\mathrm{W}}|\psi_i^{(0)}\rangle. \tag{2.2.12}$$

The coefficients can be determined by multiplying the second equation by the vector $\psi_k^{(0)}$

$$c_{ik} = \frac{\langle\psi_k^{(0)}|\hat{\mathrm{W}}|\psi_i^{(0)}\rangle}{E_i^{(0)} - E_k^{(0)}}, \qquad k \neq i. \tag{2.2.13}$$

The second-order correction is obtained in a similar way from the third equation of 2.2.10

$$E_i^{(2)} = \sum_{j\neq i} \frac{|\langle\psi_i^{(0)}|\hat{\mathrm{W}}|\psi_j^{(0)}\rangle|^2}{E_i^{(0)} - E_j^{(0)}}. \tag{2.2.14}$$

Simplified degeneracy treatment

The perturbation expressions fail when two or more *degenerate states* with the same energy occur. The perturbation operator $\hat{\mathrm{W}}$ can split the degenerate energy levels. The set of problematic degenerate states $D = \{\psi_i^{(0)}\}$ is replaced by their linear combination

$$\phi_j = \sum_{i\in D} c_{ji}\,\psi_i^{(0)} \tag{2.2.15}$$

obtained by diagonalization of the perturbation operator $\hat{\mathrm{W}}$ in the basis of the degenerate states, that is, by solving the eigenvalue problem

$$\sum_i c_{ji}\,\langle\psi_k^{(0)}|\hat{\mathrm{W}}|\psi_i^{(0)}\rangle = c_{jk}\,w_j, \qquad i,j,k \in D. \tag{2.2.16}$$

The value of the perturbed energy of the degenerate states is then

$$E_i = E_i^{(0)} + \langle\phi_i|\hat{\mathrm{W}}|\phi_i\rangle. \tag{2.2.17}$$

Because of a large number of near-degenerate and degenerate energy levels in large systems, the following simplified degeneracy-corrected formula [26] was used in practical calculations instead of the formula Eq. 2.2.14

$$E_i^{(2)\prime} = \sum_{j\neq i} \frac{1}{2}(E_j - E_i) \pm \frac{1}{2}\sqrt{(E_i - E_j)^2 + 4W_{ij}^2}, \qquad E_i = E_i^{(0)} + W_{ii}. \tag{2.2.18}$$

In the formula is used + sign when $E_i > E_j$ and − sign when $E_i < E_j$. As shown in Appendix A.1, for non-degenerate states the formula leads to the standard perturbation formula. In the case of two-fold degeneracy, the formula is exact.

Time-dependent perturbation theory

When the perturbation operator is not stationary and changes with time, the time-dependent Schrödinger equation (Eq. 2.1.2) must be used

$$i\hbar \frac{\partial \Psi}{\partial t} = \left[\hat{\mathrm{H}} + \hat{\mathrm{W}}(t)\right] \Psi(t). \tag{2.2.19}$$

The state of the system at time t can be expressed in terms of the stationary solutions ψ_j to the unperturbed Hamiltonian

$$\Psi(t) = \sum_j c_j(t)\, e^{-iE_j t/\hbar}\, \psi_j. \tag{2.2.20}$$

Inserting it into Eq. 2.2.19 and multiplying by the stationary bra vector $\langle\psi_k|$, the equation can be reduced to partial differential equations for the amplitudes

$$i\hbar \frac{d}{dt} c_k(t) = \sum_j W_{kj}(t)\, c_j(t)\, e^{-i\,\omega_{jk}\,t}, \qquad \omega_{jk} = (E_j - E_k)/\hbar. \tag{2.2.21}$$

Up to this point, the expression is exact. Similarly to the stationary PT, the approximation is introduced that the coefficients c_k can be expanded in terms of the perturbation parameter λ

$$c_k = c_k^{(0)} + \lambda\, c_k^{(1)} + \lambda^2\, c_k^{(2)} + \cdots . \tag{2.2.22}$$

By comparing terms with each power of λ, iterative solutions are obtained. The amplitudes in the first-order approximation can be written as

$$c_k(t) = c_k(0) + \frac{1}{i\hbar} \sum_j \int_0^t W_{kj}(\tau)\, c_j(0)\, e^{-i\,\omega_{jk}\,\tau}\, d\tau. \tag{2.2.23}$$

In the particular case of electromagnetic radiation, the perturbation is oscillating with angular frequency ω

$$\hat{\mathrm{W}}(t) = W e^{i\,\omega\,t} + W^* e^{-i\,\omega\,t} \tag{2.2.24}$$

and the equation can be easily integrated. To simplify the equation, assume that the system was initially in the state ψ_j. Therefore the initial values of amplitudes are $c_k(0) = \delta_{kj}$. Integrating the equation with the perturbation in the harmonic form, one obtains

$$c_k(t) = \frac{1}{\hbar}\left[W_{kj} \frac{e^{-i(\omega_{jk}-\omega)t} - 1}{\omega_{jk} - \omega} + W_{kj}^* \frac{e^{-i(\omega_{jk}+\omega)t} - 1}{\omega_{jk} + \omega} \right]. \tag{2.2.25}$$

When studying resonance effects, such as absorption of photons, the frequency of the incident light ω is close to the frequency ω_{jk}. The first term will be therefore much more significant and

we neglect the other. The probability amplitude is then

$$|c_k(t)|^2 = \frac{4\,|W_{kj}|^2}{\hbar^2}\frac{\sin^2(\omega_{jk}-\omega)t/2}{(\omega_{jk}-\omega)^2}. \tag{2.2.26}$$

This result will become useful later when discussing transition probabilities between vibrational states in Sec. 2.5.

2.3 Approximate methods of quantum chemistry

The quality of predicted vibrational frequencies and intensities undoubtedly rises and falls with the quality of the nuclear potential energy surface. Several electronic structure methods have been used in this study to test the influence of the nuclear potential on calculated spectra.

2.3.1 The Hartree-Fock approximation

The electronic wave function in Eq. 2.1.10 depends only on spatial coordinates. The spin associated with an electron gives an additional two-valued degree of freedom. The one-electron wave function with spin is represented by a product of the spatial part and one of the two *spin functions*, α or β, corresponding to spin-up and spin-down

$$\psi(\boldsymbol{x}) \equiv \psi(\boldsymbol{r})\,\alpha \quad \text{or} \quad \psi(\boldsymbol{x}) \equiv \psi(\boldsymbol{r})\,\beta. \tag{2.3.1}$$

The wave functions $\psi(\boldsymbol{x})$ are called *spin orbitals*, where $\boldsymbol{x}$ is a generalized coordinate which includes spatial and spin coordinate.

Because the electrons obey the Fermi-Dirac statistic, the wave function must change sign upon exchange of any pair of electrons. The antisymmetry of the wave function is in the Hartree-Fock theory (HF) enforced by the use of wave functions in the form of a Slater determinant. Given a set of linearly independent spin orbitals $\{\psi_i(\boldsymbol{x}_i)\}$, the n-electron *Slater determinant* is

$$\Psi_e(\boldsymbol{x}_1, \ldots, \boldsymbol{x}_n) = \frac{1}{\sqrt{n!}} \begin{vmatrix} \psi_1(\boldsymbol{x}_1) & \cdots & \psi_n(\boldsymbol{x}_1) \\ \vdots & \ddots & \vdots \\ \psi_1(\boldsymbol{x}_n) & \cdots & \psi_n(\boldsymbol{x}_n) \end{vmatrix}. \tag{2.3.2}$$

The factor $1/\sqrt{n!}$ is a normalization factor. The mathematical form of the determinant assures that upon switching two rows (i.e. exchanging two electrons), the wave function changes sign. If a single spin-orbital was occupied by two electrons, two identical columns would make the determinant zero.

For a wave function in the form of a Slater determinant, the expectation energy is given as a sum of one-electron terms

$$\langle i|\hat{\mathrm{h}}|i\rangle = -\frac{\hbar^2}{2m_e}\int \psi_i^*(\boldsymbol{r})\frac{\partial^2\psi_i(\boldsymbol{r})}{\partial \boldsymbol{r}_i^2}\,d\boldsymbol{r} - \frac{e^2}{4\pi\epsilon_0}\sum_j \int |\psi_i(\boldsymbol{r})|^2\,\frac{Z_j}{|\boldsymbol{R_j}-\boldsymbol{r}|}\,d\boldsymbol{r} \tag{2.3.3}$$

and two-electron potential terms

$$\frac{1}{2}\sum_{i,j}\left[(ij \mid ij) - (ij \mid ji)\right], \tag{2.3.4}$$

where

$$(ij \mid kl) \equiv \frac{e^2}{4\pi\epsilon_0}\iint d\boldsymbol{x}_1\, d\boldsymbol{x}_2\, \psi_i^*(\boldsymbol{x}_1)\psi_j^*(\boldsymbol{x}_2)\frac{1}{|\boldsymbol{x}_1-\boldsymbol{x}_2|}\psi_k(\boldsymbol{x}_1)\psi_l(\boldsymbol{x}_2). \tag{2.3.5}$$

The first two-electron term of the potential corresponds to the classical Coulomb repulsion, the other is the so called exchange term with no classical analog, which is not zero only for electrons with parallel spins. The integrals are usually expressed using the convenient form of the *Coulomb operator* $\hat{\mathrm{J}}_i$ and the *exchange operator* $\hat{\mathrm{K}}_i$

$$\hat{\mathrm{J}}_i\,\psi_j(\boldsymbol{x}) \equiv \frac{e^2}{4\pi\epsilon_0}\left(\int \frac{|\psi_i(\boldsymbol{x}_1)|^2}{|\boldsymbol{x}-\boldsymbol{x}_1|}\,d\boldsymbol{x}_1\right)\psi_j(\boldsymbol{x}) \tag{2.3.6}$$

$$\hat{\mathrm{K}}_i\,\psi_j(\boldsymbol{x}) \equiv \frac{e^2}{4\pi\epsilon_0}\left(\int \frac{\psi_i(\boldsymbol{x}_1)^*\psi_j(\boldsymbol{x}_1)}{|\boldsymbol{x}-\boldsymbol{x}_1|}\,d\boldsymbol{x}_1\right)\psi_i(\boldsymbol{x}). \tag{2.3.7}$$

The exchange integrals arise because of the antisymmetric nature of the wave function. The operator is non-local, in the sense that when operating on $\psi(\boldsymbol{x}_0)$, it does depend on the value of $\boldsymbol{x}$ throughout all space, not just at $\boldsymbol{x}_0$.

The Hartree-Fock theory is based on the variational principle described in Sec. 2.2.1, but instead of differentiating with respect to the coefficients, the more general technique of functional variation is used. To find the best energy, the functional $E[\Psi_e] = \langle\Psi_e|\hat{\mathrm{H}}|\Psi_e\rangle$ is minimized with respect to the spin orbitals $\{\psi_i(\boldsymbol{x}_i)\}$. Introducing the Lagrange multipliers ϵ_i and assuming orthonormality of the spin orbitals, the functional $\mathcal{L}$ has the form

$$\mathcal{L}[\{\psi_i\}] = \sum_i \langle i|\hat{\mathrm{h}}|i\rangle + \frac{1}{2}\sum_{i,j}\left[(ij\mid ij) - (ij\mid ji)\right] - \sum_i \epsilon_i(\langle\psi_i|\psi_i\rangle - 1). \tag{2.3.8}$$

Minimizing the functional $\mathcal{L}$ by setting its first variation to zero, one arrives at the *Hartree-Fock equations*

$$\left[\hat{\mathrm{h}} + \sum_j\left(\hat{\mathrm{J}}_j - \hat{\mathrm{K}}_j\right)\right]|\psi_i\rangle = \epsilon_i\,|\psi_i\rangle \qquad i = 1,\ldots,n. \tag{2.3.9}$$

Note that although the equations formally resemble linear eigenvalue equations, the Coulomb and exchange operators depend on the solutions ψ_i. Therefore the Hartree-Fock equations are usually solved by iterative procedures. Starting from an initial guess of the spin orbitals, the equations are solved to obtain new spin orbitals. The solutions are inserted into the equations again and new orbitals are calculated. The procedure is repeated until self-consistency is reached, i.e. the spin orbitals do not vary.

Only for atoms is it common to calculate the equations numerically. Molecular calculations are performed by expanding the spatial part of spin orbitals (also known as *molecular orbitals*) into a set of k known spatial basis functions (*atomic orbitals*)

$$|\psi_i\rangle = \sum_{\mu=1}^{k} c_{i\mu}\,|\phi_\mu\rangle \qquad i = 1,\ldots,n, \quad n \le k. \tag{2.3.10}$$

The problem leads to the *Roothaan equations*

$$\sum_{\mu=1}^{k} F_{\nu\mu}\,c_{i\mu} = \epsilon_i \sum_{\mu=1}^{k} S_{\nu\mu}\,c_{i\mu} \qquad i = 1,\ldots,n, \quad \nu = 1,\ldots,k, \tag{2.3.11}$$

where

$$F_{\mu\nu} = \langle\phi_\mu|\hat{\mathrm{h}} + \sum_\pi \left(\hat{\mathrm{J}}_\pi - \hat{\mathrm{K}}_\pi\right)|\phi_\nu\rangle \tag{2.3.12}$$

$$S_{\mu\nu} = \langle\phi_\mu|\phi_\nu\rangle. \tag{2.3.13}$$

The equations are solved iteratively with the aid of matrix diagonalization. Because the molecular orbitals ψ_i are in Roothaan equations approximated by a linear combination of a finite number of atomic orbitals ϕ_μ, the quality of the solution depends on the quality and the number of atomic orbitals. The problem of choice of basis set will be discussed in Sec. 2.3.7.

The Hartree-Fock approximation plays an important role in quantum chemistry. By describing the electronic wave function by a product of one-electron functions, it is possible to split the multidimensional Schrödinger equation 2.1.6 into a set of one-dimensional equations 2.3.9 and solve large many-body problems.[4] However, in this description the electrons move independently in a mean field electrostatic potential, which leads to an error in the prediction of the total molecular energy. The energy calculated by Roothaan equations in a finite basis is larger than the exact solution of Hartree-Fock equations, and the Hartree-Fock energy lies higher than the Schödinger energy. The difference between the Hartree-Fock limit and the Schödinger energy is called *correlation energy*. Although the neglect of correlation energy may lead to large deviations from experimental results, Hartree-Fock approximation serves as a starting point for more accurate methods.

2.3.2 Configuration interaction

The main deficiency of the Hartree-Fock method is the neglect of correlation between motions of electrons with different spins. A principal and conceptually simple solution to this problem is to solve the secular equation (Eq. 2.2.7) in the basis of, for example, variously configured Slater determinants, obtained by solving Roothaan's equations. The method is known as *configuration interaction* (CI). With a complete basis, the full CI method yields the exact solution. In practical applications, however, only a finite basis set can be used. A systematic approach to forming the basis set is to take the HF solution and replace a limited number of occupied spin orbitals ψ_i by virtual orbitals[5] ψ_a, to form singly, doubly, etc., excited determinants $\{\Psi_{ijk\ldots}^{abc\cdots}\}$. The number of thus created functions grows exponentially with the size of the system. Even when including only singly and doubly excited determinants, the method is impractical for all but the smallest

[4]The dominant step in Hartree-Fock calculations is the evaluation of all two-electron integrals in the basis of atomic orbitals

$$(ij \mid kl) = \sum_{\mu\nu\lambda\sigma} c_{i\mu}^* c_{j\nu}^* c_{k\lambda} c_{l\sigma} (\mu\nu \mid \lambda\sigma). \tag{2.3.14}$$

The number of the integrals grows as $O(N^4)$ with the number of atomic orbitals. Fortunately, many of the integrals are negligibly small and may be screened out by employing the Schwartz inequality. In modern quantum chemistry programs, the scaling can be reduced below $O(N^3)$ [27].

[5]For k spatial functions ϕ_μ, the eigenvalue problem 2.3.11 yields for each i a set of $2k$ orthonormal spin orbitals. The n spin orbitals with the lowest energies are called *occupied*, while the remaining $2k - n$ are called *virtual* spin orbitals.

systems.[6] Another problem of partial CI is that it is not *size consistent*, that is, a sum of energies calculated for non-interacting subsystems is not equal to the energy calculated for the whole system.

2.3.3 Coupled cluster

The size inconsistency of the CISD method is remedied by another approximate approach to full CI, called *coupled cluster* theory (CC) [28]. The exact wave function in the coupled cluster formalism is expressed in terms of the exponential operator

$$e^{\hat{\mathrm{T}}} = 1 + \hat{\mathrm{T}} + \frac{1}{2}\hat{\mathrm{T}}^2 + \frac{1}{6}\hat{\mathrm{T}}^3 + \cdots, \tag{2.3.15}$$

operating on the ground state Slater determinant. The operator $\hat{\mathrm{T}}$ is a cluster operator

$$\hat{\mathrm{T}} = \hat{\mathrm{T}}_1 + \hat{\mathrm{T}}_2 + \hat{\mathrm{T}}_3 + \cdots, \tag{2.3.16}$$

where the subscribed operators cluster linear combinations of singly, doubly, etc., excitations of the reference wave function. For instance,

$$\hat{\mathrm{T}}_1\Psi_0 = \sum_i t_i^a \Psi_i^a, \qquad \hat{\mathrm{T}}_2\Psi_0 = \sum_{\substack{i>j \\ a>b}} t_{ij}^{ab}\Psi_{ij}^{ab}, \tag{2.3.17}$$

where the expansion coefficients $t_{ij\ldots}^{ab\cdots}$ are to be determined. To better see a link, or rather a difference, between the CC and CI methods, compare the expressions for the exact CC wave function

$$\Psi_{\mathrm{CC}} = \left[1 + (\hat{\mathrm{T}}_1 + \hat{\mathrm{T}}_2 + \cdots) + \frac{1}{2}(\hat{\mathrm{T}}_1 + \hat{\mathrm{T}}_2 + \cdots)(\hat{\mathrm{T}}_1 + \hat{\mathrm{T}}_2 + \cdots) + \cdots\right]\Psi_0. \tag{2.3.18}$$

and the exact CI wave function

$$\Psi_{\mathrm{CI}} = \left[1 + \hat{\mathrm{C}}_1 + \hat{\mathrm{C}}_2 + \cdots\right]\Psi_0. \tag{2.3.19}$$

For example, the four-excitation operator $\hat{\mathrm{C}}_4$ can be decomposed into the terms

$$\hat{\mathrm{C}}_4 = \hat{\mathrm{T}}_4 + \frac{1}{2}\hat{\mathrm{T}}_2^2 + \hat{\mathrm{T}}_1\hat{\mathrm{T}}_3 + \frac{1}{2}\hat{\mathrm{T}}_1^2\hat{\mathrm{T}}_2 + \frac{1}{4!}\hat{\mathrm{T}}_1^4. \tag{2.3.20}$$

The **CCSD** method [29] truncates the operator $\hat{\mathrm{T}}$ after the second term. A rather tedious derivation of CCSD equations starts by inserting the CCSD wave function in the Schrödinger

[6] Such a calculation is referred to as singly (CIS) and doubly (CISD) excited configuration interaction. CISD scales as $O(N^6)$.

equation and projecting onto a set of functions Ψ_0, $\{\Psi_i^a\}$ and $\{\Psi_{ij}^{ab}\}$

$$\begin{aligned}\langle\Psi_0|\hat{\mathrm{H}}-E|e^{(\hat{\mathrm{T}}_1+\hat{\mathrm{T}}_2)}\,\Psi_0\rangle &= 0,\\ \langle\Psi_i^a|\hat{\mathrm{H}}-E|e^{(\hat{\mathrm{T}}_1+\hat{\mathrm{T}}_2)}\,\Psi_0\rangle &= 0,\\ \langle\Psi_{ij}^{ab}|\hat{\mathrm{H}}-E|e^{(\hat{\mathrm{T}}_1+\hat{\mathrm{T}}_2)}\,\Psi_0\rangle &= 0.\end{aligned} \tag{2.3.21}$$

Because the Hamiltonian contains at most two-electron operators, only a limited number of expansion terms are non-zero. For example, the first equation evaluates to

$$\langle\Psi_0|\hat{\mathrm{H}}-E|(1+\hat{\mathrm{T}}_1+\hat{\mathrm{T}}_2+\frac{1}{2}\hat{\mathrm{T}}_1^2)\Psi_0\rangle=0. \tag{2.3.22}$$

The energy E from the first equation is inserted into the two other equations and evaluated in terms of the coefficients t_i^a and t_{ij}^{ab} to obtain nonlinear equations, which have to be solved iteratively.

The CCSD method solves the size consistency problem of CI and effectively includes also some triple and quadruple excitation terms of the CI [29]. CCSD scales as $O(N^6)$.

2.3.4 Møller-Plesset perturbation theory

The correlation effects can be accounted for also by employing the Rayleigh-Schrödinger perturbation theory. The perturbation method where the Hartree-Fock solution appears as the zero-order approximation is known as the *Møller-Plesset perturbation theory* [30]. It is completely analogous to the vibrational perturbation theory given in Sec. 2.4.5. In this work the perturbation theory of the second order (MP2) was used. The method gives often results similar to CCSD, but scales more favorably with the size of the molecule: MP2 scales as $O(N^4)$.

2.3.5 Density functional theory

An alternative approach to the electronic problem is the *density functional theory* (DFT). In the Born-Oppenheimer approximation the electrons move in an "external" static potential of nuclei

$$\hat{\mathrm{V}}_{en}=-\frac{e^2}{4\pi\varepsilon_0}\sum_i\frac{Z_i}{|\boldsymbol{R}_i-\boldsymbol{r}|}. \tag{2.3.23}$$

The rest of the Hamiltonian

$$\hat{\mathrm{F}}=-\sum_{\alpha_i\in\boldsymbol{r}}\frac{\hbar^2}{2m_e}\frac{\partial^2}{\partial r_{\alpha_i}^2}+\frac{e^2}{4\pi\varepsilon_0}\sum_{i<j}\frac{1}{|\boldsymbol{r}_i-\boldsymbol{r}_j|} \tag{2.3.24}$$

is the same for all n-electron systems, therefore the Hamiltonian and hence the ground state $|\Psi_0\rangle$ is completely determined by the external potential $\hat{\mathrm{V}}_{en}$. The ground state wave function gives rise to the ground state *electronic density*

$$\rho_0(\boldsymbol{r})=\int|\Psi_0(\boldsymbol{r},\boldsymbol{r}_2,\ldots,\boldsymbol{r}_n)|^2\,d\boldsymbol{r}_2\ldots d\boldsymbol{r}_n. \tag{2.3.25}$$

The density functional theory is based on the concept of the electronic density as the *fundamental variable*. Formal justification for utilizing the three-dimensional function $\rho(\boldsymbol{r})$ instead of the many-dimensional wave function Ψ_0 comes from the theorems of Hohenberg and Kohn [31]. They presented an elegant proof, that the external potential $\hat{\mathrm{V}}_{en}$ (and therefore the Hamiltonian and also the ground state solution) is uniquely determined by the corresponding ground state electronic density, up to an additive constant. Consequently, the variational principle for the *energy functional*

$$E_V[\rho] = \langle \Psi_\rho | \hat{\mathrm{F}} | \Psi_\rho \rangle + \int V(\boldsymbol{r})\, \rho(\boldsymbol{r})\, d\boldsymbol{r} \tag{2.3.26}$$

can be formulated. Given any electronic density ρ' associated to a n-electron system with an external potential $\hat{\mathrm{V}}'$, the energy will be always higher than or equal to that of the ground state

$$E_V[\rho] \leq E_V[\rho']. \tag{2.3.27}$$

Thus the ground state energy may be determined by minimization with respect to the electronic density alone. The original formulation requires that the ground state is non-degenerate and that densities must be associated with some external potential. These requirements were weakened by Levy [32] in the new *constrained search* formulation, where the only requirement is that the density must be obtainable from some n-electron wave function.

Although the theorems assure the existence of the universal functional $F[\rho] = \langle \Psi_\rho | \hat{\mathrm{F}} | \Psi_\rho \rangle$, which is independent of the external potential, its exact form is not known. In the practical computational method introduced by Kohn and Sham [33], the problem of many interacting electrons is treated as the problem of non-interacting electrons, with the difference accounted for by addition of some extra terms. The electrons are described by one-dimensional functions ψ_i known as *Kohn-Sham orbitals*. The functional is formally split into three parts

$$F[\rho] = T[\rho] + \frac{1}{2} \int \frac{\rho(\boldsymbol{r})\, \rho(\boldsymbol{r}')}{|\boldsymbol{r} - \boldsymbol{r}'|}\, d\boldsymbol{r}\, d\boldsymbol{r}' + E_{xc}[\rho]. \tag{2.3.28}$$

The first term is the kinetic energy of non-interacting electron gas, the second is the classical electrostatic electron-electron interaction and the remaining term is the unknown *exchange-correlation energy*, containing non-classical electron-electron interactions and the difference between the kinetic energy of interacting and non-interacting system. The effective Kohn-Sham potential is defined

$$\hat{\mathrm{V}}_{KS} \equiv \hat{\mathrm{V}}_{en} + \int \frac{\rho(\boldsymbol{r}')}{|\boldsymbol{r} - \boldsymbol{r}'|}\, d\boldsymbol{r}' + \frac{\delta E_{xc}[\rho]}{\delta \rho} \tag{2.3.29}$$

and the *Kohn-Sham equations* are obtained by use of the variational principle

$$\left[-\frac{1}{2} \nabla_i^2 + \hat{\mathrm{V}}_{KS} \right] |\psi_i\rangle = \epsilon_i\, |\psi_i\rangle, \quad i = 1, \ldots, n. \tag{2.3.30}$$

The electronic density is determined from the Kohn-Sham orbitals by

$$\rho(\boldsymbol{r}) = 2\sum_{i=1}^{n} |\psi_i(\boldsymbol{r})|^2. \tag{2.3.31}$$

The factor of 2 is valid for systems with closed shells and comes from a double degeneracy due to the spin of electrons.

Note that HF is in a sense just a special case of DFT, with the correlation part of the energy E_c being zero and the exchange part E_x being equal to the mean value of the exchange operator $\hat{\mathrm{K}}_i$ (Eq. 2.3.7). Because the form of the exchange-correlation energy functional and its derivative is usually too complex to be integrated analytically, the exchange-correlation energy must be evaluated by numerical integration, which adds a source of numerical errors to DFT implementations, in contrast to HF.

DFT approximations

In any practical implementation, the unknown exchange-correlation energy $E_{xc}[\rho]$ must be approximated and a large number of functionals have been proposed. The construction of the functionals is not straightforward and there is no systematic way for improving them. The functionals often incorporate some empirical parameters. For instance, the exchange energy functional of Becke [34] contains one numerical parameter, which was determined by a least squares fit to exact atomic Hartree-Fock exchange energies of noble gas atoms.

The first and simplest approximation to the exchange-correlation energy is the *local density approximation* (LDA) [33]. The exchange-correlation energy is defined as a sum of local contributions $\epsilon_{xc}^{\mathrm{LDA}}$, which are set equal to that of a homogeneous electron gas

$$E_{xc}^{\mathrm{LDA}}[\rho] = \int \rho(\boldsymbol{r})\, \epsilon_{xc}^{\mathrm{LDA}}(\rho)\, d\boldsymbol{r}. \tag{2.3.32}$$

Although the approximation is simple and justified only for slow varying densities, it gives qualitatively accurate results even for systems with rapidly varying charge densities. A straightforward generalization of LDA to include electron spin is the *local spin density approximation* (LSDA), where the exchange-correlation energy per particle becomes a function of two spin densities $\epsilon_{xc}^{\mathrm{LSDA}}(\rho_\alpha, \rho_\beta)$. The local density approximations were known to overestimate bond energies. New exchange correlation functionals were devised, which depend also on density gradients and higher order density derivatives. These methods fall in the category of *generalized gradient approximation* (GGA) methods.

In this work the functionals BPW91 and B3LYP were used. The **BPW91** functional combines the exchange energy functional of Becke [34] and the correlation energy functional of Perdew and Wang [35]. The hybrid **B3LYP** functional [36] includes an empirical mixture of Hartree-Fock exchange energy with the non-local exchange-correlation energy of Lee, Yang and Parr [37].

2.3.6 Semi-empirical methods

The computational cost of quantum mechanical *ab initio* methods restricts their use only for small systems. Many molecules of interest are much larger and therefore computationally less demanding methods have been developed. In this study, the method **PM3** has been used for comparison with quantum mechanical models. It is based on the Hartree-Fock formalism described in Sec. 2.3.1, but it uses a simplified Hamiltonian, avoiding the calculation of computationally expensive two-electron integrals. To compensate for the approximations, empirical parameters are introduced.

In the PM3 method, only the valence electrons are considered. The central simplification is to not permit overlaps of atomic orbitals (ϕ_μ in Eq. 2.3.10) residing on different atomic centers. The two-electron Coulomb and exchange integrals (Eq. 2.3.14) are simplified to ignore all integrals with atomic orbitals residing on different atoms as well as all three- and four-centers integrals. The interactions with core electrons and nuclei are approximated by an average potential in which the valence electrons move.

2.3.7 Basis sets

The accuracy of electronic structure calculations is limited not only by the form of the wave function and the Hamiltonian, but also by the basis set used for the expansion of the wave function. In this section, the basis sets which were used in this study for evaluation of the nuclear potential, will be reviewed.

Any complete basis set may be used in Eq. 2.3.10. However, in practical calculations it is advantageous to use functions which resemble real atomic orbitals. For instance, the Slater type orbitals can be used for their similarity to atomic orbitals of the hydrogen atom. However, because they are not suitable for fast calculation of two-electron integrals (Eq. 2.3.5), *Gaussian type orbitals* were introduced. Atomic orbitals of this type are expressed as a linear combination of Gaussian primitives

$$\theta_{n,m,l}(\alpha, \boldsymbol{r}) = N x^n y^m z^l \, e^{-\alpha \boldsymbol{r}^2}, \tag{2.3.33}$$

where N is a normalization factor. The sum of exponents at Cartesian coordinates $L = n+m+l$ is used to mark functions as s-type (L=0), p-type (L=1), d-type (L=2), f-type (L=3), etc. The Gaussian primitives can be grouped into fixed linear combinations to form *contracted Gaussian functions*

$$\phi_\mu(\boldsymbol{r}) = \sum_p d_{p\mu} \, \theta_p(\alpha_{p\mu}, \boldsymbol{r}). \tag{2.3.34}$$

Coefficients and exponents of the Gaussian functions are chosen from a best fit to some theoretically justified function. For instance the ϕ_{1s} orbital may be chosen to be the best fit to the Slater function $e^{-\boldsymbol{r}}/\sqrt{\pi}$, which is the solution for the $1s$ orbital of the hydrogen atom. In another approach the parameters $\alpha_{p\mu}$ and $d_{p\mu}$ are varied to minimize the total energy.

Even though the contracted Gaussian functions are not optimal,[7] they permit fast calculation

[7] For example, the ϕ_{1s} function has a zero slope at zero, while Slater function has a finite slope. At large values of $\boldsymbol{r}$ the Gaussian function decays more rapidly. See Fig. 2.1.

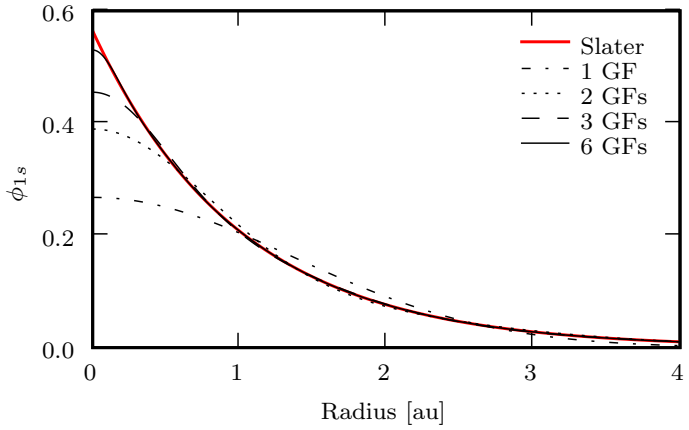

Figure 2.1: Least squares fit of variable number of Gaussian functions to the Slater 1s function. Six Gaussian functions provide enough flexibility and fit the Slater function well.

of two-electron integrals. In the simplest type of calculation, the set $\{\phi_\mu\}$ is minimal and consists of one function (1s) for hydrogen and helium, five functions (1s, 2s, 2$p_{x,y,z}$) for first row atoms Li to Ne, and so on. The minimal basis set may give qualitatively correct results of chemical bonding, but it has a limited flexibility. Extended basis sets are therefore introduced.

Split-valence basis set

The simplest basis set used in this study is the **6-31G** basis set [38]. Inner shells of heavy atoms are represented by single functions, composed of a sum of six Gaussian functions. Each valence shell is split into an inner and an outer part, expanded into three and one Gaussian functions, respectively. For instance, the valence shell of first row atoms will be described by four *sp* orbitals expanded into three Gaussian functions and four *sp* orbitals described by a single Gaussian function. The same set of exponents α may be shared in *sp* shells, which significantly speeds up calculations. If each of the minimal basis functions, not only the valence orbitals, were split into two, such a basis set is known as *double zeta*.

The 6-31G functions do not extend sufficiently far to adequately describe valence regions of oxygen and other atoms. Therefore the triple split basis set, **6-311G**, was introduced, where four additional atomic orbitals are added to the valence shell of the first row atoms [39].

Polarization functions

To create a well balanced basis set, also functions with higher angular quantum numbers must be added. A basis set with *d*-type functions added to first row atoms is usually denoted by a single star ***** or **(d)**. If in addition to that *p*-type functions are added to hydrogen, such a basis set is indicated by two stars ****** or **(d,p)**. These functions are called polarization functions, because they give electrons the potential to respond to an electric field. For instance, the spherical symmetry of the minimal 1s orbital for the hydrogen atom must be combined with a *p*-type function to enable charge redistribution in the direction of the electric field.

Diffuse functions

When the electronic density is more spread over the molecule, it is appropriate to include functions with smaller Gaussian exponents α. Diffuse functions are most important in description of anions and weakly bound complexes involving hydrogen bonding or cation-molecule interactions. A basis set with diffuse functions on heavy atoms is indicated by $+$ and a basis set with diffuse functions on heavy atoms and hydrogen is indicated by $++$. The inclusion of diffuse functions can prolong calculations significantly, but it seems to be important for evaluation of tensors responsible for Raman scattering and Raman optical activity.

Correlation consistent basis sets

Basis sets optimized for use with methods which attempt to describe correlation effects require functions with high angular momenta. For instance, the correlation consistent polarized valence triple-zeta set **cc-pVTZ** includes three s, two p and one d function for the hydrogen atom and four s, three p, two d and one f function for first row atoms [40].

2.4 Nuclear motion

The previous sections summarized the approximative methods of quantum chemistry which enable calculation of the molecular energy of a given nuclear configuration. By minimizing the energy with respect to nuclear positions, one obtains the *equilibrium geometry* of the molecule. In practical calculations, it is not easy to find such a configuration, because PES contains for larger systems a wealth of local minima. Chemical intuition and molecular dynamics simulations must be therefore often harnessed. Having found an appropriate nuclear configuration, the investigation of vibrational motions may begin.

2.4.1 Harmonic approximation

The separation of electronic and nuclear motions in Eq. 2.1.11 provided an equation which has a simple form in space-fixed Cartesian coordinates. The equation is, however, in most cases too complicated to be integrated directly. The Hamiltonian is therefore expressed in molecule-fixed coordinates, which leads to a form more complex, but containing terms with clear physical interpretation enabling meaningful simplifications [41, 42].

The new coordinate system is positioned in the nuclear center of mass and rotates with the molecule. The nuclear positions are expressed with respect to the molecule-fixed system in *normal mode coordinates* Q_i, which are defined as a linear combination of mass-weighted displacement vectors

$$\sqrt{m_j}\,(r_{\alpha_j} - r^0_{\alpha_j}) = \sum_{i=1}^{n} S_i^{\alpha_j} Q_i, \qquad j = 1, \ldots, n. \tag{2.4.1}$$

The transformation matrix $\mathbf{S}$ is determined by enforcing the (definitional) requirement that the force field matrix is diagonal in normal mode coordinates (see below). The reference nuclear configuration $\boldsymbol{r}_i^0$ is chosen to minimize the potential energy surface for a given electronic state.

Under the assumption of small amplitudes of vibrations, the nuclear potential may be expanded in power series

$$V(x_1, \ldots, z_n) = V_0 + \sum_{\alpha_i} \frac{\partial V}{\partial r_{\alpha_i}} \Delta r_{\alpha_i} + \frac{1}{2} \sum_{\alpha_i, \beta_j} \frac{\partial^2 V}{\partial r_{\alpha_i} \partial r_{\beta_j}} \Delta r_{\alpha_i} \Delta r_{\beta_j} + \cdots, \tag{2.4.2}$$

where $\Delta r_{\alpha_i} = r_{\alpha_i} - r^0_{\alpha_i}$. The term V_0 can be neglected, as it adds only a constant to the energy. Because the reference geometry $\boldsymbol{r}_i^0$ was chosen to minimize the potential, the first derivative term is also zero. Truncating the expansion after the third term, the potential can be expressed in terms of the Hessian, known also as the *force field matrix*

$$F_{\alpha_i \beta_j} = \frac{\partial^2 V}{\partial r_{\alpha_i} \partial r_{\beta_j}}. \tag{2.4.3}$$

For consequent simplification of the kinetic operator, it is convenient to introduce the diagonal

matrix of nuclear masses $\mathbf{M}$ and the mass-weighted force field matrix $\mathbf{F}'$

$$\mathbf{F}' = \mathbf{M}^{-1/2}\,\mathbf{F}\,\mathbf{M}^{-1/2}. \tag{2.4.4}$$

Since the mass-weighted force field matrix is obviously symmetric, it can be diagonalized by an orthogonal matrix, which is by definition the transformation matrix $\mathbf{S}$. In the convenient matrix notation, the potential energy can be then written as

$$\begin{aligned} 2V &= \boldsymbol{\Delta}^t\, F\, \boldsymbol{\Delta} \\ &= \boldsymbol{\Delta}^t\, \mathbf{M}^{1/2}\, \mathbf{M}^{-1/2}\, \mathbf{F}\, \mathbf{M}^{-1/2}\, \mathbf{M}^{1/2}\, \boldsymbol{\Delta} \\ &= \boldsymbol{Q}^t\, \mathbf{S}^t\, \mathbf{F}'\, \mathbf{S}\, \boldsymbol{Q} \\ &= \sum_i \frac{\partial^2 V}{\partial Q_i^2}\, Q_i^2, \end{aligned} \tag{2.4.5}$$

where $\boldsymbol{\Delta}$ is the vector of the displacements Δr_{α_i} and a matrix transpose is denoted by the superscript t.

It can be shown from the invariance of V that for nonlinear molecules, six from the total of $3n$ eigenvalues $V_{ii} = \partial^2 V/\partial Q_i^2$ will come out zero, or, due to errors in electronic calculations, close to zero. These modes correspond to translational and rotational movement. There are $3n$ variables in the space-fixed coordinate system, but only $m = 3n - 6$ degrees of freedom in the molecule-fixed system of normal mode coordinates.[8]

While the potential energy operator was significantly simplified, the kinetic operator is complicated by the rotating coordinate system. The vibration-rotation kinetic operator in normal mode coordinates derived by Watson [43] is given by

$$\hat{\mathrm{T}} = \frac{1}{2}\sum_{\alpha,\beta}(\hat{\mathrm{J}}_\alpha - \hat{\pi}_\alpha)\mu_{\alpha\beta}(\hat{\mathrm{J}}_\beta - \hat{\pi}_\beta) - \frac{\hbar^2}{8}\sum_\alpha \mu_{\alpha\alpha} - \frac{\hbar^2}{2}\sum_i \frac{\partial^2}{\partial Q_i^2}, \tag{2.4.6}$$

where $\hat{\mathrm{J}}$ is the total angular momentum operator, $\hat{\pi}$ is the vibrational angular momentum operator and $\mu_{\alpha\beta}$ is inverse of the moment of inertia tensor. It is common to neglect the vibrational angular momentum. The Hamiltonian for a non-rotating molecule is then in the *harmonic approximation* given by

$$\hat{\mathrm{H}} = -\frac{\hbar^2}{2}\sum_i \frac{\partial^2}{\partial Q_i^2} + \frac{1}{2}\sum_i \frac{\partial^2 V}{\partial Q_i^2} Q_i^2. \tag{2.4.7}$$

Thus, vibrational motions have been separated from rotations. Moreover, because of the neglect of higher-order terms in the potential in Eq. 2.4.2, the Hamiltonian does not contain any coupling between normal mode coordinates. The harmonic approximation thus enables splitting of the

[8] For linear molecules $m = 3n - 5$.

m-dimensional vibrational Schrödinger equation into a set of m one-dimensional problems

$$\left[-\frac{\hbar^2}{2}\frac{\partial^2}{\partial Q_i^2}+\frac{1}{2}\frac{\partial^2 V}{\partial Q_i^2}Q_i^2\right]\psi_i(Q_i)=\epsilon_i\,\psi_i(Q_i),\qquad i=1,\ldots,m, \tag{2.4.8}$$

with

$$\Psi_n(Q_1,\ldots,Q_m)=\prod_i \psi_i(Q_i). \tag{2.4.9}$$

The equations are known from the theory of the linear harmonic oscillator and have an analytic solution. The complicated vibrational motion of a molecule can be looked at as a superposition of independent vibrations of linear harmonic oscillators. Perhaps surprisingly, the model of atoms connected to equilibrium positions by tiny springs describes the molecular vibrations rather well. The properties of linear harmonic oscillators will be discussed in more detail in the next section.

2.4.2 Linear harmonic oscillator

The problem of the linear harmonic oscillator (LHO) is given by the equation

$$\left[-\frac{\hbar^2}{2m}\frac{\partial^2}{\partial x^2}+\frac{1}{2}m\omega^2x^2\right]\psi(x)=E\,\psi(x), \tag{2.4.10}$$

where m is the mass of the oscillating particle and ω is the characteristic frequency of the oscillation. The problem has well known solutions. The eigenvalues take discrete, equidistantly spaced values

$$E_n=(n+\frac{1}{2})\,\hbar\omega,\qquad n=0,1,\ldots \tag{2.4.11}$$

and the corresponding eigenstates are

$$\psi_n(x)=\sqrt[4]{\frac{m\omega}{\pi\hbar}}\frac{1}{\sqrt{2^n\,n!}}\,e^{-\xi^2/2}\,H_n(\xi),\qquad \xi=\sqrt{\frac{m\omega}{\hbar}}x, \tag{2.4.12}$$

where H_n are the *Hermite polynomials*

$$H_n(\xi)=(-1)^n\,e^{\xi^2}\,\frac{d^n}{d\xi^n}e^{-\xi^2}. \tag{2.4.13}$$

The first five Hermite polynomials are

$$\begin{aligned}
H_0(\xi) &= 1,\\
H_1(\xi) &= 2\xi,\\
H_2(\xi) &= 4\xi^2-2,\\
H_3(\xi) &= 8\xi^3-12\xi,\\
H_4(\xi) &= 16\xi^4-48\xi^2+12
\end{aligned}$$

and the corresponding harmonic oscillator wave functions ψ_n are plotted in Fig. 2.2. Because the

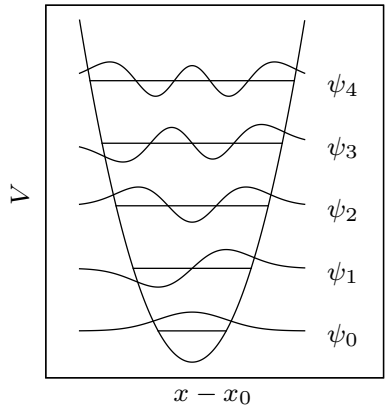

Figure 2.2: Wave functions of the linear harmonic oscillator for $n = 0, \ldots, 4$.

Hermite polynomials are orthogonal, important overlap properties of linear harmonic oscillator wave functions may be formulated, which give rise to many useful approximations and enable derivation of selection rules for spectroscopic transitions. For instance, the following identity can be derived

$$\langle \psi_n | x | \psi_k \rangle = \begin{cases} \sqrt{\frac{\hbar}{m\omega}} \sqrt{\frac{n+1}{2}} & \text{if } k = n+1, \\ \sqrt{\frac{\hbar}{m\omega}} \sqrt{\frac{n}{2}} & \text{if } k = n-1, \\ 0 & \text{otherwise} \end{cases} \tag{2.4.14}$$

and it will be used several times in Sec. 2.5 to show that a transition between two vibrational states cannot occur if their quantum numbers n do not differ by a prescribed value. This and similar identities also enable fast evaluation of multi-dimensional integrals of wave functions expanded in the basis of LHO.

2.4.3 Anharmonic potential

Despite its simplicity, the harmonic approximation gives surprisingly accurate results for energies well below the dissociation limit when the potential is expressible as a second-order polynomial. Obviously, it must fail for strongly anharmonic potentials and for highly excited vibrational states. The mathematical form of the second-order polynomial does not allow for bond breaking – when the distance between two nuclei increases, the energy would grow to infinity, instead of approaching a constant value of the bond dissociation limit. This behavior is demonstrated in Fig. 2.3 showing the plot of a scan along the symmetric C−H stretching vibration mode of formaldehyde calculated at the CCSD/cc-pVTZ level (Fig. 2.4), and the harmonic approximation of the potential. Another problem of the harmonic approximation is that it assumes that the vibrational modes are independent, i.e. can be described by independent one-dimensional Schrödinger equations. While it is sometimes reasonable to assume that the modes oscillate independently in the anharmonic potential, in other cases they are strongly correlated [44].

The most obvious way to extend the harmonic approximation is to include the higher-order terms of the Taylor expansion 2.4.2 into the Hamiltonian. The vibrational Schrödinger equation

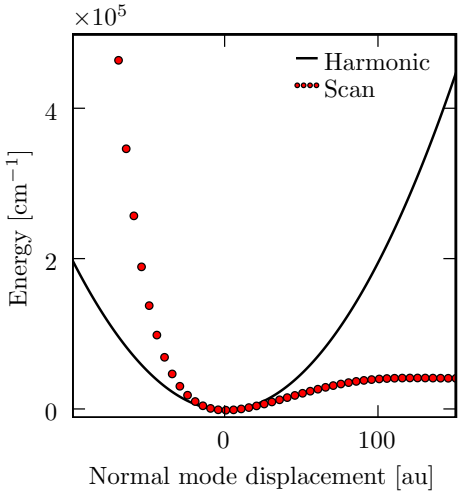

Figure 2.3: Comparison of exact (CCSD/cc-pVTZ scan) and harmonic potential of the symmetric C−H stretching vibration of formaldehyde.

is then no longer separable into a set of independent equations and the problem must be treated in its full dimensionality. Basically, all methods developed for improvement of HF described in Sec. 2.3 are in some form applicable also to the problem of molecular vibrations, as will be shown in the following sections.

Evaluation of the anharmonic potential is computationally a demanding task. In this work an approximate potential was obtained by numerical differentiation of second-order energy derivatives calculated at geometries displaced from an equilibrium geometry along nuclear coordinates. By performing $6n+1$ calculations in Cartesian coordinates (or $2m+1$ calculations for displacements along normal modes), cubic and semidiagonal quartic force field constants can be obtained. Using the shorthand notation for the force field derivatives

$$\begin{aligned} V^0_{\alpha_i\beta_j} &= \left.\frac{\partial^2 V(x_1,\ldots,z_n)}{\partial r_{\alpha_i}\partial r_{\beta_j}}\right|_{(x_1^0,y_1^0,\ldots,z_n^0)} \\ V^{\gamma_k+\Delta}_{\alpha_i\beta_j} &= \left.\frac{\partial^2 V(x_1,\ldots,z_n)}{\partial r_{\alpha_i}\partial r_{\beta_j}}\right|_{(x_1^0,\ldots,r^0_{\gamma_k}+\Delta,\ldots,z_n^0)}, \end{aligned}$$

the cubic constants were obtained from the formula

$$V^0_{\alpha_i\beta_j\gamma_k} = \frac{1}{2\Delta}(V^{\gamma_k+\Delta}_{\alpha_i\beta_j} - V^{\gamma_k-\Delta}_{\alpha_i\beta_j}). \tag{2.4.15}$$

The quartic constants were evaluated as

$$V^0_{\alpha_i\beta_j\gamma_k\gamma_k} = \frac{1}{\Delta^2}(V^{\gamma_k+\Delta}_{\alpha_i\beta_j} + V^{\gamma_k-\Delta}_{\alpha_i\beta_j} - 2V^0_{\alpha_i\beta_j}). \tag{2.4.16}$$

Note that only quartic constants with at most three indices different may be obtained from the $6n+1$ geometries. These constants will be referred to as *semidiagonal quartic constants*.[9]

[9]The precision of constants obtained by numerical differentiation is limited. As shown in Appendix A.4, the errors can be quite large.

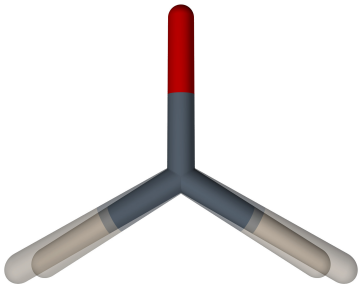

Figure 2.4: The symmetric C–H stretching vibration in formaldehyde.

Potential derivatives with respect to the normal mode coordinates are obtained from Cartesian derivatives by linear transformation. For example, the cubic terms are calculated by the formula

$$V_{ijk} = \frac{\partial V^3}{\partial Q_i \partial Q_j \partial Q_k} = \sum_{\alpha_l,\beta_m,\gamma_n} \frac{S_i^{\alpha_l}}{\sqrt{m_l}} \frac{S_j^{\alpha_m}}{\sqrt{m_m}} \frac{S_k^{\alpha_n}}{\sqrt{m_n}} V_{\alpha_l \beta_m \gamma_n}, \tag{2.4.17}$$

where $\mathbf{S}$ is the transformation matrix (Eq. 2.4.1 and Eq. 2.4.5) and m_i are the nuclear masses. It should be noted that even though the semidiagonal quartic Cartesian derivatives may be used for generating quartic normal-mode derivatives with all indices different, the normal-mode anharmonic potential used in this work was also only semidiagonal, that is, the potential of the form

$$V = \frac{1}{2}\sum_i V_{ii}\, Q_i^2 + \frac{1}{6}\sum_{i,j,k} V_{ijk}\, Q_i Q_j Q_k + \frac{1}{24}\sum_{i,j,k} V_{ijkk}\, Q_i Q_j Q_k^2 \tag{2.4.18}$$

was used. The quartic semidiagonal potential is indeed a more appropriate description of the nuclear potential, as can be seen for example in Fig. 2.5.

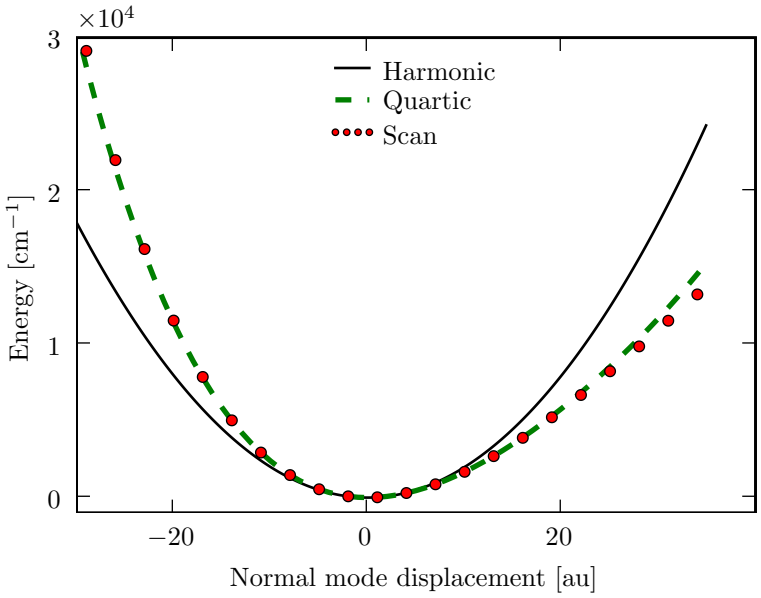

Figure 2.5: Comparison of exact (CCSD/cc-pVTZ scan), semidiagonal quartic and harmonic potential of the symmetric C–H stretching vibration in formaldehyde.

2.4.4 Vibrational self-consistent field

With the introduction of the anharmonic terms into the potential (Eq. 2.4.18), the vibrational Schrödinger equation is no longer separable into independent one-dimensional problems. The VSCF method [18] retains the low dimensionality of the harmonic approximation at the cost of neglect of coupling between vibrational modes. The method approximates the exact potential by an effective mean-field potential, a treatment conceptually identical to the HF method.

The VSCF method assumes that the vibrational wave function can be represented by a product function

$$\Psi^{\mathrm{VSCF}}(Q_1,\ldots,Q_m) = \prod_i \varphi_i(Q_i). \tag{2.4.19}$$

It is reasonable to use normal coordinates in VSCF, where separability is used only as an approximation, because in the limit of negligible coupling the use of normal coordinates will give an exact solution. Application of the variational principle for the function $\varphi_i(Q_i)$ leads to the set of equations

$$\left[-\frac{\hbar^2}{2}\frac{\partial^2}{\partial Q_i^2} + \hat{\mathrm{V}}_i^{\boldsymbol{\mu}}(Q_i)\right]\varphi_i^{\mu}(Q_i) = \epsilon_i^{\mu}\,\varphi_i^{\mu}(Q_i), \qquad i = 1,\ldots,m. \tag{2.4.20}$$

The subscripts i go over all one-mode functions and the superscripts indicate μ-th solution of the equation, so that $\mu = 0$, for example, is the ground state solution. The effective one-mode potentials are defined by

$$\hat{\mathrm{V}}_i^{\boldsymbol{\mu}}(Q_i) = \langle\prod_{j\neq i}\varphi_j^{\mu_j}(Q_j)|\hat{\mathrm{V}}(Q_1,\ldots,Q_m)|\prod_{j\neq i}\varphi_j^{\mu_j}(Q_j)\rangle \tag{2.4.21}$$

and the total VSCF energy is

$$E^{\mathrm{VSCF}} = \langle\prod_i\varphi_i|\hat{\mathrm{T}}+\hat{\mathrm{V}}|\prod_i\varphi_i\rangle = \sum_i\epsilon_i - (n-1)\langle\prod_i\varphi_i|\hat{\mathrm{V}}|\prod_i\varphi_i\rangle. \tag{2.4.22}$$

Because the potentials $V_i^{\boldsymbol{\mu}}$ in Eq. 2.4.20 depend on the unknown solutions which are to be determined, the equations are solved iteratively. First, trial wave functions φ_i are used for evaluation of the averaged potential. The new set of wave functions obtained by solving the equations is then used for evaluation of a new effective potential. The procedure is repeated until self-consistency is reached, that is, until the eigenvalues ϵ_i do not change significantly.

Note that both the ground and excited states may be obtained by inserting φ_i^{μ} into Eq. 2.4.21 with either $\mu = 0$ or $\mu \neq 0$. The notation used for the one-mode functions φ_i is therefore somewhat ambiguous. An excited VSCF function will be a product of variously excited one-mode functions, each of them depending on the excitation of others. Therefore, to explicitly refer to the μ-th solution of Eq. 2.4.20 with the effective potential

$$\hat{\mathrm{V}}_i^{\nu_1,\ldots,\nu_m} = \langle\prod_{j\neq i}\varphi_j^{\nu_j}|\hat{\mathrm{V}}|\prod_{j\neq i}\varphi_j^{\nu_j}\rangle,$$

the following notation will be used

$$\varphi_i^{\mu;\,\nu_1,\ldots,\nu_m}$$

and for the total wave function

$$\Psi_{\boldsymbol{\mu};\boldsymbol{\nu}} = \prod_i \varphi_i^{\mu_i;\,\nu_1,\ldots,\nu_m}.$$

This topic was brought to attention to emphasize the fact that although the VSCF method yields self-consistent excited states $\Psi_{\boldsymbol{\nu};\boldsymbol{\nu}}$, they are generally not orthogonal to each other. If orthogonal states are needed, excited functions $\Psi_{\boldsymbol{\mu};\boldsymbol{\nu}}$ may be used. However, they are not self-consistent. In this work, two variants of VSCF are distinguished. The standard self-consistent excited states $\Psi_{\boldsymbol{\nu};\boldsymbol{\nu}}$ are referred to as to **eVSCF**. The orthogonal excited states $\Psi_{\boldsymbol{\nu};\mathbf{0}}$ will be referred to as to **gVSCF**. Whilst in eVSCF the iterative VSCF algorithm is run for each excited state, in gVSCF the iterative procedure is run only once for the ground state.

Fig. 2.6 depicts an example of the effective VSCF potential, the ground state and first excited solution with energy levels, calculated in the harmonic and VSCF approximations. The asymptotic behavior of the VSCF potential is correct (the small embedded graph) and also low-energy states are better described by VSCF than by the harmonic approximation.

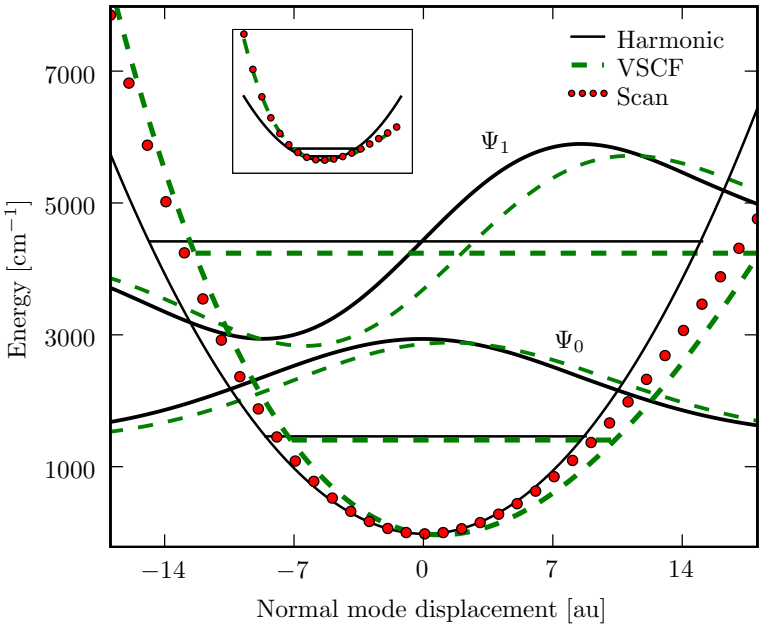

Figure 2.6: Potential of the symmetric C−H stretching vibration in formaldehyde. The black solid line is the harmonic potential with two lowest eigenstates and eigenvalues. The green dashed line is the effective VSCF potential represented by a polynomial of 4-th order and the red dots are results of a scan along the normal mode. The calculations were performed at the CCSD/cc-pVTZ level.

2.4.5 Vibrational perturbation theory

Another approach to account for the anharmonic potential and coupling effects is the perturbation theory developed in Sec. 2.2.2, page 15. Depending on the amount of anharmonicity of the system, either the harmonic approximation or VSCF may be used as starting points for the

perturbation theory. When the potential is only weakly anharmonic, the perturbation operator

$$\hat{\mathrm{W}}^{\mathrm{Harm}} = \frac{1}{6}\sum_{i,j,k} V_{ijk}\, Q_i Q_j Q_k + \frac{1}{24}\sum_{i,j,k} V_{ijkk}\, Q_i Q_j Q_k^2. \tag{2.4.23}$$

is used to correct the harmonic Hamiltonian (Eq. 2.4.7) [20, 21]. In this work, second order perturbation theory was used, and it will be denoted as PT2/Harm.

For larger anharmonicities, it is advantageous to start with VSCF solutions, which are closer to the exact solution, and to use the perturbation operator [22]

$$\hat{\mathrm{W}}^{\mathrm{VSCF}} = \hat{\mathrm{V}}(Q_1, \ldots, Q_m) - \sum_i \hat{\mathrm{V}}_i(Q_i). \tag{2.4.24}$$

The second order perturbation theory used to correct VSCF solutions will be denoted as PT2/VSCF.[10] Note that VSCF solutions are correct within first-order perturbation theory.

A comment should be made about the basis set of unperturbed VSCF solutions. The expansion functions in Eq. 2.2.11 are eigenstates of the unperturbed Hamiltonian and therefore they are orthogonal. Using the notation introduced in the previous section, the index i in the perturbation formula 2.2.14 must be replaced by $\nu_1, \ldots, \nu_m$ and the summation must go over all possible excitation combinations $\mu_1, \ldots, \mu_m$ to yield the second-order perturbation formula for eVSCF

$$E^{(2)}_{\boldsymbol{\nu};\boldsymbol{\nu}} = \sum_{\boldsymbol{\mu}} \frac{|\langle \Psi_{\boldsymbol{\nu};\boldsymbol{\nu}} | \hat{\mathrm{W}} | \Psi_{\boldsymbol{\mu};\boldsymbol{\nu}} \rangle|^2}{E^{(0)}_{\boldsymbol{\nu};\boldsymbol{\nu}} - E^{(0)}_{\boldsymbol{\mu};\boldsymbol{\nu}}}. \tag{2.4.25}$$

Similarly, the PT/gVSCF variant is given by

$$E^{(2)}_{\boldsymbol{\nu};\mathbf{0}} = \sum_{\boldsymbol{\mu}} \frac{|\langle \Psi_{\boldsymbol{\nu};\mathbf{0}} | \hat{\mathrm{W}} | \Psi_{\boldsymbol{\mu};\mathbf{0}} \rangle|^2}{E^{(0)}_{\boldsymbol{\nu};\mathbf{0}} - E^{(0)}_{\boldsymbol{\mu};\mathbf{0}}}. \tag{2.4.26}$$

2.4.6 Vibrational configuration interaction

The most general approach to the anharmonic problem is to look for a solution in the form of linear combination of some basis functions and determine the solution by use of the variational principle. It is convenient to use LHO or VSCF product functions as the expansion basis set [20, 46]. For example, the VSCF basis set is generated in a direct analogy to the electronic CI method from the ground state $\Psi_{\mathbf{0};\mathbf{0}}(Q_1, \ldots, Q_m)$ by replacing a limited number of one-mode functions $\varphi_i^{0;\mathbf{0}}(Q_i)$ by excited solutions $\varphi_i^{\mu_i;\mathbf{0}}(Q_i)$. The LHO basis set can be formed analogously.

Because the number of states thus created grows very fast with the number of vibrational modes, it is necessary to formulate a criterion for selection of functions into the basis set. First, the number of total excitations in a basis function $\Psi_{\boldsymbol{\mu};\mathbf{0}}$ must not exceed a prescribed value

[10] The method is in literature known also as the correlation-corrected VSCF (CC-VSCF) [45]. However, as pointed out already by Christiansen [23], this nomenclature is rather unfortunate, because it conflicts with abbreviations widely used for electronic structure methods. The CC abbreviation is recognized as abbreviation for coupled cluster theory.

n_{exc}, that is $\sum_i \mu_i \leq n_{\text{exc}}$. Second, only a certain number of states $\Psi_{\boldsymbol{\mu}}$ with largest ratios

$$\eta = \left| \frac{\langle \Psi_{\boldsymbol{\nu}} | \hat{\mathrm{W}} | \Psi_{\boldsymbol{\mu}} \rangle}{E_{\mathbf{0}}^{(0)} - E_{\boldsymbol{\mu}}^{(0)}} \right| \tag{2.4.27}$$

is included, where functions $\Psi_{\boldsymbol{\nu}}$ are constrained by the condition $\sum_i \nu_i \leq 1$, that is, $\Psi_{\boldsymbol{\nu}}$ is either the ground state or some of the singly excited states.

In this work, the basis of LHOs was used.

2.5 Molecules in radiation fields

2.5.1 Electromagnetic radiation

So far, stationary vibrational states of molecular nuclei have been discussed. Transitions between the states can be mediated through *electromagnetic radiation*, usually represented by a self-propagating planar wave with electric and magnetic field components oscillating at right angles to each other and to the direction of the propagation. The non-quantized electromagnetic radiation can be expressed in terms of the scalar potential $\varphi(\boldsymbol{r}, t)$ and the vector potential $\boldsymbol{A}(\boldsymbol{r}, t)$, which are related to the electric field $\boldsymbol{E}$ and the magnetic field $\boldsymbol{B}$ by

$$\begin{aligned} \boldsymbol{E} &= -\nabla\varphi - \frac{\partial \boldsymbol{A}}{\partial t}, \\ \boldsymbol{B} &= \nabla \times \boldsymbol{A}. \end{aligned} \tag{2.5.1}$$

The definition of the potentials is not unique, but depends on the gauge transformation, which may change the potentials, but preserves the electric and magnetic field vectors. For instance, using the gauge $\nabla \cdot \boldsymbol{A} = 0$ and $\varphi = 0$, the wave equations for the electromagnetic field in a vacuum may be obtained

$$\Delta \boldsymbol{A} - \varepsilon_0 \mu_0 \frac{\partial^2 \boldsymbol{A}}{\partial t^2} = \boldsymbol{0}. \tag{2.5.2}$$

ε_0 is the permittivity and μ_0 the permeability of the vacuum. The radiation vector potential is then given by

$$\boldsymbol{A}(\boldsymbol{r}, t) = \boldsymbol{A}_0 \cos(\omega t + \boldsymbol{k} \cdot \boldsymbol{r}), \tag{2.5.3}$$

where $\boldsymbol{k}$ is the wave vector in the direction of propagation.

An important concept in spectroscopy is the *polarization* of light. In a *linearly polarized* light beam, the tip of the electric field vector in a fixed plane perpendicular to the direction of propagation traces out a line with time. Linearly polarized light can be regarded as a superposition of coherent left and right *circularly polarized* light beams of equal amplitude. In a circularly polarized light beam, the tip of the electric field vector traces out a circle. Circularly polarized light is said to be right handed or left handed depending on whether the electric field vector rotates clockwise or anticlockwise, respectively, when viewed by an observer looking towards the source of light.

2.5.2 Optical activity

A structure is called optically active, if it responds differently to right and left circularly polarized light. In the phenomenon of *optical rotation*, the circularly polarized components propagate through a chiral sample with **different velocities**, which introduces a phase difference, causing a change of the orientation of the plane of polarization. A **difference in absorption** of the two circular components results in ellipticity of the initially linearly polarized light beam. The ellipticity depends on the difference of absorption indices for left and right circularly polarized light, the *circular dichroism* of the medium. In optically active molecular or crystal structures

one can also observe **difference in scattering**, for example, the Rayleigh or Raman scattering.

Optical activity is a property of crystal structures or individual molecules with sufficiently low symmetry so that the system is not superposable on its mirror image. A molecule without symmetry plane or a center of inversion is known as *chiral*. Optical activity may be associated with electronic, vibrational or rotational transitions.

2.5.3 Absorption

A system of particles with charges q_i and masses m_i in an electromagnetic field is described by the Hamiltonian

$$\hat{\mathrm{H}} = \sum_i \frac{(\boldsymbol{p}_i - q_i\boldsymbol{A})^2}{2m_i} + \hat{\mathrm{V}} = \sum_i \frac{\boldsymbol{p}_i^2 - q_i\,\boldsymbol{p}_i\boldsymbol{A} - q_i\boldsymbol{A}\,\boldsymbol{p}_i + q_i\boldsymbol{A}^2}{2m_i} + \hat{\mathrm{V}}. \tag{2.5.4}$$

Realizing that the operators $\boldsymbol{p}$ and $\boldsymbol{A}$ commute, and neglecting the second-order term $\boldsymbol{A}^2$, the term linear in $\boldsymbol{A}$ can be regarded as a time-dependent harmonic perturbation. The results of Sec. 2.2.2 may be then applied to the perturbed Hamiltonian

$$\hat{\mathrm{H}} = \hat{\mathrm{H}}_0 - \sum_i \frac{q_i}{m_i}\boldsymbol{A}\cdot\boldsymbol{p}_i. \tag{2.5.5}$$

The probability amplitude of the transition from a state ψ_j to a state ψ_k at time t was shown to be proportional to

$$f(\Delta\omega) = \frac{4\sin^2\Delta\omega t/2}{\Delta\omega^2}, \qquad \Delta\omega = \omega_{jk} - \omega. \tag{2.5.6}$$

As illustrated in Fig. 2.7, the function has large values only for the limited frequency range $|\Delta\omega| < 2\pi/t$. The transition can therefore occur only if the frequency ω of the light impinging on the molecule is very close to the frequency ω_{jk}. For example, for the value $t = 10\mu$s, the interval $(-\frac{2\pi}{t}, \frac{2\pi}{t})$ is smaller than 1.3 MHz. The laser light is not perfectly monochromatic, but has a finite line width. Having a laser with a very narrow line width of 3 MHz (0.000 1 cm^{-1}),

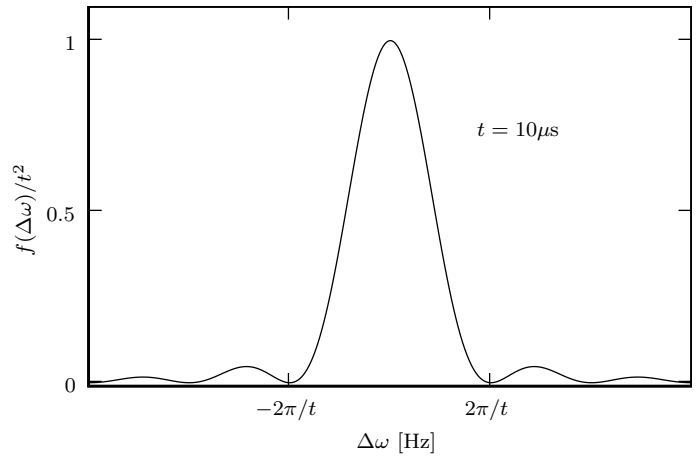

Figure 2.7: Probability amplitude of absorption as a function of frequency of incident light.

the frequency fluctuations of the incident light will greatly exceed the frequency range of the transition's maximal likelihood. Thus in experiments taking longer than, for example, 10μs, the function can be regarded as a δ function centered at ω_{jk}. Because the integral of $f(\Delta\omega)$ evaluates to $\pi\, t/2$, the function can be written in the form

$$f(\Delta\omega) = \delta(\Delta\omega)\, 2\pi t. \tag{2.5.7}$$

Another simplification can be introduced for molecules much smaller than the wavelength of the incident light. For instance, light of the argon-ion laser has wavelength 514.5 nm, dimension of a small dipeptide is 1 nm and a typical length of the C−H bond is 0.1 nm. The magnitude of the vector potential can be therefore regarded as having a constant value over the spatial extent of the vibrational motion. Expanding the coordinate-dependent part of the vector potential $\boldsymbol{A}_0(\boldsymbol{r})$ in a power series around the molecular center of mass

$$\boldsymbol{A}_0(\boldsymbol{r}) = \boldsymbol{A}_0\, e^{i\boldsymbol{k}\cdot\boldsymbol{r}} = \boldsymbol{A}_0(1 + i\boldsymbol{k}\cdot\boldsymbol{r} + \cdots), \tag{2.5.8}$$

only the first term $\boldsymbol{A}_0(\boldsymbol{r}) \simeq \boldsymbol{A}_0$ can be taken in the first approximation. The assumption of large wavelengths leads to a simplified expression for probability amplitudes of transitions, known as the *dipole approximation*: When the potential in $\hat{\mathrm{H}}_0$ in Eq. 2.5.5 commutes with the coordinate, it can be easily shown that the following relation is valid

$$\langle\psi_k|\boldsymbol{p}|\psi_j\rangle = -\frac{im}{\hbar}\,\langle\psi_k|\boldsymbol{r}|\psi_j\rangle\,(E_j - E_k). \tag{2.5.9}$$

The overlap W_{kj} from Eq. 2.2.26 can be then written as

$$\langle\psi_k|\hat{\mathrm{W}}|\psi_j\rangle = -\sum_i \frac{q_i}{m_i}\boldsymbol{A}_0\cdot\langle\psi_k|\boldsymbol{p}_i|\psi_j\rangle = -i\omega_{jk}\,\boldsymbol{A}_0\cdot\sum_i q_i\langle\psi_k|\boldsymbol{r}_i|\psi_j\rangle. \tag{2.5.10}$$

Introducing the *electric dipole moment*

$$\boldsymbol{\mu} = \sum_i q_i\,\boldsymbol{r}_i, \tag{2.5.11}$$

the probability amplitude of the transition from the state ψ_j to the state ψ_k can be written as[11]

$$\frac{d|c_k|^2}{dt} = \frac{2\pi|\boldsymbol{A}_0|^2\,\omega_{jk}^2}{3\hbar^2}\,|\langle\psi_k|\boldsymbol{\mu}|\psi_j\rangle|^2\,\delta(\omega_{jk} - \omega). \tag{2.5.12}$$

Thus a molecule in the presence of a radiation field may undergo a transition to an excited state, if the frequency of the radiation matches the energy difference between the states. The probability of the transition, and hence the observed absorption intensity, depends on the value of the *dipole strength* D

$$D(j \to k) = \boldsymbol{\mu}^{jk}\cdot\boldsymbol{\mu}^{kj} = \langle\psi_j|\boldsymbol{\mu}|\psi_k\rangle\cdot\langle\psi_k|\boldsymbol{\mu}|\psi_j\rangle. \tag{2.5.13}$$

[11] The factor of three in the denominator comes from averaging for isotropic samples.

Because no assumption was made about the wave functions ψ, the result is valid for the overall wave functions including the electronic, vibrational and spin part. Important relations, such as Franck and Condon principle [47,48] may be derived. However, in this text we are interested in transitions between vibrational states with an unchanged electronic state (usually the ground state).

Absorption observables

The connection between the theory of absorption and experiment is the Lambert-Beer law

$$A = \log_{10} I_0/I = \varepsilon\, c\, L, \tag{2.5.14}$$

which relates the absorbance A to the molecular property of molar extinction coefficient ε and to the experimental conditions, the concentration c, and the path length L of the light through the sample. The molar extinction coefficient ε is usually expressed in $\mathrm{L\,mol^{-1}\,cm^{-1}}$.

Integrated contributions of a molecular transition $\Psi^j \rightarrow \Psi^k$ to ε are proportional to the dipole strength of the transition $D(j \rightarrow k)$.

Selection rules

Because of the separability of the total wave function into the electronic and the nuclear part (Eq. 2.1.8), the *transition dipole moment* $\boldsymbol{\mu}^{kj}$ between the states Ψ^k and Ψ^j may be written as

$$\boldsymbol{\mu}^{kj} = \langle \Psi_n^k(\boldsymbol{R}) | \boldsymbol{\mu}_e^{kj}(\boldsymbol{R}) | \Psi_n^j(\boldsymbol{R}) \rangle, \tag{2.5.15}$$

where

$$\boldsymbol{\mu}_e^{kj}(\boldsymbol{R}) = \langle \Psi_e^k(\boldsymbol{r};\boldsymbol{R}) | e \sum_{i,\alpha} Z_i R_{i\alpha} - e \sum_{i,\alpha} r_{i\alpha} | \Psi_e^j(\boldsymbol{r};\boldsymbol{R}) \rangle. \tag{2.5.16}$$

When the electronic part of the transition dipole moment is expressed in normal coordinates and expanded in Taylor series

$$\boldsymbol{\mu}_e(Q_1,\ldots,Q_m) = \boldsymbol{\mu}_e(\mathbf{0}) + \sum_i \frac{\partial \boldsymbol{\mu}_e}{\partial Q_i} Q_i + \frac{1}{2} \sum_{i,j} \frac{\partial^2 \boldsymbol{\mu}_e}{\partial Q_i \partial Q_j} Q_i Q_j + \cdots, \tag{2.5.17}$$

the overlap properties of LHO wave functions (Eq. 2.4.14) cause only the terms linear in Q_i to evaluate to non-zero in Eq. 2.5.15. Thus in the harmonic approximation, only transitions between vibrational states $\Psi^j \rightarrow \Psi^k$ for which $k = j \pm 1$ are permitted. Moreover, only transitions of those modes are allowed which change the magnitude of the electric dipole moment in the course of the vibration. Closer inspection of the wave functions and the transition dipole moment operator leads to symmetry-based selection rules for molecules with high symmetry. For example, for molecules with a center of inversion, bands that are active in IR spectra are not active in Raman spectra, and *vice versa*. For general systems no such rule can be applied, but the value of the transition dipole moment can be evaluated numerically.

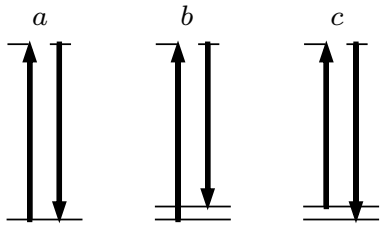

Figure 2.8: Energy-level diagram illustrating Rayleigh (a), Stokes (b) and anti-Stokes (c) Raman scattering.

The tensor of first order derivatives of the electronic part of the transition dipole moment with respect to nuclear positions is called *atomic polar tensor* (APT). For anharmonic vibrational wave functions, also higher-order terms of the Taylor expansion Eq. 2.5.17 may evaluate to non-zero.

2.5.4 Raman scattering

In absorption spectroscopy, a beam of light is passed through a sample and its attenuation is monitored as a function of wavelength, that is, weakening of photon flow with frequencies already present in the incident light is detected. On the other hand, in Raman spectroscopy the sample is illuminated by monochromatic light and the intensity of photon flow with frequencies originally absent from incident light is monitored.

Raman scattering is a two-photon process, where the impinging photon is annihilated and a new photon is scattered. Most of the light is scattered elastically with unchanged frequency, when the initial and the final states have the same energy (*Rayleigh scattering*, Fig. 2.8*a*). A small fraction of photons may end up in a state with higher (2.8*b*) or lower (2.8*c*) energy. In the case *b*, the scattered light has lower frequency and is known as *Stokes scattering*. It is a distinct phenomenon from fluorescence, because Raman scattering is observed for any frequency of the incident light, not only for a particular resonant frequency. The process depicted in Fig. 2.8*c* is *anti-Stokes scattering*, which yields photons with higher frequency than the frequency of the incident light. It occurs much less frequently, because higher-energy levels are less populated, as dictated by Boltzmann's law. Raman spectra are usually recorded in the visible or near-UV region of the electromagnetic radiation, but are plotted as differences from the wavelength of incident light. The frequency differences correspond to frequencies measured by IR spectroscopy. Clearly, for any Stokes transition there is a corresponding anti-Stokes transition with the same frequency difference from the central peak of the elastic Rayleigh scattering.

Classical description

In a classical treatment, scattered light is generated by oscillations of electric and magnetic multipoles which are induced in a molecule by the incident light wave. The most significant contribution to light scattering comes from the induced electric dipole moment

$$\boldsymbol{\mu}^{\mathrm{ind}} = \boldsymbol{\alpha} \cdot \boldsymbol{E}, \tag{2.5.18}$$

where $\boldsymbol{\alpha}$ is the *electric dipole-electric dipole polarizability tensor* and $\boldsymbol{E}$ is the electric field vector. An oscillating electric field will result in an oscillating induced dipole moment, which in turn will produce an electromagnetic field oscillating at the frequency of the incident light, modulated by intrinsic frequencies of molecular vibrations. The polarizability can be expanded into a power series with respect to nuclear displacements along vibrational modes Q_i and the expansion truncated after the second term

$$\boldsymbol{\alpha} \simeq \boldsymbol{\alpha}_0 + \sum_i \frac{\partial \boldsymbol{\alpha}}{\partial Q_i} Q_i. \tag{2.5.19}$$

Denoting the frequency of the electric field oscillations by ω, the intrinsic frequencies of nuclear vibrations by ω_i,

$$\begin{aligned} \boldsymbol{E} &= \boldsymbol{E}_0 \cos \omega t, \\ Q_i &= Q_i^0 \cos \omega_i t, \end{aligned}$$

and inserting in Eq. 2.5.18, one obtains the expression

$$\boldsymbol{\mu}^{\text{ind}} = \boldsymbol{E}_0 \cdot \boldsymbol{\alpha}_0 \cos \omega t + \frac{1}{2} \boldsymbol{E}_0 \cdot \sum_i Q_i^0 \frac{\partial \boldsymbol{\alpha}}{\partial Q_i} \left[\cos(\omega - \omega_i)t + \cos(\omega + \omega_i)t \right]. \tag{2.5.20}$$

The induced electric dipole thus oscillates at multiple frequencies. The first harmonic term with the frequency of the incident light corresponds to Rayleigh scattering. Additionally, for each vibrational mode Q_i there are two terms that correspond to Stokes and anti-Stokes scattering.

Quantum-mechanical description

Although the classical description provides a valuable insight into the origin of Raman scattering, it does not explain quantization of energy levels and does not give a quantitatively correct recipe for evaluation of transition probabilities. Quantum-mechanical expressions for transition probabilities of Raman scattering can be found from time-dependent perturbation theory of the second order. Similarly to Eq. 2.5.15 and Eq. 2.5.16, the polarizability transition element between states $\Psi^i \rightarrow \Psi^j$ may be then written in terms of electronic polarizability. In so-called Placzek approximation [49], an adiabatic wave function is used. Assuming that the electronic part of the state $\Psi^j = \Psi_e^i \Psi_n^j$ does not change during the transition, the components of the electronic polarizability tensor are then given by

$$(\alpha_e)_{\alpha\beta}^{ii} = \frac{2}{\hbar} \sum_{k \neq i} \frac{\omega_{ki}}{\omega_{ki}^2 - \omega^2} \operatorname{Re} \left[\langle \Psi_e^i | \mu_\alpha | \Psi_e^k \rangle \langle \Psi_e^k | \mu_\beta | \Psi_e^i \rangle \right], \qquad \alpha, \beta = x, y, z. \tag{2.5.21}$$

The summation goes over all excited electronic states Ψ_e^k of the molecule and $\omega_{ki} = \omega_k - \omega_i$ is the difference between angular frequency of the initial state Ψ_e^i and the state Ψ_e^k. The vibrational

transition polarizability between the vibrational states Ψ_n^i and Ψ_n^j is then

$$\boldsymbol{\alpha}^{ij} = \langle \Psi_n^i(\boldsymbol{R}) | \boldsymbol{\alpha}_e | \Psi_n^j(\boldsymbol{R}) \rangle. \tag{2.5.22}$$

Raman observables

The transition polarizability is a second rank tensor. Therefore the electric dipole moment $\boldsymbol{\mu}^{\text{ind}} = \boldsymbol{\alpha} \cdot \boldsymbol{E}$, and hence the probability of a transition, depends on the orientation of a molecule with respect to the incident light. The intensity of light scattered by a sample of randomly oriented molecules may be expressed in terms of tensor invariants, which are independent of the coordinate system rotations. The resultant expressions are dependent only on the scattering geometry, that is, on the angle between the direction of the incident and the scattered light. In particular, the Raman and ROA instrument at the Institute of Physics collects light scattered backwards. The total intensity of the back-scattering experimental setup is given by

$$I(180^\circ) = 45\alpha^2 + 7\beta(\alpha)^2. \tag{2.5.23}$$

Here α is the isotropic invariant of the polarizability tensor

$$\alpha = \frac{1}{3}(\alpha_{xx} + \alpha_{yy} + \alpha_{zz}), \tag{2.5.24}$$

and $\beta(\alpha)^2$ is the symmetric anisotropic invariant of the polarizability tensor

$$\beta(\alpha)^2 = \frac{1}{2} \sum_{\alpha,\beta=x,y,z} 3\alpha_{\alpha\beta}^2 - \alpha_{\alpha\alpha}\alpha_{\beta\beta}, \tag{2.5.25}$$

where $\alpha_{\alpha\beta}$ are components of the transition polarizability 2.5.22.

Selection rules

When the electronic polarizability 2.5.22 is expanded in Taylor series with respect to nuclear positions and expressed in normal mode coordinates

$$\boldsymbol{\alpha}_e(Q_1, \ldots, Q_m) = \boldsymbol{\alpha}_e(\mathbf{0}) + \sum_i \frac{\partial \boldsymbol{\alpha}_e}{\partial Q_i} Q_i + \frac{1}{2} \sum_{i,j} \frac{\partial^2 \boldsymbol{\alpha}_e}{\partial Q_i \partial Q_j} Q_i Q_j + \cdots, \tag{2.5.26}$$

the overlap properties of LHO wave functions may be used again to formulate selection rules for Raman transitions. Taking terms of polarizability linear in Q_i, only transitions between vibrational states $\Psi^i \to \Psi^j$ such that $i = j \pm 1$ are allowed within the harmonic approximation. The polarizability must change in course of the vibration so that $\partial \boldsymbol{\alpha}_e / \partial Q_i$ is non-zero. For anharmonic wave functions, also higher-order terms may become significant.

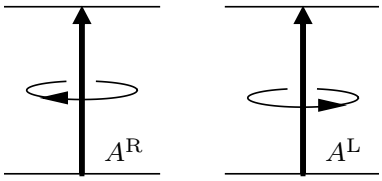

Figure 2.9: Energy-level diagram illustrating VCD.

2.5.5 Vibrational circular dichroism

Vibrational circular dichroism detects differences in attenuation of left and right circularly polarized light passing through a sample (Fig. 2.9). The fundamental quantity associated with the infrared absorption was the dipole strength (Eq. 2.5.13), a quantity which depends on the transition electric dipole moment. When the next term of the vector potential expansion (Eq. 2.5.8) is included in the perturbation operator, the transition probability for absorption of circularly polarized light can be found to be proportional not only to the dipole strength, but also to the quantity of the *rotational strength*. The differential absorption $\Delta A = A^{\mathrm{L}} - A^{\mathrm{R}}$ is therefore proportional to the rotational strength R which depends on both the electric and magnetic dipole transition moments

$$R(j \to k) = \boldsymbol{\mu}^{jk} \cdot \boldsymbol{m}^{kj} = \mathrm{Im}\left[\langle\psi_j|\boldsymbol{\mu}|\psi_k\rangle \cdot \langle\psi_k|\boldsymbol{m}|\psi_j\rangle\right]. \tag{2.5.27}$$

The magnetic dipole moment is defined as

$$\boldsymbol{m} = \sum_i \frac{q_i}{2m_i}(\boldsymbol{r}_i \times \boldsymbol{p}_i), \tag{2.5.28}$$

where particle i at $\boldsymbol{r}_i$ has charge q_i, mass m_i and linear momentum $\boldsymbol{p}_i$. Sensitivity of the handedness of a molecule toward circularly polarized light results from the form of the rotational strength (Fig. 2.10).

The magnetic transition dipole moment $\boldsymbol{m}^{kj}$ can be expanded in Taylor series with respect to nuclear momenta.[12] The tensor of first derivatives with respect to nuclear momenta is called *atomic axial tensor* (AAT). It should be noted that the appearance of the magnetic dipole moment in the transition probability expression brings a difficulty to practical calculations of VCD intensities, because the AAT tensor generally depends on the choice of coordinate system origin.

2.5.6 Raman optical activity

Light scattered from chiral samples carries a small degree of circular polarization, and the scattered intensity is slightly different in right and left circularly polarized light. ROA can be

[12] Derivatives with respect to nuclear positions vanish in the Born-Oppenheimer approximation.

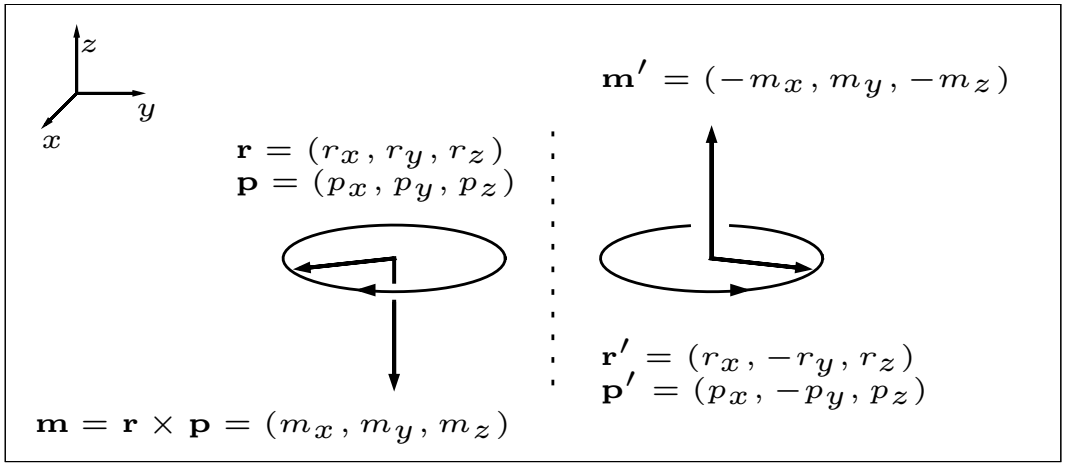

Figure 2.10: The mirror plane on the picture contains the axes x and z. Electric dipole moments of two enantiomers differ in sign of the y component ($\boldsymbol{\mu} = (\mu_x, \mu_y, \mu_z)$ and $\boldsymbol{\mu}' = (\mu_x, -\mu_y, \mu_z)$), while magnetic dipole moments differ in sign of the x and z components. Therefore, the rotational strength must have opposite sign for two enantiomers.

observed in a number of forms, depending on the polarization of the incident and the scattered light. For instance, in the scattered circular polarization (SCP) experiment, the incident light is linearly polarized and differences in circular polarization of the scattered light are measured. In the dual circular polarization (DCP), both the incident and the scattered light are circularly polarized, either in phase ($\mathrm{DCP_I}$) or out of phase ($\mathrm{DCP_{II}}$). The calculations in this work were performed for the incident circular polarization (ICP) form, where the sample is illuminated by a circularly polarized light and the total scattered intensity is measured.

Similarly to Raman scattering, the theory of ROA intensities may be derived by employing time-dependent perturbation method of second order. Analogously to VCD, the term linear in $\boldsymbol{r}$ of the vector potential expansion 2.5.8 must be included in the perturbation operator to describe Raman optical activity. The multipoles associated with ROA are then the electric dipole moment $\boldsymbol{\mu}$ (Eq. 2.5.11), the magnetic dipole moment $\boldsymbol{m}$ (Eq. 2.5.28), and the traceless electric quadrupole moment $\boldsymbol{\Theta}$,

$$\Theta_{\alpha\beta} = \frac{1}{2}\sum_i q_i(3r_{i_\alpha}r_{i_\beta} - r_i^2\delta_{\alpha\beta}), \qquad \alpha,\beta = x,y,z, \tag{2.5.29}$$

where particle i at $\boldsymbol{r}_i$ has charge q_i. In the weak-field approximation, it turns out that the multipoles induced in a molecule by electromagnetic radiation are given as

$$\mu_\alpha^{\mathrm{ind}} = \sum_\beta \alpha_{\alpha\beta}E_\beta + \frac{1}{\omega}\sum_\beta G'_{\alpha\beta}\frac{\partial B_\beta}{\partial t} + \frac{1}{3}\sum_{\beta,\gamma} A_{\alpha\beta\gamma}\frac{\partial E_\gamma}{\partial R_\beta} + \cdots, \tag{2.5.30}$$

$$m_\alpha^{\mathrm{ind}} = -\frac{1}{\omega}\sum_\beta G'_{\beta\alpha}\frac{\partial E_\beta}{\partial t} + \cdots, \tag{2.5.31}$$

$$\Theta_{\alpha\beta}^{\mathrm{ind}} = \sum_{\beta,\gamma} A_{\alpha\beta\gamma}E_\gamma + \cdots, \qquad \alpha,\beta,\gamma = x,y,z, \tag{2.5.32}$$

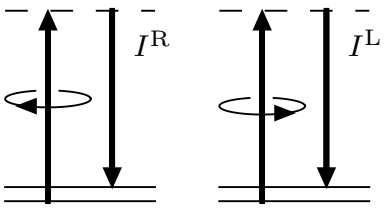

Figure 2.11: Energy-level diagram illustrating ICP ROA experiment.

where $\boldsymbol{E}$ is the electric field vector and $\boldsymbol{B}$ is the magnetic field vector. The tensor $\boldsymbol{\alpha}$ is the linear polarization of the electric dipole moment by an electric field (the electric dipole-electric dipole polarizability, see Eq. 2.5.21), $\boldsymbol{G'}$ determines the linear polarization of the electric dipole moment by the magnetic field component of the incident light (the *electric dipole-magnetic dipole polarizability*) and $\boldsymbol{A}$ determines the linear polarization of the electric dipole moment by the electric field gradient of the incident light (the *electric dipole-electric quadrupole polarizability*). In Placzek approximation, the tensors are given by the formulae

$$G'_{\alpha\beta} = -\frac{2}{\hbar} \sum_{k \neq i} \frac{\omega}{\omega_{ki}^2 - \omega^2} \operatorname{Im} \left[\langle \Psi_e^i | \mu_\alpha | \Psi_e^k \rangle \, \langle \Psi_e^k | m_\beta | \Psi_e^i \rangle \right], \tag{2.5.33}$$

$$A_{\alpha\beta\gamma} = \frac{2}{\hbar} \sum_{k \neq i} \frac{\omega_{ki}}{\omega_{ki}^2 - \omega^2} \operatorname{Re} \left[\langle \Psi_e^i | \mu_\alpha | \Psi_e^k \rangle \, \langle \Psi_e^k | \Theta_{\beta\gamma} | \Psi_e^i \rangle \right]. \tag{2.5.34}$$

Analogously to the transition dipole moment (Eq. 2.5.17) and electric dipole-electric dipole polarizability (Eq. 2.5.26), also the tensors $\boldsymbol{G'}$ and $\boldsymbol{A}$ can be expanded in Taylor series with respect to nuclear positions and transformed into normal modes. Thus obtained derivatives are then used in practical calculations of ROA intensities.

ROA observables

For a sample of randomly oriented molecules, the difference in scattering of circularly polarized light for the back-scattering geometry is proportional to

$$I^{\mathrm{R}} - I^{\mathrm{L}} = \frac{48}{c} \left[\beta(G')^2 + (1/3)\beta(A)^2 \right], \tag{2.5.35}$$

where c is the speed of light, I^{R} and I^{L} are the intensities scattered in right and left circularly polarized incident light. The invariants $\beta(G')^2$ and $\beta(A)^2$ are defined as

$$\beta(G')^2 = \frac{1}{2} \sum_{\alpha,\beta} \left(3\alpha_{\alpha\beta} \, G'_{\alpha\beta} - \alpha_{\alpha\alpha} \, G'_{\beta\beta} \right), \tag{2.5.36}$$

$$\beta(A)^2 = \frac{1}{2} \omega \sum_{\alpha,\beta,\gamma,\delta} \alpha_{\alpha\beta} \, \varepsilon_{\alpha\gamma\delta} \, A_{\gamma\delta\beta}, \tag{2.5.37}$$

where ω is the frequency of the incident light, $\alpha, \beta, \gamma, \delta = x, y, z$ and ε is the permutation symbol.

2.6 Spectral shapes

Spectra were simulated using Lorentz band shapes, so that a peak centered at $\tilde{\nu}_i$ with intensity I_i contributes to a spectrum by

$$S_i(\tilde{\nu}) = \frac{I_i}{4(\tilde{\nu} - \tilde{\nu}_i)^2/\Delta^2 + 1}, \tag{2.6.1}$$

where Δ is a full width at half-maximum height (FWHM). For absorption spectra, I_i was calculated using Eq. A.2.8. Raman spectra were evaluated using Eq. 2.5.23 and ROA spectra using Eq. 2.5.35. When contributions from multiple conformers were averaged in Raman and ROA spectra (see Sec. 3.2.2), the curve S_i was multiplied by the Boltzmann factor

$$B_j = \left[1 - e^{-\Delta E_j/kT}\right]^{-1}, \tag{2.6.2}$$

where ΔE_j is the relative energy of j-th conformer.

2.7 Solvation models

Vibrational spectra may be strongly affected by interactions with molecules of the same kind or by interactions with molecules of a solvent. In biochemical applications, solvent effects are particularly important because hydration is often responsible for three-dimensional structure and conformational flexibility of many biologically active molecules. There are two major types of methods for evaluating solvent effects: those treating the solvent as a continuous medium and those that include individual solvent molecules.

Inclusion of explicit solvent molecules in *ab initio* calculations is computationally very demanding. For example, quantum mechanical dynamics simulations of hydration shells of alanine zwitterion revealed that there are on average six water molecules in the first hydration shell in the vicinity of the charged CO_2^- and NH_3^+ alanine sites [50]. Therefore 18 atoms of water molecules must be included in calculations in addition to the 13 atoms of the alanine molecule.

In continuum models, the solute molecule (possibly supplemented by some solvent molecules from the first solvation shell) is placed in a cavity surrounded by a continuum medium. The *polarizable continuum model* (PCM) [24] represents the solvent by an infinite polarizable medium characterized mainly by its dielectric constant. The cavity is formed by spheres centered on each atom and the surface of the cavity is divided into small regions (called tesserae) on which are evaluated charges induced by the solute. The *conductor-like screening model* (COSMO) which is based on the assumption that the solvent may be represented by a conducting cavity, became extremely popular [51]. COSMO uses a scaled conductor boundary condition instead of the much more complicated dielectric boundary condition. The most important practical aspect is that the procedure replaces the normal component of the electric field on the cavity tesserae with the electrostatic potential, arriving at a noticeable reduction in computational costs. The *conductor-like PCM* (CPCM) [25] used in this work is an implementation of COSMO in the

PCM framework, where a correction for dielectric behavior is included. Some practical aspects of CPCM calculations are discussed in Appendix A.4.

3.1 Performance of anharmonic methods

3.1.1 Model potentials

The anharmonic methods reviewed in Sec. 2.4 were implemented in the Gvib software package [52] and applied to a number of systems. The correctness of the program was verified on simple potentials studied previously, for example, by Bowman, Christoffel and Norris [18, 22, 46].

The two-dimensional Henon-Heiles potential is defined as

$$V = \frac{1}{2}\left(\omega_1^2 Q_1^2 + \omega_2^2 Q_2^2\right) + \lambda\left(Q_1 Q_2^2 + \eta Q_1^3\right), \tag{3.1.1}$$

the parameters were set to $\omega_1^2 = 0.29375$, $\omega_2^2 = 2.12581$, $\lambda = -0.1116$ and $\eta = 0.08414$. The three-dimensional Christoffel potential

$$V = \frac{1}{2}(\omega_1^2 Q_1^2 + \omega_2^2 Q_2^2 + \omega_3^2 Q_3^2) + \lambda\eta Q_1^3 + \mu\zeta Q_2^3 + \lambda Q_1 Q_2^2 + \mu Q_2 Q_3^2 \tag{3.1.2}$$

was used with the values $\omega_1^2 = 0.49$, $\omega_2^2 = 1.69$, $\omega_3^2 = 1.00$, $\lambda = \mu = -0.10$ and $\eta = \zeta = 0.10$.

The vibrational Schrödinger equation was solved for these potentials using the harmonic approximation, VSCF, VCI and perturbation methods. The calculated energies are shown in Tables 3.1 and 3.2 as differences from the VCI results. All methods improve harmonic approximation. Both VSCF variants give similar results, but eVSCF gives consistently smaller errors. The differences can be for some modes exceptionally large. For example, the energy of the $|01\rangle$ state (Table 3.1) is predicted by gVSCF with an error five times larger than by eVSCF. On the other hand, the value obtained from the eVSCF calculation is comparable to PT2/Harm. The perturbation theory improves results of both the harmonic and the VSCF approximation.

The best results are given by the PT2/eVSCF method. The results of the PT2/Harm approach indicate that the harmonic approximation is a poor starting point for perturbation calculations, at least in the case of the model potentials. However, the results of all perturbation methods are comparable for real molecules and none of them gives clearly better energies than any of the others.

$E - E$(VCI)	$\|00\rangle$	$\|10\rangle$	$\|20\rangle$	$\|01\rangle$
Harmonic	0.00837	0.02604	0.05313	0.03911
gVSCF	0.00084	0.00307	0.00564	0.01404
eVSCF	0.00084	0.00303	0.00546	0.00277
PT2/Harm	0.00031	0.00162	0.00469	0.00276
PT2/gVSCF	0.00001	0.00013	0.00045	0.00075
PT2/eVSCF	0.00001	0.00003	0.00008	0.00006
E(VCI)	0.99163	1.51595	2.03085	2.41891

Table 3.1: State energies obtained for the Henon-Heiles potential by various methods, shown as differences from the values obtained by VCI. (Dimensionless numbers.)

$E - E$(VCI)	$\|000\rangle$	$\|001\rangle$	$\|010\rangle$	$\|100\rangle$	$\|101\rangle$	$\|200\rangle$
Harmonic	0.00625	0.01433	0.02814	0.01485	0.02328	0.02689
gVSCF	0.00128	0.00564	0.01259	0.00323	0.00793	0.00532
eVSCF	0.00128	0.00258	0.00618	0.00322	0.00478	0.00528
PT2/Harm	0.00013	0.00045	0.00103	0.00049	0.00116	0.00117
PT2/gVSCF	0.00002	0.00015	0.00036	0.00009	0.00053	0.00028
PT2/eVSCF	0.00002	0.00004	0.00012	0.00004	0.00009	0.00011
E(VCI)	1.49375	2.48567	2.77186	2.18515	3.17672	2.87311

Table 3.2: State energies obtained for the Christoffel potential by various methods, shown as differences from the values obtained by VCI. (Dimensionless numbers.)

3.1.2 Water

One of the smallest real-world systems available for modeling of vibrational spectra is a molecule of water. Biomolecules are preferably studied in their natural environment, that is, dissolved in water, and therefore vibrational transitions of water often interfere in the spectra of molecules of interest. Although the water molecule with only three fundamental vibrational modes may look deceptively simple for calculations, in fact it is not. Being very light and polar, water molecules in the liquid phase form non-covalently bonded clusters. Some of the vibrational motions in these clusters are strongly anharmonic and correlated, therefore the applicability of the potential expansion into a fourth-order polynomial is questionable [12]. The large number of possible configurations of water molecules in the clusters results in broad peaks, which can be simulated *ab initio* possibly only by calculating spectra for each orientation and consequent Boltzmann averaging.

Table 3.3 compares experimental frequencies of water vapor [53] with anharmonic calculations performed at four different levels of electronic theory: CCSD, MP2, B3LYP, and BPW91, all with the large cc-pVTZ basis set. In the harmonic approximation, all internuclear potentials behave similarly: Best is described the bending mode δ, while the strongly anharmonic O−H stretching modes ν_s and ν_{as} show much larger deviation. This is particularly true for CCSD, MP2 and B3LYP, but to a lesser extent also for BPW91. This behavior is quite general and can be observed also for other molecules. All anharmonic methods significantly improve harmonic frequencies calculated at the CCSD, MP2 and B3LYP levels. The internuclear potential calculated by BPW91 strongly underestimates both the angle and bonds stiffness, which results in

	Methods	$\omega_{\text{calc}} - \omega_{\text{exp}}$			$\omega_{\text{calc}} - \omega_{\text{harm}}$		
		δ	ν_s	ν_{as}	δ	ν_s	ν_{as}
CCSD/cc-pVTZ	Harmonic	84	224	223			
	gVSCF	29	134	176	-54	-89	-47
	eVSCF	26	134	66	-57	-90	-157
	PT2/Harm	21	86	35	-63	-138	-187
	PT2/gVSCF	19	91	39	-65	-132	-184
	PT2/eVSCF	17	92	37	-66	-131	-186
	VCI	17	91	39	-67	-132	-183
MP2/cc-pVTZ	Harmonic	57	204	220			
	gVSCF	2	116	174	-55	-88	-47
	eVSCF	-1	115	65	-58	-89	-156
	PT2/Harm	-6	68	34	-63	-136	-186
	PT2/gVSCF	-8	74	39	-65	-130	-182
	PT2/eVSCF	-10	75	36	-67	-129	-184
	VCI	-10	74	39	-67	-130	-182
B3LYP/cc-pVTZ	Harmonic	44	152	148			
	gVSCF	-11	68	107	-55	-83	-41
	eVSCF	-14	67	-2	-58	-84	-149
	PT2/Harm	-20	19	-34	-64	-133	-182
	PT2/gVSCF	-22	27	-28	-66	-125	-176
	PT2/eVSCF	-23	27	-30	-67	-124	-178
	VCI	-24	27	-28	-68	-125	-175
BPW91/cc-pVTZ	Harmonic	18	54	52			
	gVSCF	-38	-36	4	-56	-90	-48
	eVSCF	-41	-37	-107	-59	-91	-159
	PT2/Harm	-47	-84	-136	-64	-138	-188
	PT2/gVSCF	-49	-79	-133	-67	-133	-185
	PT2/eVSCF	-50	-78	-136	-68	-133	-188
	VCI	-51	-79	-133	-68	-133	-185
	Expt. (ω_{exp})	1595	3652	3756			

Table 3.3: Calculated and measured [53] frequencies of water vapor. Frequencies of three fundamental vibrations (bending δ, symmetric stretch ν_s, and antisymmetric stretch ν_{as}) are shown as differences from experimental values (the middle columns). In the columns on the right the magnitudes of anharmonic corrections are shown. The vibrational potential was evaluated at the CCSD/cc-pVTZ, MP2/cc-pVTZ, B3LYP/cc-pVTZ and BPW91/cc-pVTZ levels. All frequencies and frequency differences in cm^{-1}. The maximal deviations are emphasized by different color, as explained in the text.

too low anharmonic frequencies.

Somewhat surprising may be the exceptionally good overall agreement in the magnitude of the anharmonic corrections calculated using different electronic methods, as listed in the right part of Table 3.3. In particular, the maximal difference in anharmonic contributions for a given anharmonic method is only 10 cm^{-1} (the asymmetric stretch ν_{as} calculated at the B3LYP and BPW91 level using PT2/eVSCF, the numbers are printed in green color), while the maximal difference in the harmonic frequencies is 171 cm^{-1} (the asymmetric stretch ν_{as} calculated at CCSD and BPW91 levels, the numbers are printed in red color). This result is in accordance with the well known fact that anharmonic contributions are usually smaller than 10% of harmonic values.

Electronic calculations with the cc-pVTZ basis set are computationally very demanding and are feasible only for small molecules. To evaluate the vibrational potential of medium-sized and large systems, it is necessary to reduce the size of the basis set and employ electronic methods with favorable scaling. Table 3.4 shows the results from using several electronic methods

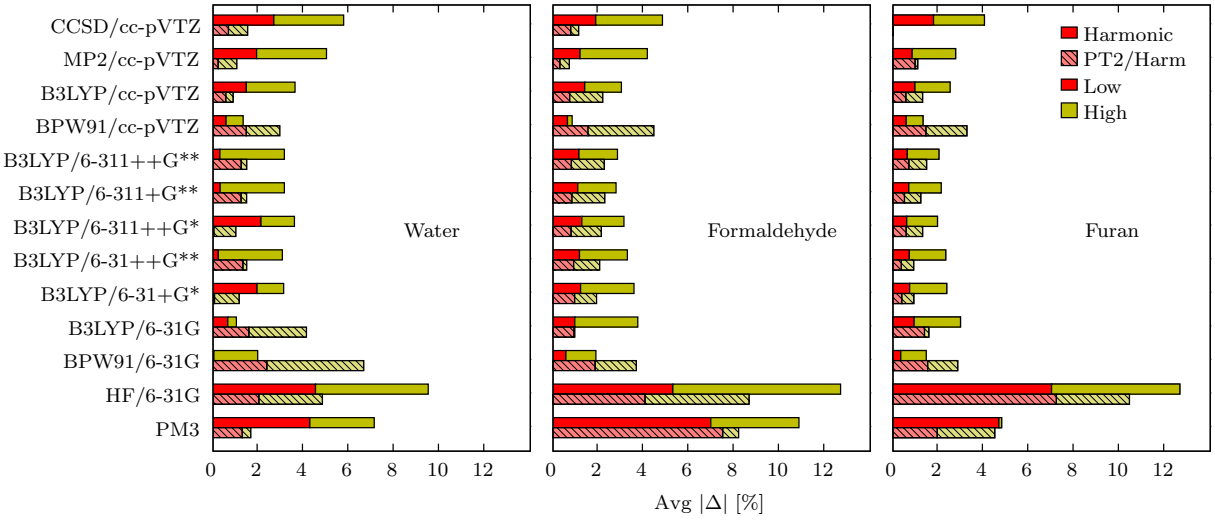

Figure 3.1: Average absolute deviations of fundamental frequencies of water, formaldehyde and furan from experimental frequencies observed in the gas phase, as calculated at various levels of the electronic theory using the harmonic approximation and the PT2/Harm method. The deviations of hydrogen stretching modes are printed in a color different (yellow) from low- and mid-frequency modes (red).

(B3LYP, BPW91, HF and PM3) and basis sets (6-311++G**, 6-31+G*, 6-31G). Similarly to the calculations performed using the cc-pVTZ basis set, the difference in harmonic frequencies greatly exceeds the differences in anharmonic corrections. The largest difference in the harmonic frequencies of 477 cm^{-1} (the symmetric stretch ν_s calculated with BPW91/6-31G and HF/6-31G) greatly exceeds the maximal difference 39 cm^{-1} in the anharmonic contributions (the asymmetric stretch ν_{as} calculated at BPW91/6-31G and B3LYP/6-31+G* using PT2/eVSCF).[1]

3.1.3 Formaldehyde

The results of calculations on formaldehyde follow the general pattern observed for water and, as will be seen later, also for other molecules. Usually, the hydrogen stretching vibrations come out too large from the harmonic approximation and all anharmonic methods tend to improve the agreement with the experiment in this region. The low- and mid-frequency modes, however, are often quite close to the experimental values already within the harmonic approximation. Anharmonic methods shift the harmonic frequencies toward the red end of the spectrum and occasionally change the order of modes.

As shown in Fig. 3.1, very good agreement with experiment can be observed for anharmonic frequencies calculated at the CCSD/cc-pVTZ and MP2/cc-pVTZ levels. With the exception of the asymmetric C−H stretching vibration ν_{as} (Table 3.5), both VSCF methods as well as the perturbation methods give consistently similar results and do not exhibit dramatic differences observed for model potentials in Sec. 3.1.1. The largest deviation of anharmonic frequencies from experimental values in the CCSD/cc-pVTZ calculation is observed for the symmetric C=O

[1]The semi-empirical method PM3 was not included in the comparison.

	Methods	$\omega_{\text{calc}} - \omega_{\text{exp}}$			$\omega_{\text{calc}} - \omega_{\text{harm}}$		
		δ	ν_s	ν_{as}	δ	ν_s	ν_{as}
B3LYP 6-311++G**	Harmonic	8	166	166			
	gVSCF	-42	76	121	-49	-90	-46
	eVSCF	-45	75	10	-53	-90	-156
	PT2/Harm	-51	28	-19	-59	-138	-185
	PT2/gVSCF	-53	33	-15	-61	-132	-182
	PT2/eVSCF	-54	34	-19	-62	-132	-185
	VCI	-55	33	-16	-63	-132	-183
B3LYP/6-31+G*	Harmonic	68	85	105			
	gVSCF	9	2	64	-58	-83	-41
	eVSCF	7	1	-43	-61	-84	-148
	PT2/Harm	2	-49	-76	-66	-134	-181
	PT2/gVSCF	-1	-41	-70	-68	-125	-175
	PT2/eVSCF	-2	-40	-71	-69	-124	-176
	VCI	-2	-40	-69	-70	-125	-174
B3LYP/6-31G	Harmonic	23	-33	29			
	gVSCF	-37	-122	-21	-60	-89	-50
	eVSCF	-40	-124	-138	-62	-91	-167
	PT2/Harm	-47	-174	-175	-70	-142	-203
	PT2/gVSCF	-49	-163	-166	-72	-131	-195
	PT2/eVSCF	-51	-163	-168	-74	-130	-197
	VCI	-51	-163	-165	-74	-130	-193
BPW91/6-31G	Harmonic	1	-140	-76			
	gVSCF	-59	-241	-138	-60	-101	-63
	eVSCF	-62	-243	-259	-63	-103	-183
	PT2/Harm	-69	-289	-289	-70	-149	-213
	PT2/gVSCF	-72	-283	-286	-73	-143	-210
	PT2/eVSCF	-73	-283	-290	-74	-143	-215
	VCI	-74	-283	-286	-75	-143	-210
HF/6-31G	Harmonic	142	337	389			
	gVSCF	71	248	348	-71	-88	-42
	eVSCF	68	247	233	-74	-90	-156
	PT2/Harm	61	196	198	-81	-141	-191
	PT2/gVSCF	59	204	205	-83	-132	-184
	PT2/eVSCF	58	205	204	-84	-131	-186
	VCI	57	205	206	-85	-132	-183
PM3	Harmonic	146	217	234			
	gVSCF	70	99	65	-76	-119	-169
	eVSCF	62	13	59	-84	-204	-175
	PT2/Harm	50	16	53	-96	-202	-180
	PT2/gVSCF	50	-9	40	-97	-226	-194
	PT2/eVSCF	47	-18	38	-99	-235	-196
	VCI	47	-13	37	-99	-231	-197
	Expt. (ω_{exp})	1595	3652	3756			

Table 3.4: Calculated and measured [53] frequencies of water vapor. Comparison of frequencies calculated with different electronic methods and lower-quality basis sets. See also Table 3.3. All frequencies and frequency differences are in cm^{-1}. The maximal deviations are emphasized by different color, as explained in the text.

stretching mode ν_{s_1}. The anharmonicity of the mode is weak (1% of the harmonic frequency) and therefore all anharmonic methods yield essentially the same value. The large difference from experiment must be therefore attributed to an inadequate description of the C=O bond strength by the CCSD/cc-pVTZ method. The same mode is described exceptionally well by the MP2 and BPW91 methods. However, the behavior of the electronic methods is too complex to draw straightforward conclusions. For example, it is interesting to notice that the frequency

	Methods	$\omega_{\text{calc}} - \omega_{\text{exp}}$						$\omega_{\text{calc}} - \omega_{\text{harm}}$					
		δ_{oop}	δ_{as}	δ_s	ν_{s_1}	ν_{s_2}	ν_{as}	δ_{oop}	δ_{as}	δ_s	ν_{s_1}	ν_{s_2}	ν_{as}
CCSD/cc-pVTZ	Harmonic	48	41	61	85	175	182						
	gVSCF	5	-5	25	70	52	94	-43	-46	-36	-15	-123	-88
	eVSCF	2	-7	24	69	50	15	-45	-48	-37	-16	-125	-167
	PT2/Harm	3	-5	19	64	4	31	-45	-45	-41	-21	-171	-151
	PT2/gVSCF	0	-9	19	63	7	-13	-47	-50	-42	-21	-169	-195
	PT2/eVSCF	-1	-10	19	63	7	6	-48	-51	-42	-22	-169	-176
	VCI	0	-10	19	63	8	-3	-48	-51	-42	-21	-167	-185
MP2/cc-pVTZ	Harmonic	41	31	54	28	189	201						
	gVSCF	-1	-14	22	9	68	115	-42	-45	-32	-18	-121	-86
	eVSCF	-4	-16	20	8	66	36	-45	-47	-33	-20	-123	-165
	PT2/Harm	-4	-14	14	5	15	35	-45	-44	-40	-23	-174	-166
	PT2/gVSCF	-6	-18	15	3	23	-5	-47	-48	-39	-24	-166	-205
	PT2/eVSCF	-7	-19	15	3	23	16	-48	-50	-39	-25	-166	-185
	VCI	-7	-18	15	3	24	13	-48	-49	-39	-24	-165	-187
B3LYP/cc-pVTZ	Harmonic	36	20	36	78	97	90						
	gVSCF	-8	-26	0	66	-38	-8	-44	-46	-36	-12	-134	-98
	eVSCF	-11	-28	-1	65	-40	-92	-47	-48	-37	-13	-136	-182
	PT2/Harm	-11	-26	-4	58	-78	-107	-46	-45	-41	-19	-174	-197
	PT2/gVSCF	-14	-30	-5	59	-85	-116	-49	-50	-41	-19	-182	-206
	PT2/eVSCF	-15	-32	-6	58	-85	-125	-50	-51	-42	-19	-182	-215
	VCI	-14	-31	-5	58	-84	-140	-50	-51	-41	-19	-180	-230
BPW91/cc-pVTZ	Harmonic	-11	-20	-8	23	14	-6						
	gVSCF	-55	-67	-45	11	-119	-101	-45	-47	-37	-11	-133	-95
	eVSCF	-59	-69	-46	10	-121	-187	-48	-49	-38	-13	-135	-181
	PT2/Harm	-57	-66	-50	4	-162	-204	-47	-46	-42	-19	-176	-198
	PT2/gVSCF	-61	-71	-51	4	-168	-210	-50	-51	-42	-19	-181	-204
	PT2/eVSCF	-62	-72	-51	4	-168	-220	-51	-52	-43	-19	-181	-214
	VCI	-61	-72	-51	4	-166	-232	-51	-52	-43	-19	-180	-226
	Expt. (ω_{exp})	1167	1249	1500	1746	2782	2843						

Table 3.5: Calculated and measured [54] frequencies of formaldehyde in the gas phase. All frequencies and frequency differences in cm^{-1}.

of the C=O stretching mode ν_{s_1} is predicted with similar deviation by the CCSD and B3LYP methods ($\approx$ 80 cm^{-1}) and by the MP2 and BPW91 methods ($\approx$ 25 cm^{-1}). On the other hand, the C–H stretching vibrations ν_{s_2} and ν_{as} are predicted similarly by the CCSD and MP2 methods, while the B3LYP and BPW91 methods predict the frequencies far too low.

Similarly to the behavior observed for water, the magnitudes of the anharmonic contributions differ much less than the harmonic frequencies (Tables 3.5 and 3.6). The maximal difference in anharmonic contributions for a given anharmonic method is 68 cm^{-1} (the asymmetric stretching mode ν_{as} calculated at the CCSD/cc-pVTZ and B3LYP/6-31+G* levels using PT2/Harm), while the maximal difference in harmonic frequencies is 462 cm^{-1} (ν_{as} calculated at the BPW91/cc-pVTZ and HF/6-31G levels).

3.1.4 Furan

Furan is a rigid planar molecule made of an aromatic cycle containing oxygen. Consisting of nine atoms, furan has 21 vibrational modes. As mentioned in Sec. 2.4.6, the size of the basis set used in VCI calculations grows very fast with the number of normal modes and only a fraction of the states can be included in a practical computation. In particular, the value of

	Methods	$\omega_{\text{calc}} - \omega_{\text{exp}}$						$\omega_{\text{calc}} - \omega_{\text{harm}}$					
		δ_{oop}	δ_{as}	δ_s	ν_{s_1}	ν_{s_2}	ν_{as}	δ_{oop}	δ_{as}	δ_s	ν_{s_1}	ν_{s_2}	ν_{as}
B3LYP 6-311++G**	Harmonic	35	11	31	68	104	101						
	gVSCF	-11	-33	-4	56	-36	-1	-47	-44	-34	-11	-140	-102
	eVSCF	-15	-36	-5	55	-38	-86	-50	-46	-36	-12	-142	-187
	PT2/Harm	-14	-33	-8	49	-76	-104	-49	-44	-39	-19	-180	-205
	PT2/gVSCF	-17	-38	-9	49	-84	-111	-52	-49	-40	-19	-188	-212
	PT2/eVSCF	-18	-39	-10	49	-85	-122	-53	-50	-40	-19	-189	-223
	VCI	-17	-39	-9	49	-83	-93	-53	-49	-40	-19	-187	-194
B3LYP/6-31+G*	Harmonic	24	18	44	77	149	147						
	gVSCF	-20	-28	9	65	7	45	-43	-46	-36	-12	-142	-103
	eVSCF	-23	-31	8	64	5	-41	-47	-49	-37	-13	-144	-189
	PT2/Harm	-22	-28	4	57	-38	-71	-46	-46	-41	-20	-187	-219
	PT2/gVSCF	-25	-33	3	58	-42	-69	-49	-51	-41	-20	-191	-217
	PT2/eVSCF	-26	-34	3	57	-42	-81	-50	-52	-42	-20	-191	-229
	VCI	-26	-34	3	57	-41	-57	-50	-52	-42	-20	-189	-204
B3LYP/6-31G	Harmonic	36	25	60	2	181	192						
	gVSCF	-11	-25	33	-19	35	86	-47	-49	-27	-21	-147	-106
	eVSCF	-14	-27	31	-21	33	-2	-49	-51	-29	-23	-149	-194
	PT2/Harm	-12	-23	22	-23	-2	1	-48	-48	-38	-25	-184	-191
	PT2/gVSCF	-15	-29	24	-25	-15	-50	-51	-53	-36	-27	-196	-242
	PT2/eVSCF	-17	-30	25	-26	-16	-42	-53	-55	-35	-28	-197	-234
	VCI	-16	-29	25	-26	-14	-28	-52	-54	-35	-28	-195	-220
BPW91/6-31G	Harmonic	-4	-10	20	-49	87	84						
	gVSCF	-52	-61	-7	-72	-59	-21	-48	-51	-26	-23	-147	-106
	eVSCF	-55	-63	-9	-74	-62	-111	-51	-53	-29	-25	-149	-196
	PT2/Harm	-53	-59	-19	-74	-96	-108	-49	-49	-39	-26	-183	-192
	PT2/gVSCF	-57	-65	-16	-78	-110	-154	-53	-55	-36	-29	-197	-239
	PT2/eVSCF	-58	-66	-16	-79	-111	-145	-54	-57	-35	-30	-198	-230
	VCI	-57	-66	-16	-78	-108	-131	-53	-56	-36	-29	-195	-215
HF/6-31G	Harmonic	162	125	173	164	425	456						
	gVSCF	117	78	143	144	294	364	-45	-46	-30	-20	-131	-93
	eVSCF	114	76	141	142	292	282	-48	-48	-32	-21	-133	-174
	PT2/Harm	115	79	135	140	247	280	-47	-46	-38	-24	-179	-176
	PT2/gVSCF	113	74	136	138	247	232	-49	-50	-37	-26	-178	-224
	PT2/eVSCF	112	73	136	137	247	255	-50	-51	-37	-26	-178	-201
	VCI	112	73	136	138	248	254	-50	-51	-37	-26	-177	-203
PM3	Harmonic	-119	-159	-212	242	216	184						
	gVSCF	-87	-160	-210	240	19	38	32	-2	2	-1	-197	-145
	eVSCF	-92	-166	-211	240	13	-49	27	-8	1	-2	-203	-232
	PT2/Harm	-94	-167	-215	195	5	-57	25	-8	-3	-47	-211	-241
	PT2/gVSCF	-97	-170	-216	203	-34	-81	22	-11	-3	-38	-250	-265
	PT2/eVSCF	-99	-171	-216	204	-38	-83	20	-13	-4	-38	-254	-267
	VCI	-98	-170	-216	203	-34	-78	21	-12	-3	-39	-249	-262
	Expt. (ω_{exp})	1167	1249	1500	1746	2782	2843						

Table 3.6: Calculated and measured [54] frequencies of formaldehyde in the gas phase. All frequencies and frequency differences in cm^{-1}.

1000 states, used by default in this work, constitutes only 1.5% of the 65780 possible states with at most 5 excitations. The VCI calculation was therefore repeated for the MP2/cc-pVTZ potential also with 4000, 5000 and 6000 basis functions to check the convergence behavior of VCI. The calculation in the smallest basis set yielded absolute average error of 26 cm^{-1}, which is nearly half of the error of the harmonic approximation (49 cm^{-1}). With 4000 states (6% of the possible states), the error is reduced below 20 cm^{-1}. With 5000 (7.6%) and 6000 (9.1%) functions, the VCI results do not differ significantly and can be thus regarded as converged (see

Table 3.8, page 60, and also Ref. 26).

The best agreement with the experiment give the perturbation methods with the potential calculated at the MP2/cc-pVTZ level: the absolute average error was only 10 cm^{-1}.

3.1.5 N-methyl acetamide

N-methyl acetamide (NMA) serves as a model system for understanding spectroscopic properties of the peptide bond. In Table 3.7 are shown calculated frequencies of selected vibrational transitions (amide A, I, II, III, IV, and a collective stretching vibration ν) in comparison to experimental values. As discussed in Appendix A.3, five lowest-energy modes had to be left out from the calculations to avoid numerical instabilities. Although the 6000 functions included in the basis set for the VCI diagonalization constitute only 4% of the total states, the VCI frequencies changed no more than few cm^{-1} from the values calculated in the basis of 5000 functions. (Data not shown.) The best agreement of anharmonic frequencies with experiment was achieved by the B3LYP potential using the perturbation methods.

3.1.6 α-Pinene

α-Pinene is an organic compound of the terpene class (Fig. 3.2) which is routinely used as a standard for measurements of vibrational optical activity. The molecule is rigid and non-polar.

	Methods	$\omega_{calc} - \omega_{exp}$						$\omega_{calc} - \omega_{harm}$					
		IV	ν	III	II	I	A	IV	ν	III	II	I	A
MP2/cc-pVTZ	Harmonic	12	35	33	63	41	203						
	gVSCF	-4	30	15	32	25	32	-16	-5	-18	-31	-16	-171
	eVSCF	-5	26	11	27	21	31	-17	-8	-21	-35	-21	-172
	PT2/Harm	-12	15	-4	20	17	48	-24	-19	-37	-43	-24	-155
	PT2/gVSCF	-13	15	-1	16	18	50	-25	-20	-34	-47	-23	-153
	PT2/eVSCF	-14	14	-2	14	14	51	-26	-21	-34	-48	-27	-152
	VCI (6000)	6	32	12	41	43	85	-6	-2	-21	-22	1	-119
B3LYP/cc-pVTZ	Harmonic	4	14	21	44	29	152						
	gVSCF	-13	5	4	16	10	-21	-17	-8	-16	-28	-18	-172
	eVSCF	-15	2	0	11	6	-22	-19	-12	-20	-33	-23	-173
	PT2/Harm	-21	-8	-14	2	2	-2	-25	-22	-35	-42	-27	-154
	PT2/gVSCF	-22	-10	-10	-1	3	-2	-26	-23	-30	-45	-25	-153
	PT2/eVSCF	-23	-10	-10	-2	1	-1	-27	-24	-30	-47	-28	-153
	VCI (6000)	-2	13	4	26	29	35	-6	-0	-17	-18	1	-116
BPW91/cc-pVTZ	Harmonic	-15	-14	-23	-5	-25	68						
	gVSCF	-33	-21	-39	-35	-43	-119	-18	-7	-16	-30	-18	-187
	eVSCF	-34	-25	-43	-39	-48	-120	-19	-11	-20	-34	-22	-188
	PT2/Harm	-41	-35	-59	-47	-53	-100	-26	-22	-35	-41	-27	-167
	PT2/gVSCF	-43	-36	-54	-50	-51	-102	-28	-23	-31	-45	-26	-169
	PT2/eVSCF	-44	-37	-54	-52	-55	-101	-29	-24	-31	-47	-30	-169
	VCI (6000)	-21	-15	-39	-23	-24	-63	-7	-1	-16	-18	2	-131
	Expt. (ω_{exp})	[b)]626	[a)]1089	[b)]1259	[b)]1500	[b)]1728	[a)]3498						

[a)] Exp. values from Ref. 55.
[b)] Exp. values from Ref. 56.

Table 3.7: Calculated and experimental frequencies of selected vibrational transitions of N-methyl acetamide in the gas phase. The experimental values were obtained by infrared measurements in low-temperature nitrogen matrix (a) and by resonance Raman spectroscopy (b). All frequencies and frequency differences are in cm^{-1}.

	Methods	$\omega_{calc} - \omega_{exp}$																				
		ν_{11}	ν_{14}	ν_{10}	ν_{13}	ν_{12}	ν_9	ν_8	ν_{21}	ν_7	ν_{20}	ν_6	ν_5	ν_{19}	ν_{18}	ν_4	ν_3	ν_{17}	ν_{16}	ν_2	ν_{15}	ν_1
[a]	Harmonic	16	19	39	36	41	28	22	23	32	39	37	40	61	44	57	67	74	152	153	152	151
MP2/cc-pVTZ	Harmonic	14	29	5	17	1	4	7	11	31	24	47	25	68	26	37	19	21	160	161	158	156
	gVSCF	46	45	58	73	42	50	0	7	33	25	34	22	53	12	20	4	2	51	41	45	16
	eVSCF	46	44	50	61	37	38	-0	7	29	23	33	20	44	11	15	-0	-5	-6	10	-13	13
	PT2/Harm	33	29	3	-3	1	-8	-8	4	9	2	21	6	31	1	-11	-14	-13	-3	-5	-7	-3
	PT2/gVSCF	33	28	14	12	6	3	-8	3	10	3	22	5	32	-1	-8	-9	-9	-13	-21	-20	-3
	PT2/eVSCF	34	29	16	12	9	3	-9	3	9	1	21	4	31	-2	-7	-9	-4	5	-13	-9	-0
	VCI (1000)	53	48	34	21	18	14	9	20	30	20	42	28	54	21	23	-4	-6	55	31	9	8
	VCI (4000)	45	42	29	21	19	11	-1	12	17	9	31	13	44	7	10	-18	-13	52	6	-8	8
	VCI (5000)	44	41	28	21	19	10	-2	12	17	9	31	12	45	6	9	-20	-13	45	2	-12	9
	VCI (6000)	44	41	28	21	18	9	-2	11	17	9	30	13	43	6	9	-21	-14	41	1	-18	7
B3LYP/cc-pVTZ	Harmonic	19	22	15	16	19	23	21	21	20	19	20	26	18	27	31	22	37	113	114	116	113
	gVSCF	51	41	59	68	53	17	55	17	22	17	7	24	3	13	16	7	21	7	-17	-6	-41
	eVSCF	50	41	53	57	48	16	45	16	18	15	6	23	-4	12	12	3	14	-57	-37	-72	-46
	PT2/Harm	36	23	10	-0	15	9	2	13	-0	-5	-5	7	-19	2	-12	-10	6	-51	-51	-53	-45
	PT2/gVSCF	35	22	18	12	18	9	11	12	0	-5	-5	7	-18	1	-10	-6	10	-56	-61	-66	-75
	PT2/eVSCF	36	23	20	11	21	8	10	12	-1	-6	-5	6	-18	0	-10	-6	15	-16	-55	-96	-89
	VCI (6000)	46	35	30	18	30	15	16	20	6	2	5	14	-8	8	2	13	3	15	-40	-56	-108
BPW91/cc-pVTZ	Harmonic	1	7	-25	-15	-26	-12	-11	-8	-6	-14	-0	-5	-17	-19	-7	-22	-12	51	51	51	49
	gVSCF	33	25	28	46	13	22	-18	-13	-4	-15	-13	-8	-33	-33	-22	-37	-28	-66	-83	-73	-105
	eVSCF	32	24	21	33	8	11	-18	-14	-8	-17	-14	-9	-40	-34	-27	-41	-36	-130	-110	-137	-110
	PT2/Harm	15	6	-27	-31	-27	-33	-26	-17	-28	-39	-26	-25	-55	-45	-52	-55	-45	-122	-125	-122	-118
	PT2/gVSCF	15	6	-16	-15	-23	-23	-26	-18	-27	-38	-25	-26	-55	-45	-49	-50	-42	-132	-145	-136	-109
	PT2/eVSCF	16	7	-13	-15	-20	-24	-27	-18	-29	-40	-26	-27	-54	-47	-49	-50	-38	-102	-131	-175	-149
	VCI (6000)	28	20	-1	-6	-10	-17	-20	-9	-20	-30	-15	-18	-43	-38	-36	-67	-46	-65	-112	-113	-112
[b]	Harmonic	10	16	9	10	12	16	17	20	17	14	16	22	14	17	25	16	30	111	113	118	115
	gVSCF	53	36	60	65	56	79	10	16	20	14	4	21	0	5	11	1	15	7	-22	-6	-44
	eVSCF	52	35	53	54	51	69	10	15	17	12	3	19	-7	5	7	-2	8	-58	-38	-75	-50
	PT2/Harm	42	17	9	-5	17	23	2	12	-2	-9	-8	3	-22	-6	-15	-15	4	-48	-51	-58	-46
	PT2/gVSCF	42	17	19	10	22	35	2	11	-2	-8	-7	3	-21	-6	-14	-11	8	-55	-61	-67	-79
	PT2/eVSCF	43	18	21	8	24	35	2	11	-3	-10	-8	2	-20	-7	-14	-11	15	-16	-59	-94	-93
	VCI (6000)	49	30	32	15	33	42	8	19	5	-1	2	10	-10	0	-4	-3	-0	11	-41	-53	-54
	Expt. (ω_{exp})	600	603	722	745	838	864	870	873	995	1043	1067	1140	1181	1267	1385	1491	1558	3130	3140	3161	3169

[a] CCSD/cc-pVTZ (The evaluation of the anharmonic potential was not possible at this level.)
[b] B3LYP/6-311++G**

Table 3.8: Calculated and measured frequencies of fundamental vibrational transitions of furan in the gas phase. The mode numbering and experimental values were taken from Ref. 57. All frequencies and frequency differences are in cm^{-1}. The number of states included in VCI calculations is indicated by the numbers in brackets.

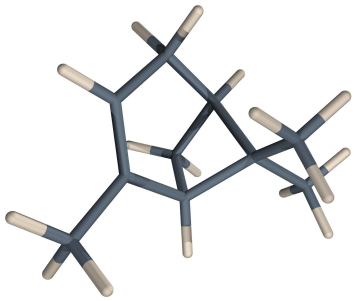

Figure 3.2: (+)-α-Pinene

Although α-pinene exists in the liquid form, calculations performed for a single molecule in the vacuum yield agreeable results. The size of the molecule (26 atoms) restricts the level of electronic *ab initio* calculations to HF or DFT methods and smaller basis sets. Fig. 3.3 (page 62) shows Raman spectra calculated using different anharmonic methods at the B3LYP/6-31G** level. By visual inspection of dominant peaks in calculated and measured [5] spectra, it is obvious that the VCI method gives in this region the worst agreement with the experiment. This fact is not surprising, because the diagonalization was performed in the basis of 6000 functions, which is only 0.04% of the total of almost 14 million states. The best agreement was attained by the perturbation methods, as indicated by the red dotted lines. Fig. 3.4 shows calculated and measured ROA spectra of (-)-α-pinene.

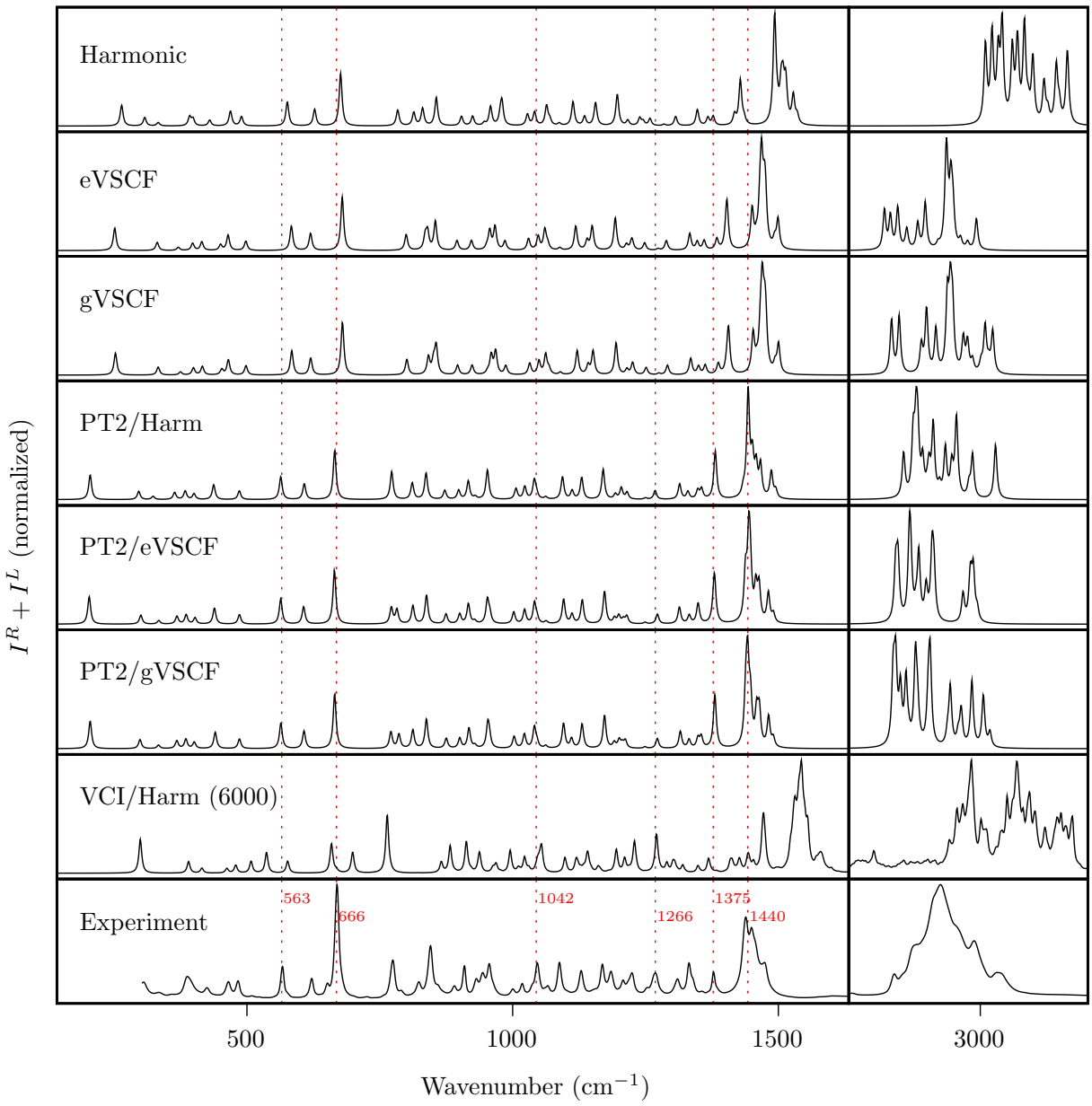

Figure 3.3: Calculated and measured Raman spectra of α-Pinene (neat liquid). The vibrational potential was calculated using the B3LYP/6-31G** method. Five of the lowest-energy modes were left out from the calculations to avoid numerical instabilities. Only first derivatives of intensity tensors were considered. The VCI calculation was performed in the basis of 6000 functions.

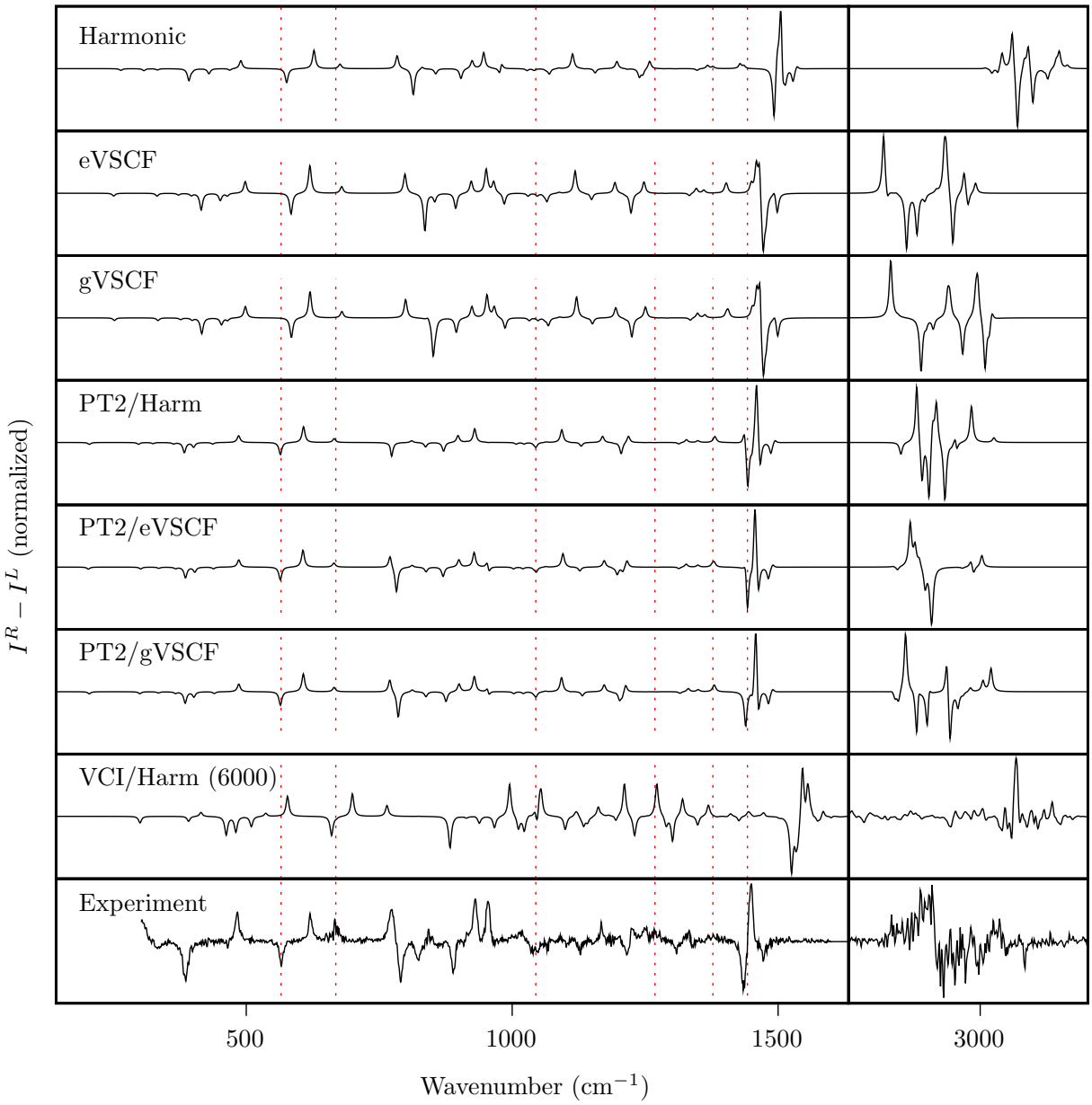

Figure 3.4: Calculated and measured ROA spectra of (-)-α-Pinene (neat liquid). The vibrational potential was calculated using the B3LYP/6-31G** method. Five of the lowest-energy modes were left out from the calculations to avoid numerical instabilities. Only first derivatives of intensity tensors were considered. The VCI calculation was performed in the basis of 6000 functions. The red dotted lines correspond to peaks emphasized in Fig. 3.3.

3.2 Publications

3.2.1 Numerical stability of anharmonic methods (summary)

The accuracy of calculated vibrational energies depends on the quality of input data (the potential energy surface), involved vibrational approximation (harmonic, VSCF, etc.) and numerical stability of the method under consideration.

Because the accuracy of electronic calculations is limited, the cubic and semi-diagonal quartic constants obtained by numerical differentiation from second derivatives can differ significantly not only for different levels of the electronic theory, but also for different options and parameters used in the potential evaluation. For example, harmonic frequencies of alanine evaluated at the B3LYP/6-31G**/CPCM level can occasionally differ as much as 136 cm^{-1} when calculated by GAUSSIAN with the default grid (75,302)[2] or with the "UltraFine" grid (99,590). The maximal difference in frequencies corrected by anharmonic methods is magnified to almost 400 cm^{-1} by some methods. It is expected that different anharmonic methods will respond differently to small potential variations. For example, in the mathematical formalism of the perturbation method of the second order there is a term which contains summation over many terms with the same sign (Eq. 2.2.14). One may expect that the perturbation methods will amplify the differences in the anharmonic potential to a different level than, for example, VSCF.

In Ref. 26 (see Appendix B) we focused on the numerical stability of anharmonic vibrational methods with respect to random variations of anharmonic constants of furan. While VSCF proved to be the most resistant to potential variations, the second-order perturbation methods turned out to be very sensitive to random degeneracies and provided the least stable results. However, the stability could be significantly improved by a simple modification of perturbation formula (Eq. 2.2.18).

Performance of the anharmonic methods was investigated also for other molecules.

3.2.2 Anharmonic methods applied to solvated systems (summary)

In an aqueous environment, many amino acids occur in the zwitterionic form.[3] Zwitterions interact strongly with water, which makes them ideal model systems for studying properties of molecules strongly interacting with polar solvents.

In Ref. 58 (see Appendix B) we analyzed anharmonic contributions to IR, Raman and ROA spectra of alanine and proline zwitterions (Fig. 3.5), studied previously also in [59, 60]. It was found that anharmonic effects dominate in the region of C−H and N−H stretching vibrations. All of the anharmonic methods significantly improved harmonic results in this region. Due to inaccuracies of the vibrational potential and involved approximations, none of the methods enabled peak-to-peak agreement with experiment though. The lower-frequency vibrations (less

[2] The default grid has 75 radial shells and 302 angular points per shell.

[3] A *zwitterion* contains positively and negatively charged groups, but its total charge is zero. In amino acids, a hydrogen ion from the carboxyl group is removed leaving the carboxyl group negatively charged, while the amino group is protonated and positively charged.

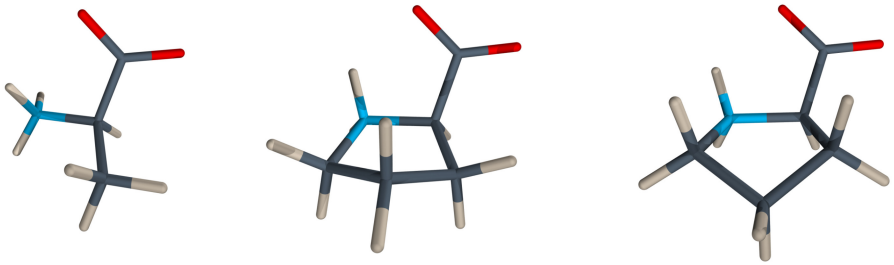

L-Alanine L-Proline A L-Proline B

Figure 3.5: L-alanine and L-proline zwitterions. The A and B proline conformers have approximately the same energy and equal populations in aqueous solutions at room temperature [60].

than 2000 cm^{-1}) are in general well described by the harmonic potential. The anharmonic methods improved the agreement only occasionally for some C−H and N−H bending modes.

Conformational flexibility of the molecules contributes to the broadening of peaks, as was demonstrated by the Boltzmann averaging of the spectra calculated for different conformers.

3.2.3 Conformational flexibility (preliminary results)

Raman and ROA spectra are sensitive to molecular conformation. If a molecule can exist in multiple conformations under the given experimental conditions, each of the conformers will contribute to the spectra. For flexible molecules, it is expected that some of the spectral bands will change their relative intensity and will become broader with increased temperature, as more conformers will become energetically accessible. Experimental evidence suggested that more flexible molecules have less complex spectral features than the rigid ones. For example, experimental Raman and ROA spectra of some small dipeptides (Gly-Pro and Ala-Pro) seem to have sharper bands than others (Pro-Gly and Pro-Ala) within 200–750 cm^{-1} [59].

In the paper under preparation, we try to verify that the decreased complexity of the Pro-Gly and Pro-Ala spectra is due to larger conformational flexibility of these molecules: in the "rigid" molecules (Gly-Pro and Ala-Pro), the torsion angle φ is fixed by the covalent bond in the proline ring and only the torsion angle ψ is allowed to move. In the "flexible" molecules (Pro-Gly and Pro-Ala) both torsion angles ψ and φ are allowed to move (Fig. 3.6). To identify possible conformers, systematic scanning of the conformation space was performed: one-dimensional scans along the angle ψ for the rigid molecules and two-dimensional scans along the angles ψ and φ for the flexible molecules.

Four local minima have been found for Gly-Pro and Ala-Pro, differing in the puckering phase[4] or in the *cis* and *trans* form (Table 3.9). For Ala-Pro, both *cis* conformers have significantly lower energy, but their geometries appear unrealistic: according to the calculation, one of the hydrogens from the NH_3 group forms a hydrogen bond with one of the oxygens from the CO_2 group. The calculation shows the vibrational transition associated with this hypothetical

[4]The puckering phase is a characterization of the five-membered ring in proline and it is defined in terms of torsion angles [61]. There are two proline conformers differing in the puckering phase. They have approximately the same energy in aqueous solutions at room temperature (Fig. 3.5).

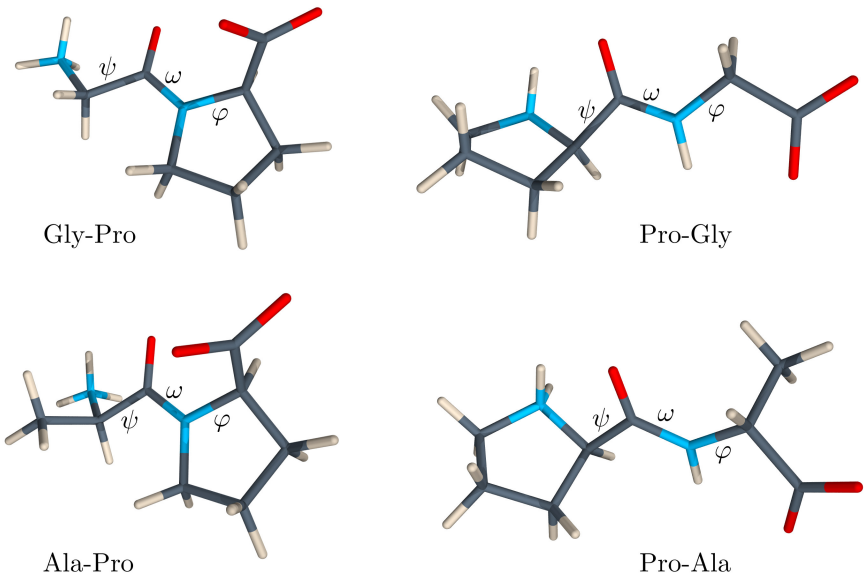

Figure 3.6: *Trans* conformers of Gly-Pro, Pro-Gly, Ala-Pro and Pro-Ala zwitterions. The angle φ is fixed in Gly-Pro and Ala-Pro, but is allowed to move in Pro-Gly and Pro-Ala.

bond as an isolated peak near 2400 cm^{-1}, but there is no such peak present in experimental spectra. For Gly-Pro, the two *cis* conformers also have lower energies, but both appear realistic. Each of the conformers was then used to generate another two geometries by rotating the angle ψ and optimizing with ψ held constant. Ideally, the rotation should be large enough to estimate the effect on the vibrational spectra, but still allowing decent Boltzmann population of the rotamers at room temperature. In Fig. 3.7 the results of the preliminary calculations are plotted for Gly-Pro. Although the limited number of conformers does not exactly reproduce the smooth experimental bands, broadening of the peaks is clearly visible.

The flexible dipeptides Pro-Gly and Pro-Ala were treated in a similar way. Four local minima differing in the puckering phase and in the *cis* and *trans* form of the amide bond can exist for both molecules. The *cis* form is known to be energetically much less favorable and therefore only the *trans* form was investigated. For both molecules, two-dimensional PES were generated by interpolation between 100 scan points calculated at the B3LYP/6-31G*/CPCM level with φ and ψ ranging from 0° to 360°. Raman spectra were then calculated for 26 conformers and averaged according to Boltzmann populations at room temperature. Because the evaluation of the optical activity tensors is very demanding, the ROA tensors were calculated only for the equilibrium geometries. For other conformers, the algorithm described in Ref. 62 was used to

Gly-Pro	*cis*	*trans*
P_1	0	0.75
P_2	0.17	0.89

Ala-Pro	*cis*	*trans*
P_1	0	4.8
P_2	<1.1	5.0

Table 3.9: Relative energies of Gly-Pro and Ala-Pro conformers calculated at the B3LYP/6-31++G**/CPCM level. They differ in the puckering phase (P_1 and P_2) or in the *cis* and *trans* form. The P_2/*cis* conformer reached a local minimum. The global minimum was not pursued, because the geometry seemed unrealistic, as described in the text. [kcal/mol]

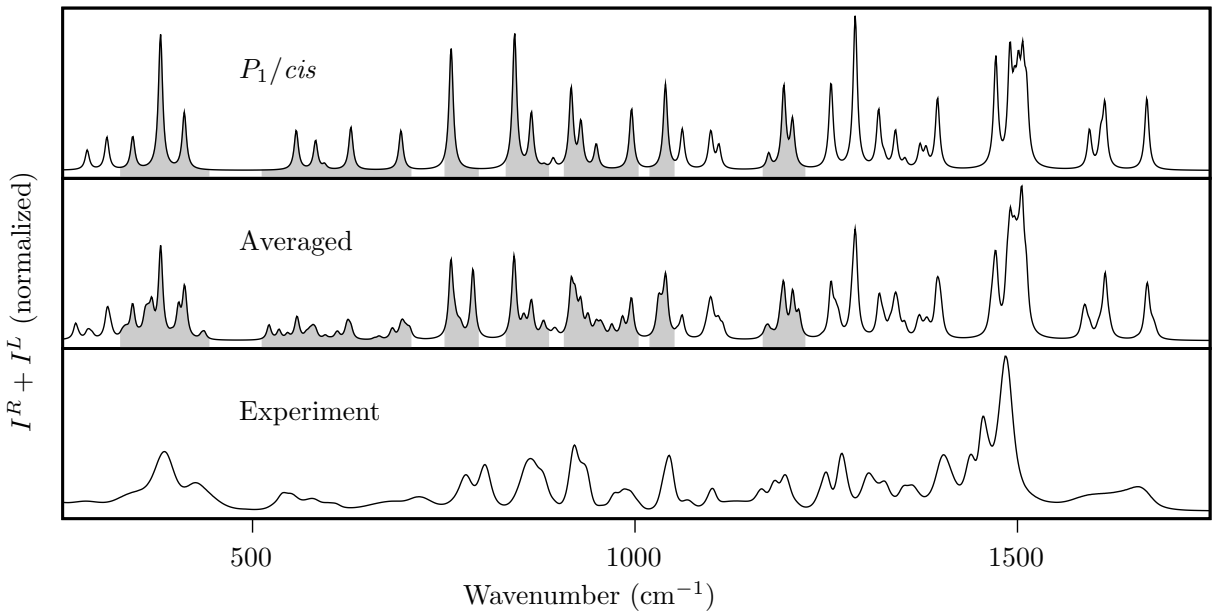

Figure 3.7: Calculated and experimental Raman spectra of Gly-Pro (preliminary results). The top panel shows Raman spectra calculated for the equilibrium geometry P_1/cis, the middle panel shows Boltzmann-averaged spectra of 11 conformers, and in the bottom panel is plotted the measured spectrum. The parts of the spectra susceptible to improvement by Boltzmann averaging are emphasized by gray color. All calculations were performed at the B3LYP/6-31++G**/CPCM level using the harmonic approximation.

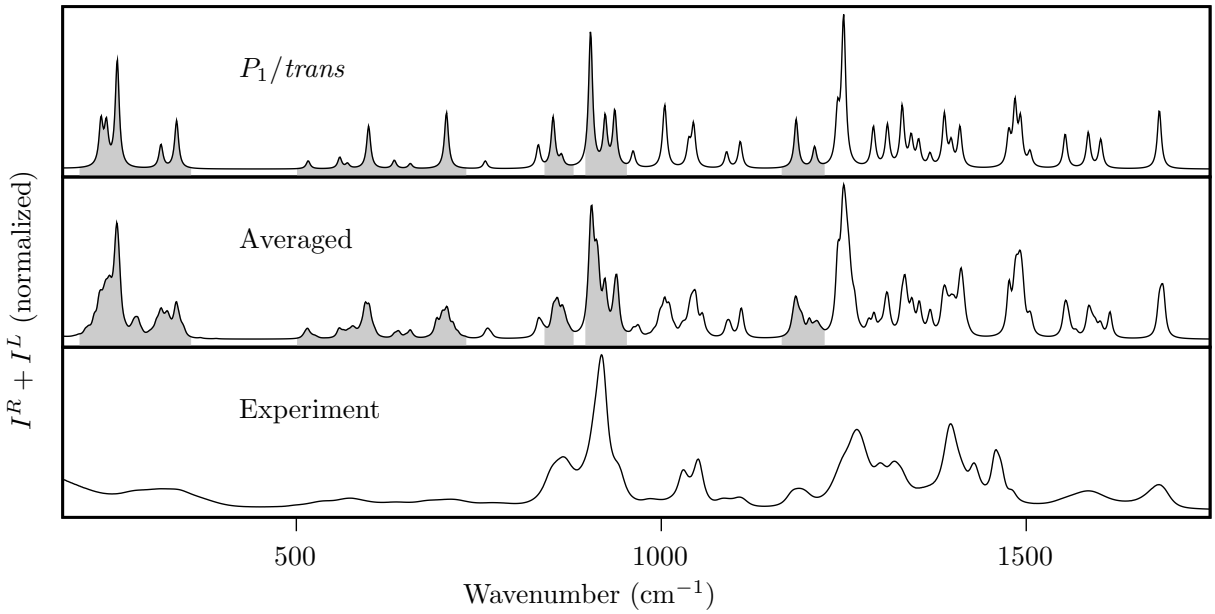

Figure 3.8: Calculated and experimental Raman spectra of Pro-Gly (preliminary results). The top panel shows Raman spectra calculated for the equilibrium geometry $P_1/trans$, the middle panel shows Boltzmann-averaged spectra of 26 conformers, and in the bottom panel is plotted the measured spectrum. The parts of the spectra susceptible to improvement by Boltzmann averaging are emphasized by gray color. All calculations were performed at the B3LYP/6-31++G**/CPCM level using the harmonic approximation.

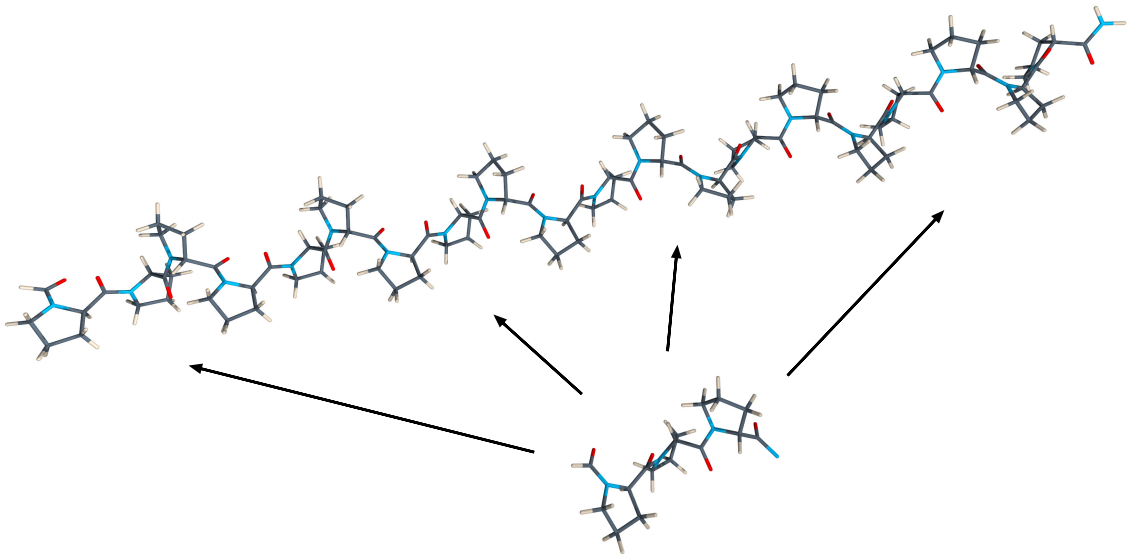

Figure 3.9: Transfer of molecular property tensors from a tripeptide to poly-proline II.

transfer the tensors to the desired geometries.

In Fig. 3.8 the results of the preliminary calculations are plotted. The results obtained so far for Gly-Pro and Pro-Gly do not seem to confirm the hypothesis that the lesser complexity of the Raman and ROA spectra of Pro-Gly and Pro-Ala origin in larger number of conformers. The averaging seems to play a role equally important for all of the studied dipeptides.

3.2.4 Transfer of molecular property tensors (in progress)

The evaluation of *ab initio* force fields and molecular property tensors is feasible only for small molecules. Large systems can be treated only approximately, for example, by dividing them into smaller pieces, then evaluating the properties on a decent electronic level, and transferring the properties to the large molecule (Fig. 3.9). Because the evaluation of the anharmonic potential requires a large amount of computer-time, the algorithm described in Ref. 62 was implemented also for anharmonic force constants. The method will be used for anharmonic frequencies of poly-proline II, the calculations are already in progress.

CHAPTER 4

Conclusions

The aim of this work was to investigate anharmonic and solvation effects in vibrational spectra. Several vibrational anharmonic methods were coded in two implementations using two different programming languages (Fortran and C) to verify the correctness of the software, and thoroughly tested on model potentials studied previously by other authors. The anharmonic methods were then applied to a number of systems, both small and large (water and α-pinene), rigid and flexible (furan and NMA).

For small molecules, several calculations were performed with potentials obtained at various levels of the electronic theory. The most computer-time demanding method CCSD/cc-pVTZ could be used only for water and formaldehyde. In both cases, the anharmonic frequencies based on the CCSD potential deviated from experiment more than the frequencies obtained with the MP2/cc-pVTZ potential. The MP2 method gave the best agreement with experiment in calculations performed for formaldehyde and furan, while for water and NMA the MP2 method was outperformed by the B3LYP/cc-pVTZ calculation. The BPW91/cc-pVTZ method seems to be biased toward the harmonic approximation, so that the harmonic frequencies often give the best results, but anharmonic corrections shift the frequencies far too low.

For larger molecules, the evaluation of the anharmonic potential is restricted to less accurate electronic methods and smaller basis sets. The B3LYP method was tested with several basis sets, but the small number of tested molecules (water, formaldehyde and furan) did not allow generalization. For furan and formaldehyde, the calculations performed with the cc-pVTZ basis set yielded results similar to the results obtained with the 6-311++G** set. Whereas for water, a significant difference between the two was observed. Diffuse functions on hydrogens (++) seemed not to be crucial for water and formaldehyde, but were found important for furan. The double split set (6-31++G**) gave identical results for water as for the triple split basis set (6-311++G**), but very different for furan. Perhaps expectedly, the polarization functions on hydrogen (**) are important for water, but not so much for formaldehyde and furan. Clearly, the basis set must be selected on an individual basis to respect the nature of the studied system.

As expected, the anharmonic effects dominate in the region of C-H and N-H stretching vibrations. All of the anharmonic methods investigated in this work significantly improved harmonic results in this region. Due to inaccuracies of the vibrational potential and involved approximations, none of the methods enabled peak-to-peak agreement with experiment though. The low- and mid-frequency vibrations are in general described well by the harmonic potential and anharmonic corrections do not inevitably improve the agreement with experiment in this

region.

The solvent interactions were accounted for by means of the conductor solvent model CPCM. The model correctly stabilized the zwitterionic peptides and provided reasonable vibrational frequencies. However, due to numerical instabilities, the conductor model sometimes yields inconsistent results and therefore it requires tighter geometry optimization and a higher-density integration grid with DFT calculations. Although the treatment of solvation prolongs the computation time, the effects of solvation often cannot be neglected.

Some of the bands in experimental spectra are less intensive and broader, probably because of direct interactions with solvent molecules and larger molecular flexibility. To reproduce these spectral shapes, full energy scans and the Boltzmann averaging were used successfully. The averaging allowed to partially include the anharmonicity of the low-frequency vibrations which could not be properly treated by the anharmonic methods.

Appendix A

A.1 Simplified degeneracy treatment

This Appendix justifies usage of the degeneracy-corrected perturbation formula. It is shown that for non-degenerate states the formula reduces to the standard second-order perturbation treatment.

Non-degenerated states

The second term in Eq. 2.2.18 may written as

$$\sqrt{(E_i - E_j)^2 + 4W_{ij}^2} = |E_i - E_j|\sqrt{1+\epsilon}, \qquad \epsilon = \frac{4W_{ij}^2}{(E_i - E_j)^2}, \tag{A.1.1}$$

where ϵ is proportional to second power of the perturbation parameter λ from Eq. 2.2.8. Using first two terms of the expansion

$$\sqrt{x+\epsilon} = \sqrt{x} + \frac{1}{2}x^{-1/2}\epsilon - \frac{1}{8}x^{-3/2}\epsilon^2 + \cdots, \tag{A.1.2}$$

the expression may be then approximated by

$$|E_i - E_j|\left[1 + \frac{2W_{ij}^2}{(E_i - E_j)^2}\right]. \tag{A.1.3}$$

Respecting the $\pm$ convention introduced on page 16, it is easy to show that Eq. 2.2.18 then evaluates to

$$\sum_{j\neq i}\frac{1}{2}(E_j - E_i) \pm \frac{1}{2}\sqrt{(E_i - E_j)^2 + 4W_{ij}^2} \;=\; \sum_{j\neq i}\frac{W_{ij}^2}{E_i - E_j}. \tag{A.1.4}$$

By use of the expansion

$$\frac{1}{x+\epsilon} = \frac{1}{x} - \frac{\epsilon}{x^2} + \cdots, \tag{A.1.5}$$

the formula may be modified as

$$\sum_{j\neq i}\frac{W_{ij}^2}{E_i - E_j} = \sum_{j\neq i}\frac{W_{ij}^2}{E_i^{(0)} - E_j^{(0)}} - \frac{W_{ij}^2(W_{ii} - W_{jj})}{(E_i^{(0)} - E_j^{(0)})^2} + \cdots. \tag{A.1.6}$$

The terms which are proportional to higher powers of the perturbation coefficient λ are neglected. Thus taking only the first term, one arrives to the standard perturbation formula.

Two-fold degenerated states

When two or more states occur with the same energy, the second-order perturbation formula fails. If there are only two degenerate states, it is straightforward to show that the eigenvalues from Eq. 2.2.16 are

$$w_{\pm} = \frac{1}{2}(W_{11} + W_{22}) \pm \frac{1}{2}\sqrt{(W_{11} - W_{22})^2 + 4W_{12}^2}. \tag{A.1.7}$$

Therefore Eq. 2.2.17 evaluates to

$$E_{\pm} = E_1^{(0)} + \frac{1}{2}(W_{11} + W_{22}) \pm \frac{1}{2}\sqrt{(W_{11} - W_{22})^2 + 4W_{12}^2}. \tag{A.1.8}$$

When also interactions with other states are included, an expression identical to

$$E_1^0 + W_{11} + E_1^{(2)\prime} \tag{A.1.9}$$

is obtained.

A.2 Units

Frequencies

In vibrational spectroscopy frequencies are traditionally expressed as wave numbers $\tilde{\nu}$ in the cm^{-1} units. The wave number is defined as

$$\tilde{\nu} = 1/\lambda, \tag{A.2.1}$$

where λ is the wave length of the radiation in a vacuum.

Experimental absorption intensities

Absorption spectra in this work were plotted as the molar extinction coefficient ε, with peaks simulated by Lorentz curves of a fixed width Δ. A peak of height h centered at $\tilde{\nu}_i$ is given as

$$L_i(\tilde{\nu}) = \frac{h}{4(\tilde{\nu} - \tilde{\nu}_i)^2/\Delta^2 + 1}. \tag{A.2.2}$$

Calculated absorption intensities I are usually given in km/mol [63]. These units are related to the experimental quantity ε ($\mathrm{L\,mol^{-1}cm^{-1}}$) by [64]

$$I_i = 9.184 \times 10^{-3}\, \tilde{\nu}_i \sqrt{2\pi} \int \frac{\varepsilon}{\tilde{\nu}}\, d\tilde{\nu}. \tag{A.2.3}$$

Using the approximation that

$$\int \frac{\varepsilon}{\tilde{\nu}}\, d\tilde{\nu} \simeq \frac{1}{\tilde{\nu}_i} \int \varepsilon\, d\tilde{\nu}, \tag{A.2.4}$$

the unknown height h of the Lorentz curve is determined from the requirement that the area under the curve L has to be equal to the area under ε

$$\int_{-\infty}^{\infty} \varepsilon\, d\tilde{\nu} = \int_{-\infty}^{\infty} \frac{h}{4(\tilde{\nu} - \tilde{\nu}_i)^2/\Delta^2 + 1}\, d\tilde{\nu} \tag{A.2.5}$$

$$= -\frac{1}{2}\, h\, \Delta\, \tan^{-1}\left[\frac{2(\tilde{\nu}_i - \tilde{\nu})}{\Delta}\right]_{-\infty}^{+\infty} \tag{A.2.6}$$

$$= \frac{\pi}{2}\, h\, \Delta. \tag{A.2.7}$$

Inserting this result in Eq. A.2.3, the height of the Lorentz curve is found to be

$$h = \frac{1}{9.184 \times 10^{-3}}\, \frac{I}{\Delta} \sqrt{\frac{2}{\pi^3}}. \tag{A.2.8}$$

A.3 Computation details

The force fields and molecular properties were calculated using the GAUSSIAN software [63]. The results of anharmonic methods presented in this work were calculated using the GVIB program package implemented by the author of this work. The code is freely available for download [52].

Unless explicitly stated otherwise, all calculations were performed using the following default parameters:

Force field constants

- The anharmonic constants were calculated by numerical differentiation with a displacement step of 0.025Å.

VSCF parameters

- VSCF functions were represented by a linear combination of 15 LHOs.
- The convergence criterion for VSCF energy was set to 10^{-6} cm^{-1}. Typically, the energy converged after less than 50 iterations.

VCI and perturbation methods

- The maximal number of allowed excitations in product functions used in VCI and the perturbation calculus was set to $n_{\mathrm{exc}} = 5$.
- Unless stated otherwise, the VCI calculations were performed in the basis of 1000 functions.

Spectra simulations

- The default width (FWHM) of Lorentzian peaks was 6.5 cm^{-1}.
- The evaluation of second-order derivatives of tensors required for anharmonic Raman and ROA intensities is very computer-time demanding. Therefore, the computation may be performed using first-order derivatives only.
- For perturbation methods, the calculation of intensities was not implemented. Instead, intensities are taken from the unperturbed solutions.

For some molecules, the anharmonic methods exhibit convergence problems. The most sensitive is the eVSCF method, which often fails to converge unless the lowest-energy modes are left out from the calculations. Their coupling to higher-frequency modes is believed to be negligible and was in some cases partially accounted for by Boltzmann averaging.

A.4 Numerical differentiation and CPCM

As discussed in Sec. 2.4.3, the vibrational potential can be near a minimum approximated by a Taylor expansion. Cubic and semidiagonal quartic derivatives can be calculated by numerical differentiation of second order derivatives evaluated at geometries displaced from the equilibrium geometry along nuclear coordinates. Some of the constants can be obtained multiple times. For instance, the quartic constant $V^0_{\alpha_i\alpha_i\beta_j\beta_j}$ can be obtained twice

$$V^0_{\alpha_i\alpha_i\beta_j\beta_j} = \frac{1}{\Delta^2}(V^{\beta_j+\Delta}_{\alpha_i\alpha_i} + V^{\beta_j-\Delta}_{\alpha_i\alpha_i} - 2V^0_{\alpha_i\alpha_i}) = \frac{1}{\Delta^2}(V^{\alpha_i+\Delta}_{\beta_j\beta_j} + V^{\alpha_i-\Delta}_{\beta_j\beta_j} - 2V^0_{\beta_j\beta_j}). \qquad \text{(A.4.1)}$$

If the second order derivatives were exact, both formulae would yield exactly the same values. However, due to numerical errors of electronic calculations, the values differ in practice. For example, calculations performed for alanine at the B3LYP/6-31G**/CPCM level with the dif-

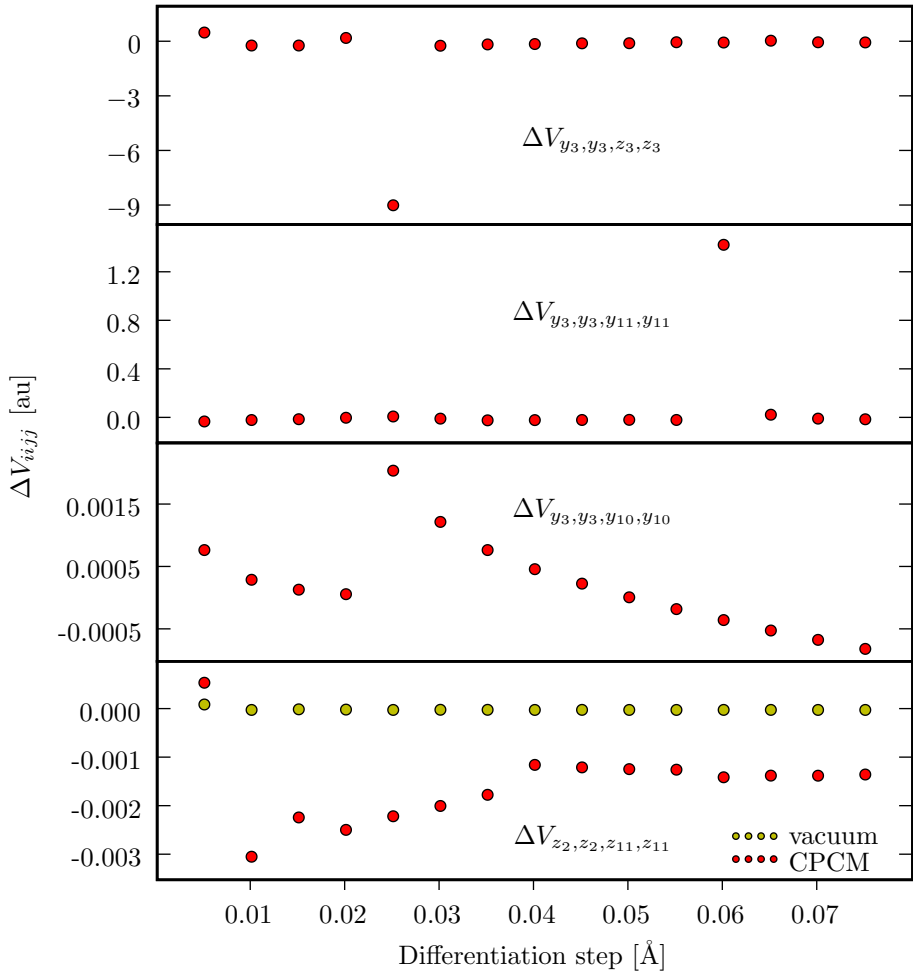

Figure 4.1: Deviations from expected symmetry of semidiagonal quartic constants calculated at the B3LYP/6-31G**/CPCM (red) and the B3LYP/6-31G** (yellow) levels. The two pictures at the top illustrate that there is no best differentiation step: the error of the constant V_{y_3,y_3,z_3,z_3} is minimal for the step of 0.06 Å. Using this step size will, however, magnify the error of the constant $V_{y_3,y_3,y_{11},y_{11}}$. The third picture shows a well-behaved constant. On the last picture are compared errors of CPCM and vacuum calculations.

ferentiation step $\Delta = 0.025$ Å give an alarmingly large error: the maximal error is almost 95% of the value of the largest quartic constant! The magnitude of the error depends on the size of the differentiation step. For example, if the step size is increased to 0.06 Å, the maximal error is reduced below 24%. However, the most significant improvement is achieved when the calculations are performed without the CPCM model or when the CPCM cavities are held fixed at the equilibrium positions and are not allowed to move along with the displaced atoms.[1]

Fig. 4.1 shows deviations of selected symmetric quartic constants, calculated for particular steps. As shown, a randomly chosen quartic constant is much less stable when calculated using the CPCM model (the bottom picture). For most constants, the error changes gradually with the step size (the third picture from the top), but it can be significantly larger for some particular step (the top picture). Choosing a different step size does not help, because different constants have largest deviations for different steps (the second picture from the top).

The results in this Appendix were obtained by the GAUSSIAN 03 software, rev. C.02. Obviously, the results are dependent on a number of the program's options, parameters and optimization criteria. Calculations performed by the same version of the software at a different level of theory (HF/6-31G) or for slightly different starting geometry either did not reproduce these dramatic errors or gave different error curves. In contrast to the suggestion of Barone [21, 65], practical tests (with the CPCM model) favored larger differentiation steps of about 0.05 Å. It was not investigated whether larger steps may contaminate the constants by higher order force constants or if the constants can be affected by coupling between modes for larger steps.

[1] The results of CPCM calculations presented throughout this work were obtained with cavities following the displaced atoms.

References

[1] C. V. Raman and R. S. Krishnan, *A new type of secondary radiation*, Nature **121** (1928), 501.

[2] P. W. Atkins and L. D. Barron, *Rayleigh scattering of polarized photons by molecules*, Mol. Phys. **16** (1969), 453–466.

[3] L. D. Barron and A. D. Buckingham, *Rayleigh and Raman scattering from optically active molecules*, Mol. Phys. **20** (1971), 1111–1119.

[4] W. Hug, S. Kint, G. F. Bailey, and J. R. Scherer, *Raman circular intensity differential spectroscopy.*, J. Am. Chem. Soc. **97** (1975), 5589–5590.

[5] P. Bouř, V. Baumruk, and J. Hanzlíková, *Measurement and calculation of the Raman optical activity of α-pinene and* trans-*pinane*, Collect. Czech. Chem. Commun. **62** (1997), 1384–1395.

[6] J. Hanzlíková, P. Praus, and V. Baumruk, *Raman optical activity spectrometer for peptide studies*, J. Mol. Struct. **480–481** (1999), 431–435.

[7] J. Kapitán, *Teoretický a experimentální rozvoj Ramanovy optické aktivity jako metody studia biomolekul ve vodném prostředí*, Ph.D. thesis, MFF UK, 2006.

[8] T. Hrenar, H. J. Werner, and G. Rauhut, *Accurate calculation of anharmonic vibrational frequencies of medium sized molecules using local coupled cluster methods*, J. Chem. Phys. **126** (2007), 134108–1–134108–9.

[9] P. Pulay and W. Meyer, *Comparison of the ab initio force constants of ethane, ethylene and acetylene*, Mol. Phys. **27** (1974), 473–490.

[10] C. E. Blom and C. Altona, *Scale factor method for the calculation of vibrational frequencies from ab initio force constants*, Mol. Phys. **31** (1976), 1377–1391.

[11] J. Haesler, I. Schindelholz, E. Riguet, C. G. Bochet, and W Hug, *Absolute configuration of chirally deuterated neopentane*, Nature **446** (2007), 526–529.

[12] J. O. Jung and R. B. Gerber, *SCF for $(H_2O)_n$ wave functions*, J. Chem. Phys. **105** (1996), 10332–10348.

[13] A. E. Roitberg and R. B. Gerber, *A vibrational eigenfunction of BPTI*, J. Phys. Chem. B **101** (1997), 1700–1706.

[14] G. Rauhut, *Efficient calculation of potential energy surfaces for the generation of vibrational wave functions*, J. Chem. Phys. **121** (2004), 9313–9322.

[15] S. Carter, J. M. Bowman, and L. B. Harding, *Ab initio calculations of force fields for H_2CN and ClHCN and vibrational energies of H_2CN*, Spec. Chim. Acta A **53** (1997), 1179–1188.

[16] S. Carter, S. J. Culik, and J. M. Bowman, *Vibrational self-consistent field method for many-mode systems*, J. Chem. Phys. **107** (1997), 10458–10469.

[17] W. Schneider and W. Thiel, *Anharmonic force fields from analytic second derivatives: Method and application to methyl bromide*, Chem. Phys. Lett. **157** (1989), 367–373.

[18] J. M. Bowman, *Self-consistent field energies nad wavefunctions for coupled oscillators*, J. Chem. Phys. **68** (1978), 608–610.

[19] J. M. Bowman, K. Christoffel, and F. Tobid, *Application of SCF-SI theory to vibrational motion in polyatomic molecules*, J. Phys. Chem. **83** (1979), 905–912.

[20] P. Bouř and L. Bednárová, *Anharmonic force field of formamide. a computational study.*, J. Phys. Chem. **99** (1995), 5961–5966.

[21] V. Barone, *Anharmonic vibrational properties by a fully automated second-order perturbative approach*, J. Chem. Phys. **122** (2005), 014108.

[22] L. S. Norris, M. A. Ratner, A. E. Roitberg, and R. B. Gerber, *Møller Plesset perturbation theory applied to vibrational problems*, J. Chem. Phys. **105** (1996), 11261–11267.

[23] O. Christiansen, *Vibrational coupled cluster theory*, J. Chem. Phys. **120** (2004), 2149–2159.

[24] S. Miertus, E. Scrocco, and J. Tomasi, *Electrostatic interaction of a solute with a continuum*, Chem. Phys. **55** (1981), 117–129.

[25] V. Barone and M. Cossi, *Quantum calculation of molecular energies and energy gradients in solution by a conductor solvent model*, J. Phys. Chem. A **102** (1998), 1995–2001.

[26] P. Daněček and P. Bouř, *Comparison of the numerical stability of methods for anharmonic calculations of vibrational molecular energies*, J. Comp. Chem. **28** (2007), 1617–1624.

[27] D. L. Strout and G. E. Scuseria, *A quantitative study of the scaling properties of the Hartree-Fock method*, J. Chem. Phys. **102** (1995), 8448–8452.

[28] J. Čížek, *On the correlation problem in atomic and molecular systems*, J. Chem. Phys. **45** (1966), 4256–4266.

[29] G. D. Purvis and R. J. Bartlett, *Coupled-clusters singles and doubles model*, J. Chem. Phys. **76** (1982), 1910–1918.

[30] C. Møller and M. S. Plesset, *Note on an approximation treatment for many-electron systems*, Phys. Rev. **46** (1934), 618–622.

[31] P. Hohenberg and W. Kohn, *Inhomogeneous electron gas*, Phys. Rev. **136** (1964), B864–B871.

[32] M. Levy, *Universal variational functionals of electron densities, first-order density matrices, and natural spin-orbitals and solution of the v-representability problem*, Proc. Natl. Acad. Sci. **76** (1979), 6062–6065.

[33] W. Kohn and L. J. Sham, *Self-consistent equations including exchange and correlation effects*, Phys. Rev. **140** (1965), A1133–A1138.

[34] A. D. Becke, *Density-functional exchange-energy approximation with correct asymptotic behavior*, Phys. Rev. A **38** (1988), 3098–3100.

[35] J. P. Perdew, in *Electronic structure of solids '91*, P. Ziesche and H. Eschrig (eds.), p. 11, Akademie Verlag, Berlin, 1991.

[36] A. D. Becke, *Density-functional thermochemistry. The role of exact exchange*, J. Chem. Phys. **98** (1993), 5648–5652.

[37] C. Lee, W. Yang, and R. G. Parr, *Development of the Colle-Salvetti correlation-energy formula into a functional of the electron density*, Phys. Rev. B **37** (1988), 785–789.

[38] W. J. Hehre, R. Ditchfield, and J. A. Pople, *Further extensions of gaussian-type basis sets for use in molecular orbital studies of organic molecules*, J. Chem. Phys. **56** (1971), 2257–2261.

[39] R. Krishnan, J. S. Binkley, R. Seeger, and J. A. Pople, *A basis set for correlated wave functions*, J. Chem. Phys. **72** (1980), 650–654.

[40] T. H. Dunning, Jr., *Gaussian basis sets for use in correlated molecular calculations*, J. Chem. Phys. **90** (1989), 1007–1023.

[41] E. B. Wilson and J. B. Howard, *The vibration-rotation energy levels of polyatomic molecules*, J. Chem. Phys. **4** (1936), 260–268.

[42] D. Papoušek and M. R. Aliev, *Molecular vibrational-rotational spectra*, Elsevier, 1982.

[43] K. G. Watson, *Simplification of the molecular vibration-rotation hamiltonian*, Mol. Phys. **15** (1968), 479–490.

[44] J. Antony, G. von Helden, G. Meijer, and B. Schmidt, *Anharmonic midinfrared vibrational spectra of benzoic acid monomer and dimer*, J. Chem. Phys. **123** (2005), 014305–1–014305–11.

[45] G. M. Chaban, J. O. Jung, and R. B. Gerber, *Ab initio calculation of anharmonic vibrational states of polyatomic systems: Electronic structure combined with vibrational self-consistent field*, J. Chem. Phys. **111** (1999), 1823–1829.

[46] K. M. Christoffel and J. M. Bowman, *Investigations of self-consistent field, SCF CI and virtual state configuration interaction vibrational energies for a model three-mode system*, Chem. Phys. Lett. **85** (1982), 220–224.

[47] J. Franck, *Elementary processes of photochemical reactions*, Trans. Faraday Society **21** (1926), 536–542.

[48] E. Condon, *A theory of intensity distribution in band systems*, Phys. Rev. **28** (1926), 1182–1201.

[49] G. Placzek, in *Handbuch der radiologie*, E. Marx (ed.), pp. Vol. VI, Pt. 2, Academische Verlagsgesellschaft, Leipzig, 1934.

[50] I. M. Degtyarenko, K. J. Jalkanen, A. A. Gurtovenko, and R. M. Nieminen, *L-alanine in a droplet of water: A density-functional molecular dynamics study*, J. Phys. Chem. B **111** (2007), 4227–4234.

[51] A. Klamt and G. Schürmann, *COSMO: A new approach to dielectric screening in solvents with explicit expressions for the screening energy and its gradient*, J. Chem. Soc. Perkin Trans. **2** (1993), 799–805.

[52] P. Daněček, *Gvib: A package for vibrational analysis*, http://gvib.sf.net.

[53] M. Diem, *Introduction to modern vibrational spectroscopy*, John Wiley & Sons, 1993.

[54] M. M. Wohar and P. W. Jagodzinski, *Infrared spectra of H_2CO, $H_2{}^{13}CO$, D_2CO, and $D_2{}^{13}CO$ and anomalous values in vibrational force fields*, J. Mol. Spectrosc. **148** (1991), 13–19.

[55] S. Ataka, H. Takeuchi, and M. Tasuni, *Infrared studies of N-methylformamide and N-methylacetamide in low-temperature nitrogen matrices*, J. Mol. Struct. **113** (1984), 147–160.

[56] L. C. Mayne and B. Hudson, *Resonance Raman spectroscopy of N-Methylacetamide*, J. Phys. Chem. **95** (1991), 2962–2961.

[57] A. Mellouki, J. Liévin, and M. Herman, *The vibrational spectrum of pyrrole and furan in the gas phase*, Chem. Phys. **271** (2001), 239–266.

[58] P. Daněček, J. Kapitán, V. Baumruk, L. Bednárová, V. Kopecký, Jr., and P. Bouř, *Anharmonic effects in IR, Raman, and Raman optical activity spectra of alanine and proline zwitterions*, J. Chem. Phys. **126** (2007), 224513.

[59] J. Kapitán, V. Baumruk, V. Kopecký, Jr., and P. Bouř, *Conformational flexibility of L-alanine zwitterion determines shapes of Raman and ROA spectral bands*, J. Chem. Phys. A **110** (2006), 4689–4696.

[60] J. Kapitán, V. Baumruk, V. Kopecký, Jr., R. Pohl, and P. Bouř, *Proline zwitterion dynamics in solution, glass, and crystalline state*, J. Am. Chem. Soc. **128** (2006), 13451–13462.

[61] C. Altona and M. Sundaralingam, *Conformational analysis of the sugar ring in nucleosides and nucleotides. A new description using the concept of pseudorotation*, J. Am. Chem. Soc. **94** (1972), 8205–8212.

[62] P. Bouř, J. Sopková, L. Bednárová, P. Maloň, and T. A. Keiderling, *Transfer of molecular property tensors in cartesian coordinates: A new algorithm for simulation of vibrational spectra*, J. Comp. Chem. **18** (1997), 646–659.

[63] M. J. Frisch, G. W. Trucks, H. B. Schlegel, et al., *Gaussian 03, Revision C.02*, Gaussian, Inc., Wallingford, CT, 2004.

[64] E. Charney, *The molecular basis of optical activity*, John Wiley & Sons, 1979.

[65] V. Barone, *Vibrational spectra of large molecules by density functional computations beyond the harmonic approximation: the case of pyrrole and furan*, Chem. Phys. Lett. **383** (2004), 528–532.

[66] A. Szabo and N. S. Ostlund, *Modern quantum chemistry*, MacGraw-Hill, Inc., 1989.

[67] L. D. Barron, *Molecular light scattering and optical activity*, Cambridge University Press, 1982.

[68] D. A. Long, *The Raman effect*, John Wiley & Sons, 2002.

List of Figures

List of Tables

Acronyms

AAT	Atomic axial tensor	46
APT	Atomic polar tensor	43
BOA	Born-Oppenheimer approximation	12
CC	Coupled cluster	22
CI	Configuration interaction	21
CIS	Singly excited CI	22
CISD	Singly and doubly excited CI	22
CPCM	Conductor-like PCM	50
COSMO	Conductor-like screening model	??
DFT	Density functional theory	23
eVSCF	Excited-state VSCF with self-consistent excited states	36
FWHM	Full width at half maximum	50
GGA	Generalized gradient approximation	25
gVSCF	Ground-state VSCF with orthogonal excited states	36
HF	Hartree-Fock theory	19
ICP	Incident circular polarization	47
IR	Infrared absorption spectroscopy	7
LDA	Local density approximation	25
LHO	Linear harmonic oscillator	9
LSDA	Local spin density approximation	25
MP2	Møller-Plesset perturbation theory	23
PCM	Polarizable continuum model	50
PES	Potential energy surface	8
PT2/Harm	Perturbation theory applied to harmonic approximation	37
PT2/VSCF	Perturbation theory applied to VSCF	37
ROA	Raman optical activity	7
VCD	Vibrational circular dichroism	7
VCI	Vibrational configuration interactions	9
VOA	Vibrational optical activity - VCD and ROA	7
VPT	Vibrational perturbation theory	9
VSCF	Vibrational self consistent field	9

Index

Appendix B: Publications